

University of Alberta

**The search for High-Affinity Carbohydrate Inhibitors: Investigation of
Macromolecular Trisaccharide Derivatives Containing Functional Group
Modifications**

by

Robert S. McGavin

A thesis submitted to the Faculty of Graduate Studies and Research in partial
fulfillment of the requirements for the degree of Doctor of Philosophy

Department of Chemistry

Edmonton, Alberta

Spring 2006



Library and
Archives Canada

Bibliothèque et
Archives Canada

Published Heritage
Branch

Direction du
Patrimoine de l'édition

395 Wellington Street
Ottawa ON K1A 0N4
Canada

395, rue Wellington
Ottawa ON K1A 0N4
Canada

Your file *Votre référence*

ISBN: 0-494-14019-4

Our file *Notre référence*

ISBN: 0-494-14019-4

NOTICE:

The author has granted a non-exclusive license allowing Library and Archives Canada to reproduce, publish, archive, preserve, conserve, communicate to the public by telecommunication or on the Internet, loan, distribute and sell theses worldwide, for commercial or non-commercial purposes, in microform, paper, electronic and/or any other formats.

The author retains copyright ownership and moral rights in this thesis. Neither the thesis nor substantial extracts from it may be printed or otherwise reproduced without the author's permission.

AVIS:

L'auteur a accordé une licence non exclusive permettant à la Bibliothèque et Archives Canada de reproduire, publier, archiver, sauvegarder, conserver, transmettre au public par télécommunication ou par l'Internet, prêter, distribuer et vendre des thèses partout dans le monde, à des fins commerciales ou autres, sur support microforme, papier, électronique et/ou autres formats.

L'auteur conserve la propriété du droit d'auteur et des droits moraux qui protègent cette thèse. Ni la thèse ni des extraits substantiels de celle-ci ne doivent être imprimés ou autrement reproduits sans son autorisation.

In compliance with the Canadian Privacy Act some supporting forms may have been removed from this thesis.

Conformément à la loi canadienne sur la protection de la vie privée, quelques formulaires secondaires ont été enlevés de cette thèse.

While these forms may be included in the document page count, their removal does not represent any loss of content from the thesis.

Bien que ces formulaires aient inclus dans la pagination, il n'y aura aucun contenu manquant.


Canada

Abstract

Univalent oligosaccharides protein interactions with few exceptions are characterized by weak affinity. Increasing the affinity would provide carbohydrate derivatives with therapeutic potential for treating cancer and infections. A crystallographically defined monoclonal antibody, SYA/J6, produced against the lipopolysaccharide of *Shigella flexneri* was used to investigate and design tighter binding oligosaccharides.

The goals of this work were to unambiguously identify the energy gains observed for macrocyclic trisaccharide epitope **21** as either entropic or enthalpic, and to design and synthesize macrocyclic trisaccharides incorporating selected functional group modifications that were anticipated to yield high affinity, submicromolar, ligands.

Synthesis of tethered, macrocyclic derivatives of the trisaccharide α -L-Rha-(1 \rightarrow 3)- α -L-Rha-(1 \rightarrow 3)- β -D-GlcNAc-OMe modified at the central Rha residue to incorporate either 2'-deoxy or 2'-chloro-2'-deoxy groups gave two univalent trisaccharides **25** and **26**.

ELISA assays and isothermal titration microcalorimetry were used to evaluate the binding affinities of a series of acyclic and tethered trisaccharide derivatives. Acyclic derivatives of the macrocyclic trisaccharide **21** exhibited a decreased affinity for SYA/J6, confirming that a β -alanine tether was responsible for its affinity gains. Compound **25** showed the highest affinity of all ligands tested, although the free energies gains from tethering and functional group modification were not additive. The 2-deoxy-macrocyclic trisaccharide **26** exhibited a binding affinity that was considerably lower than expected.

Molecular dynamics that **26** was pre-organized in a bioactive conformation and acyclic trisaccharides **23** and **24** had greater conformational flexibility than macrocyclic **21**. Docking analysis indicated that the tether of **26** could clash with the protein when bound in the preferred mode of its 2'-deoxygenated parent trisaccharide **2**.

Saturation transfer difference (STD) NMR was optimized to measure oligosaccharide-protein interactions. Structural changes, such as tethering and functional group modification, caused subtle changes in the mode of binding. Data from NMR experiments are consistent with x-ray data for non-tethered derivatives and suggests that the tether-protein interactions prevent penetration of **26** into the deepest part of the binding site.

Acknowledgements

I gratefully thank my supervisor, Dr. David R. Bundle for his guidance, patience, support, and insight, especially in the latter stages of my degree.

During my time spent in the group, I had the opportunity to train with excellent chemists of a wide range of expertise. Dr. Chang-Chung Ling spent a great deal of time dealing with numerous computer issues, and his help with molecular modeling and insightful discussions, along with Dr. Pavel Kitov are truly appreciated. For the contribution of their time to program the STD-NMR pulse sequence, and guide me through the latter stages of this work, I am indebted to Dr. Albin Otter and Dr. Thomas Peters. Also critical to this work was Joanna Sadowska, who generated antibody in plentiful quantities, and performed all the ELISA assays. I also thank the members of the Bundle group, past and present, whose kindness and generosity will never be forgotten. It was a great pleasure to work with you. Finally, I would like to thank Karin Fodor, and Lynne Lechelt for their superior organizational skills.

On a personal note, I would like to thank my parents: Mom and Marvin, and Dad and Gayle whose loving support was truly appreciated. I want to mention and thank some of the people who have made my time here one of the most enjoyable of my life. I gratefully acknowledge Jamie, Nolan, Corwin and Dean for their tremendous friendship, support and motivation. My time in Edmonton was made truly memorable by the following people: Jen, Jakie and Maggie, Hanna, Marc, Steven, Bailey, Graham, Duane, Karl, Fuzzer the Cat, Soren, Sebastian and Birgit, Sandra, Steph, and last but certainly not least, Jaime.

Table of Contents

Title	Page
CHAPTER ONE	
INTRODUCTION	
1.1 The Prevalence of Carbohydrates and Their Interactions with Proteins	1
1.2 The Thermodynamics of Carbohydrate-Protein Interactions.	3
1.2.1. Intermolecular Forces and the Association Constant.	3
1.2.2. Thermodynamic Forces of Binding.	4
1.2.3. The Thermodynamic Consequence of Aqueous Media.	6
1.3. Monoclonal IgG Antibodies: Structure and Production.	7
1.3.1 The General Structure of the IgG Antibody.	7
1.3.2. Production and Purification of Monoclonal Antibodies.	8
1.3.3. Quantification of Carbohydrate-Protein Interactions.	10
1.4. Description of the System Used in this Project	11
1.4.1. The <i>Shigella flexneri</i> IgG Monoclonal Antibody, SYA/J6.	11
1.4.2. Crystal Structure of the SYA/J6 Antibody.	12
1.4.3. Increased Affinity <i>via</i> Functional Group Modification.	16
1.5. Intramolecular Pre-Organization of Carbohydrate Structures.	17
1.5.1. Literature Precedent for Intramolecular Pre-Organization.	19
1.5.2. Pre-Organization of the <i>S. flexneri</i> LPS BCD Trisaccharide.	24
1.6. Scope of Project.	26
CHAPTER 2	
THE SYNTHESSES OF BCD TRISACCHARIDES	
2.1. Stereo and Electronic Factors in Glycosylation Chemistry.	29
2.1.1. The Anomeric Effect.	29
2.1.2. Substituents at C-2 and Neighboring Group Participation.	30
2.2 Acyclic BCD Trisaccharide Variants.	32
2.2.1. General considerations and Retrosynthetic Analysis.	32

2.2.2. Synthesis of Monosaccharide Components.	34
2.2.3. Assembly of the Acyclic Trisaccharides	36
2.3 Macrocyclic BCD Trisaccharides Containing Functional Group Modifications	40
2.3.1. Synthesis of a 2'-chloro-2'-deoxy Rhamnosyl Donor and L-Mannosyl Donor	40
2.3.2. Assembly of Macrocyclic Trisaccharides 25 and 26 .	45

CHAPTER 3

ANALYSIS OF THE BINDING OF SYNTHETIC LIGANDS TO MONOCLONAL ANTIBODY SYA/J6

3.1. Initial Binding Assessment Using ELISA.	53
3.1.1. The ELISA Protocol.	53
3.1.2. Thermodynamic Binding Analysis by Isothermal Titration Microcalorimetry.	59
3.2. ITC Analysis for Ligands Used in This Study.	63

CHAPTER 4

A MOLECULAR MODELING INVESTIGATION OF LIGAND FLEXIBILITY

TO UNDERSTAND BINDING WITH MONOCLONAL ANTIBODY SYA/J6

4.1. Determining the Conformation of Oligosaccharides in Solution.	68
4.1.1. NMR Methods.	68
4.1.2. Molecular Modeling.	69
4.2. Molecular Dynamics of Trisaccharide Ligands.	70
4.2.1. Definition of Torsional Angles of Oligosaccharides.	70
4.2.2. Comparison of HSEA Results with Molecular Dynamics Simulation.	71
4.2.3. Dynamics Calculations of Acyclic Trisaccharides 23 and 24 .	74
4.2.4. Conformation of the 2'-Chloro-2'-Deoxy Cyclic Trisaccharide.	77
4.2.5. Calculated Conformation of Tethered 2'-Deoxy Trisaccharide 26 .	80
4.3. Docking of 26 into the SYA/J6 Binding Site.	83

CHAPTER 5	
QUALITATIVE COMPARISON OF TRISACCHARIDE BINDING MODES USING SATURATION TRANSFER DIFFERENCE NMR	
5.1. Detecting Binding with NMR Techniques.	87
5.1.1. General Features of the Saturation Transfer Difference NMR Technique.	88
5.1.2. Specific Features of the STD-NMR Experiment.	90
5.2. Optimal STD-NMR Pulse Sequence Parameters.	92
5.2.1. Placement of the Selective On-Resonance Pulse Cascade.	93
5.2.2. Optimization of HOD Suppression.	99
5.3. STD-NMR Analysis of <i>Shigella flexneri</i> BCD Trisaccharide Congeners.	
5.3.1. Comparison of STD-NMR Derived Epitope Maps: General Considerations.	103
5.3.2. Comparison of STD-NMR Derived Epitope Maps.	106
CHAPTER 6	
SUMMARY AND CONCLUSIONS	112
CHAPTER 7	
EXPERIMENTAL SECTION	115
CHAPTER 8	
BIBLIOGRAPHY	153

List of Tables

Table	Title	Page
2.1	Conditions attempted for the chlorination of L-rhamnol derivative 51 .	44
3.1	Measured IC_{50} values with their corresponding structures for targets 23-26 .	57
3.2	Microcalorimetry results from measurement with each ligand and mAb SYA/J6.	63

List of Figures

Figure	Title	Page
1.1	The general structure of an IgG antibody.	8
1.2	ABCD A' pentasaccharide (1), 2'-deoxy BCD trisaccharide (2) and their calorimetric binding parameters.	14
1.3	Hydrogen bond map for 1 and 2 .	15
1.4	BCD trisaccharide derivatives 2 and 3 modified at the 2'-positions.	17
1.5	Examples of conformationally pre-arranged oligosaccharides.	20
1.6	Conformationally restricted H-Type II trisaccharide derivative 13 .	22
1.7	Pre-organized derivatives of the mAb Se155.4 epitope.	23
1.8	The bound ABCD A' pentasaccharide 1 .	25
1.9	Glyciny- (20) and β -alanyl-tethered (21) with native trisaccharide 22 .	25
1.10	Synthetic targets 23 and 24 .	26
1.11	The energetic penalties for the indicated modification of 2 .	27
1.12	Macrocyclic BCD trisaccharide targets 25 and 26 .	28
2.1	Orbital overlap that leads to the anomeric effect.	30
3.1	The general ELISA protocol for the evaluation of ligands with SYA/J6.	55
3.2	ELISA results for cyclic-deoxy 26 and acyclic control 23 .	56
3.3	ELISA results for cyclic-chloro 25 and acyclic control 24 .	56
3.4	Ligands grouped based on structural similarities to compared with ELISA binding data.	57
3.5	ITC results for native trisaccharide 22 and acyclic compounds 23 and 24 .	61
3.6	ITC results for native trisaccharide 22 and acyclic compounds 25 and 26 .	62
3.7	Relative comparisons of the change in free energies of the ligands measured by ITC.	66
4.1	Definitions of glycosidic torsion angles.	71
4.2	The ϕ vs. time and ψ vs. time for the BC and CD portions of the native trisaccharide 22 .	72
4.3	Comparisons of the dynamics calculations of native 22 from Insight II and potential energy surfaces from GEGOP.	73
4.4	Molecular dynamics for 23 .	75
4.5	Molecular dynamics for 24 .	76

4.6	The calculated conformation of the ω angle of 24 .	77
4.7	The potential energy diagrams for native 22 and the 2'-chloro-2'-deoxy BCD derivative 3 .	79
4.8	Molecular dynamics calculations for macrocyclic 21 .	80
4.9	ϕ and ψ torsional diagrams for compounds 2 .	81
4.10	ϕ and ψ torsional diagrams for compounds 26 .	82
4.11	The global energy minimum of 26 (yellow) superimposed on the bound structure of 2 (cyan).	83
4.12	Molecular dynamics of rotation around the C5 ² -C6 ² bond, ω .	84
4.13	A view of docked 26 in the SYA/J6 binding site with both the protein and 26 are colored by atom.	85
4.14a/b	Additional views of docked 26 with SYA/J6. In the top picture, carbon and hydrogen are both colored white.	86
5.1	A cartoon representation of the STD technique	89
5.2	The STD-NMR pulse sequence	93
5.3	Array of the gaussian on-resonance pulse in the aromatic region.	95
5.4	Array of the gaussian on-resonance pulse in the aliphatic region.	96
5.5	Array of the on-resonance pulse using the E-BURP-1 pulse profile in the aromatic region.	97
5.6	Array of the on-resonance pulse using the E-BURP-1 pulse profile in the aliphatic region.	98
5.7	The 1D spectrum of a “wet” sample of SYA/J6.	99
5.8	The effect of precise water suppression.	100
5.9	Array of reference spectra for determination of an optimal WATERGATE d3 values.	102
5.10	The three groups of ligands compared by epitope mapping derived by STD-NMR.	104
5.11	Representative STD-NMR (bottom) and reference spectrum (top) for 25 .	105
5.12	The epitope maps of 21 , 23 , and 24 .	107
5.13	The epitope maps for 2 , 26 , and 23 .	108
5.14	Epitope map values for 3 , 21 , 22 , and 26 .	109

List of Schemes

Scheme	Title	Page
2.1	A general glycosylation pathway showing the four possible configurational outcomes for standard hexoses.	31
2.2	Neighboring group participation and the Halide-Ion method of glycosylation.	32
2.3	Retrosynthetic analysis of acyclic BCD trisaccharides.	33
2.4	Synthesis of <i>N</i> -Phthalimido protected glucosamine acceptor 30 .	34
2.5	Synthesis of rhamnosyl thioglycoside donor 34 .	35
2.6	Synthesis of the L-mannosyl thioglycoside donor 38 .	36
2.7	Assembly of the protected core trisaccharide 41 .	37
2.8	Final synthesis of acyclic BCD derivatives 23 and 24 .	39
2.9	Retrosynthetic analysis of cyclic 25 and 26 .	41
2.10	Synthesis of protected L-rhamnol derivative 51 .	43
2.11	Successful chlorination of protected rhamnol derivative 51 and its elaboration to thioglycoside donor 56 .	44
2.12	Synthesis of L-mannosyl thioglycoside 59 .	45
2.13	Synthesis of protected trisaccharide 62 , containing the 2'-chloro-2'-deoxy modification.	46
2.14	Synthesis of macrocyclic 25 and 26 .	47
2.15	Synthesis of macrocyclic 21 .	50
2.16	Synthesis of the native BCD trisaccharide.	51

Abbreviations

Ac	acetyl
Ala	alanine
AMBER	assisted model building with energy refinement
Arg	Arginine
Bn	benzyl
Bz	benzoyl
1D	one-dimensional
2D	two-dimensional
DMF	<i>N,N'</i> -dimethylformamide
EIA	enzyme immunosorbent assay
ELISA	Enzyme linked immunosorbent assay
ES HRMS	electrospray high resolution mass spectrometry
Et	ethyl
Fab	antigen-binding fragment
Fmoc	9-fluorenylmethoxycarbonyl
GCOSY	gradient coupling correlated spectroscopy
GlcNAc	<i>N</i> -acetylglucosamine, 2-acetamido-2-deoxy- <i>D</i> -glucose
GlcNPhth	<i>N</i> -phthaloylglucosamine, 2-deoxy-2-phthalimido- <i>D</i> -glucose
Glu	glutamic acid
Gly	glycine
HIA	Hemagglutinin inhibition assay
His	histidine
HMQC	heteronuclear multiple quantum coherence
HOBt	1-hydroxybenzotriazole
HPLC	high performance liquid chromatography
HRP	horseradish peroxidase
IC ₅₀	inhibitor concentration required giving 50% inhibition
Man	mannose
MD	molecular dynamics

Me	methyl
M.S.	molecular sieves
NEM	<i>N</i> -ethylmorpholine
NIS	<i>N</i> -iodosuccinamide
NOE	nuclear Overhauser effect
PBS	phosphate buffer saline
PBST	phosphate buffer saline containing Tween 20
Ph	phenyl
PhthN	phthalimido
ppm	parts per million
Pyr	pyridine
Qui	L-quinovose, 6-deoxy-L-glucose
ROE	rotating-frame nuclear Overhauser effect
Rha	L-rhamnose, 6-deoxy-L-mannose
STD	saturation transfer difference
TBAF	tetrabutylammonium fluoride
TBDMS	<i>t</i> -butyldimethylsilyl
TBDPS	<i>t</i> -butyldiphenylsilyl
TBTU	2-(1H-benzotriazole-1-yl)-1,1,3,3,-tetramethyluronium tetrafluoroborate
TEMPO	2,2,6,6-tetramethyl-1-piperidinyloxy, free radical
TfOH	trifluoromethanesulphonic acid
Thr	threonine
TLC	thin layer chromatography
TMB	3,3',5,5'-tetramethylbenzidine
Trp	tryptophan
Tyr	tyrosine
UV	ultraviolet

Chapter 1

Introduction

1.1. The Prevalence of Carbohydrates and Their Interactions with Proteins.

The current impetus for the study of carbohydrates is their widespread role in biological systems. Oligosaccharides are found on the surface of virtually every cell in the mammalian body, and are also found on viruses, fungi, and bacteria. They are present as glycoconjugates and are commonly found in the form of glycoproteins, glycopeptides, glycolipids, and peptidoglycan and lipopolysaccharides of bacteria. These macromolecules can be structural and transport proteins, enzymes, immunoglobulins, cell adhesion molecules, hormones, toxins and lectins.^[1, 2]

As part of such conjugates, oligosaccharides function in many ways and are involved in numerous important biological roles. Commonly, they function by altering the conjugate's conformation, stability, or solubility.^[3] Oligo- and monosaccharides can also alter the activity of a protein *via* covalent attachment.^[4] While oligosaccharide structures can be displayed at the cell surface for recognition, if they are of sufficient size protein epitopes can be masked.^[5] Important examples of these interactions involving carbohydrates include reproductive fertilization, immunological responses, host-pathogen attachment, and cell-cell interactions necessary for recognition and proliferation. Consequently, the study of oligosaccharide interactions is of major interest.^[6]

The complexity of oligosaccharide structures allows a great diversity of interactions in biological systems due to the many stereogenic centers in a monosaccharide. The array of potential oligosaccharide structures grows due to the nature and position of attachment. In contrast to the other main classes of biomacromolecules – DNA, protein, and lipids – oligosaccharides can be highly branched structures. However, the length of these types of oligosaccharides is typically less than 20 residues.^[7]

Glycoconjugates bind to complementary protein receptors with typically weak affinity with dissociation constants of univalent interactions that range from sub-millimolar to micromolar. Many biological systems depend on the interaction of multivalent receptors with displays of multiple ligands, termed ordered multivalency, and increased avidity or apparent affinity has been observed. A notable example of ordered multivalency is the pentameric *Escherichia coli* O157:H7 Shiga-like toxin I that binds the P^k trisaccharide (α -D-Gal-(1→4)- β -D-Gal-(1→4)- β -D-Glc).^[8] Other examples include glyco-polymers, dendrimers and clusters.^[9]

There is considerable interest in the development of higher-affinity univalent oligosaccharide derivatives that could feasibly modulate complex biological systems. These compounds would have therapeutic value for the treatment of viral, bacterial, fungal, and parasitic infections. These types of molecules could be of potential use for the neutralization of certain autoimmune conditions^[10] and human cancers.^[6] Such inhibitors would also contribute to knowledge of the binding of carbohydrates to protein receptors and ultimately could be combined with multivalent platforms to increase avidity even further.

1.2 The Thermodynamics of Carbohydrate-Protein Interactions.

1.2.1. Intermolecular Forces and the Association Constant.

In aqueous solution, two complementary binding partners will associate if their cohesive forces are greater than the total of the detrimental, or repulsive, interactions between them. Non-covalent interactions between molecules are substantially weaker than a covalent bond and are individually extremely weak. Almost without exception there is more than one type of driving force governing the binding process.^[11] Identifying the contributions of the individual attractive forces is almost impossible using NMR and crystallography, but an increased understanding of the binding process has come from the measurement of binding of various systems.^[12-15]

The association of a single ligand and receptor at equilibrium is described by the following equation, where [L] and [P] are the equilibrium concentrations of unbound ligand and protein and [LP] is that of the bound complex:



The position of the equilibrium is described by a constant K_A :

$$K_A = [LP] / [L] [P] \quad (2)$$

The association constant can be related to the Gibbs free energy equation (3) to give a quantitative measure of the strength of binding in the system, where R is the universal gas constant and T is the absolute temperature.

$$\Delta G = \Delta H - T\Delta S = -RT \ln K_A \quad (3)$$

1.2.2. Thermodynamic Forces of Binding.

The enthalpic term contributing to the free energy of binding can be divided into separate commutative terms:

$$\Delta H = \Delta H_{\text{bind}} + \Delta H_{\text{conf}} \quad (4)$$

ΔH_{bind} encompasses the favorable forces of association and includes such forces as ionic interactions between protein and ligand (including metal-chelated contacts), hydrogen bonding, and van der Waal's forces.^[16]

Hydrogen bonds form between the lone pairs of electronegative heteroatoms such as nitrogen, sulfur, and oxygen (hydrogen bond acceptors) and a hydrogen covalently attached to an atom with a Pauling electronegativity greater than 3.0 (donor). These forces are directional, as the interacting partners are oriented at angles dependant on the bonds and lone pairs around the heteroatoms involved. The strongest hydrogen bond occurs when the angle A-H---B is 180°. Water molecules can mediate hydrogen bonds, as observed *via* protein crystallography. The distance between the hydrogen bonding donors and acceptors decreases with a concomitant lengthening of the σ -bound proton. There is an approximate correlation to the number of hydrogen bonds and higher affinity.^[16-18] The hydrogen bond results in a force that strongly orients the ligand in the binding site. ΔH_{conf} refers to unfavorable penalties resulting from steric or strain energies upon forming a complex with the ligand.

An equally important contribution to cohesive binding are the hydrophobic, or van der Waal's interactions. These forces exist between all atoms but are often emphasized for lipophilic surfaces and the strength of interaction is generally

proportional to increasing surface area between binding partners. Although oligo- and polysaccharides are water soluble, certain areas or faces of monosaccharide residues can be lipophilic, as demonstrated by the association of benzene with the α -face of methyl β -D-galactopyranoside.^[19] Apolar compounds are poorly soluble in water, a liquid characterized by an extensive network of hydrogen bonding, and complementary lipophilic surfaces will associate to exclude the polar liquid. Examples are known where ligands bind to protein solely through lipophilic interactions.^[18] Antibodies against oligosaccharides typically contain a number of aromatic residues in their binding site that are capable of forming high-affinity hydrophobic contacts with a ligand.^[20, 21]

Entropic contributions to binding has been described as follows:

$$\Delta S = \Delta S_{\text{solv}} + \Delta S_{\text{config}} + \Delta S_{\text{rot}} + \Delta S_{\text{trans}} \quad (5)$$

The unfavorable entropy associated with the loss of translational and rotational movement in solution upon a ligand binding to a protein is termed ΔS_{rot} and ΔS_{trans} . Configurational entropy includes energetic penalties that occur upon binding. An example being the freezing of bond rotamers that decreases molecular movement when the ligand and binding site arrange into a more static environment. Solvation effects arise from the desolvation (release of water) of the ligand as it prepares to bind. This interaction is typically favorable as water molecules are then in a more dynamic environment and more hydrogen bonds are formed when these water molecules are released back to bulk solution than existed when solvating the ligand.^[22, 23]

1.2.3. The Thermodynamic Consequence of Aqueous Media.

In an aqueous environment, all ligand-protein interactions compete with water that is present in approximately 55 M excess. When the protein and ligand are dissolved, their entire surfaces must interact directly with water. However, the epitope and its complementary protein surface (paratope) must be formally desolvated to facilitate association. Polar amino acids exposed at the protein exterior cause water to be more strongly attracted to these regions, forming transient hydrogen bonds.^[24] In the case of polar residues, hydrogen bonding limits the movement and freedom of bound water, at least transiently, producing a higher energy species less capable of forming ideal hydrogen bonds with bulk solvent. This water is of higher energy and would therefore make an enthalpic contribution as desolvation restores their ability to form optimal hydrogen bonds with other water molecules.

It has been shown from isothermal titration microcalorimetry that the substitution of water for deuterium oxide caused a reduction in the amount of heat liberated upon binding ligands to a variety of proteins. Assuming the conformation of the binding partners remained unchanged in heavy water, this reduction in enthalpy can be attributed to solvent reorganization. It was discovered that 25-100% of the observed enthalpies were due to these solvent effects.^[25]

Calculations have shown that water molecules at the interface of hydrophobic areas have weaker inter-solvent interactions, supporting Lemieux's hypothesis that water becomes more ordered in these regions. This increased translational and rotational restriction imposed on these water molecules would result in favorable entropic gains upon release.^[26, 27]

1.3. Monoclonal IgG Antibodies: Structure and Production.

1.3.1 The General Structure of the IgG Antibody.

Immunoglobulin proteins are an essential element of defense for the mammalian immune system. The monoclonal antibody, SYA/J6 used in this project, belongs to the murine IgG3 isotype. IgG is the most abundant antibody in serum and is the marker of a mature humoral response against a pathogenic challenge.

The general monomeric unit of an antibody is a symmetrical polypeptide assembly of two heavy chains complexed with two light chains. They associate via disulfide bonds and non-covalent interactions. There are five types of heavy chains that differentiate IgG classes: α , δ , ϵ , γ , and μ that correspond to IgA, IgD, IgE, IgG, and IgM, respectively. For the IgG antibody, subtle differences in the part of the γ heavy chain denote subclasses, or isotypes, that are numbered in the order of decreasing serum concentration. In addition, there are two versions of light chains, κ and λ .^[28] SYA/J6 is an IgG3 (κ) monoclonal antibody (Figure 1.1).

The light chain consists of a variable (V_L) and constant region (C_L) whereas the heavy chain has one variable (V_H) and three constant regions (C_{H1} , C_{H2} , and C_{H3}). Regions C_{H2} and C_{H3} of each heavy chain are termed the Fc region. These chains are glycosylated to varying extents by an *N*-linked glycan. The V_L and V_H sequences, combined with the C_L and C_{H1} motifs, make up the Fab fragment. The so-called hinge region of the immunoglobulin heavy chain is readily cleaved by papain. The V_H and V_L regions are not uniformly variable. Each segment has three short hypervariable

sequences that make up the antigen-binding site of the V_L and V_H chains at the N -terminus of each polypeptide, resulting in the bivalent immunoglobulin.^[29]

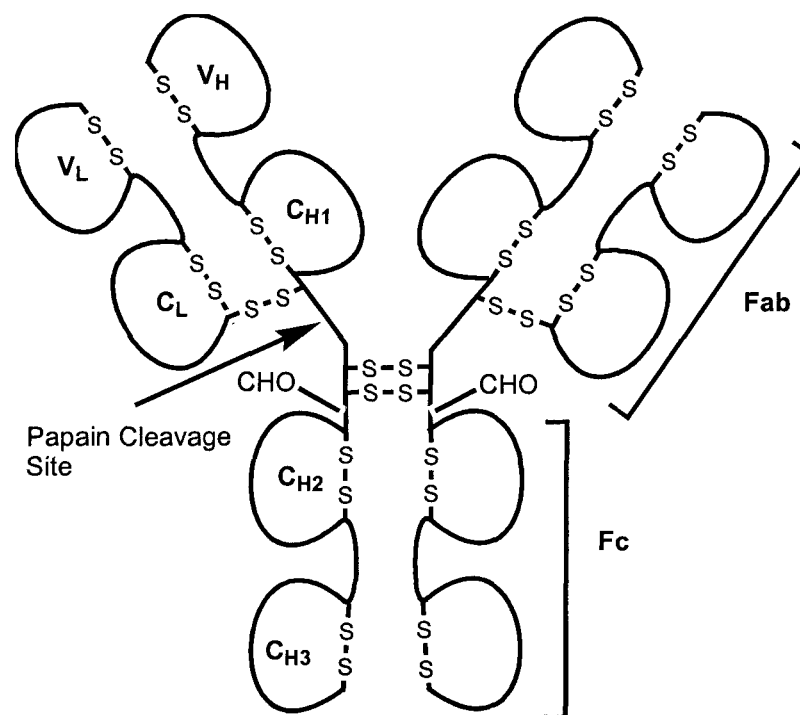


Figure 1.1: *The general structure of an IgG antibody. CHO indicates sites of glycosylation.*

1.3.2. Production and Purification of Monoclonal Antibodies.

Homogenous or monoclonal antibodies can be prepared in almost limitless quantities using the hybrid-myeloma technique.^[30] Advantages of this technology benefit biochemical research, as monoclonal antibodies are able to detect extremely small quantities of almost any specific antigen.

When a mouse is immunized with an antigen of interest, lymphocytes within the spleen produce specific antibodies. These cells can be fused with a mutant cell line of myeloma cells. These cancerous cells lack hypoxanthine-guanine phosphoribosyl transferase, an enzyme in the metabolic pathway responsible for inosine monophosphate

(IMP) synthesis. The fusion of spleen and myeloma cells takes place in HAT media, which contains hypoxanthine, amethopterin, and thymine. Ultimately, all un-fused spleen or myeloma cells cannot live in HAT media and the cell colonies that grow have the advantage of producing monoclonal antibodies coupled with the longevity of myeloma cells. These hybridoma cells are then cloned and assayed in microtitre plates against the antigen of interest. Antigen-positive clones can be grown in culture or injected into mice to generate solid tumors and ascites fluid that is rich in soluble antibody.^[28] The antibodies can then be purified from the mouse serum.

The purification of monoclonal antibodies is most effectively done *via* affinity chromatography specific for, in our case, IgG class antibodies. Proteins such as protein A or protein G immobilized on resins can be used to purify Ig molecules, which are specifically bound by these molecules. Elution is then achieved by decreasing the pH of the eluent. Ascitic fluid taken from mice inoculated with a hybridoma is taken and centrifuged and filtered to remove solid debris. The resultant fluid is passed through a column containing bacterial Protein A immobilized on sepharose. This bacterial membrane protein binds the Fc region of the IgG antibody, and elution of the bound antibody is accomplished by lowering the pH to 4.0, which is often within the stability range of the antibody.^[31, 32] Occasionally, elution conditions may have to be so drastic that the Ig is deactivated. Also, immobilized antigen can be used as an affinity chromatography sorbent.

1.3.3. Quantification of Carbohydrate-Protein Interactions.

As carbohydrates regulate and control a wide range of biological processes and recognition, a significant effort has been put in to increasing the affinity of these systems. The systems of interest are almost without exception, of low affinity and have dissociation constants that typically fall within a millimolar to micromolar range. Often, the quantities of carbohydrates from natural sources are limited, necessitating laborious chemical synthesis. Also, detection of ligands is hampered by a lack of ultraviolet absorbance that is common to many oligosaccharides. Despite these issues, a number of methods have been developed to quantify protein-oligosaccharide interactions. Two of the most widely used are the hemagglutinin inhibition assay (HIA) and the enzyme-linked immunosorbent assay (ELISA).

One of the earliest and most widely used measurements of protein-carbohydrate interactions is the HIA.^[33] Many lectins cross-link erythrocyte cells due to the high levels of oligosaccharide present on their surface. Incubation with a multivalent lectin and serial dilutions of soluble oligosaccharide inhibitor determines an IC_{50} value, or the minimum concentration of oligosaccharide at which 50% inhibition of agglutination has occurred. Because of the serial two-fold dilutions, the assay is not very precise and IC_{50} values do not give an accurate measure of a binding constant.

ELISA is a precise solid-phase assay with detection of a colorimetric response. Ligand or receptor can be immobilized on a microtitre plate and then treated with its complementary binding partner. The latter is often labeled, or able to be labeled, so that a colorimetric signal can be generated. Competitive assays are established by the addition of increasing concentrations of soluble ligand, thus reducing binding to the

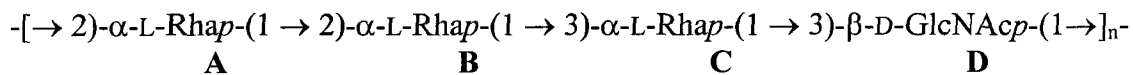
immobilized substrate. The addition of an enzyme-linked colorimetric substrate, such as horseradish peroxidase produces a response that can be measured by ultraviolet-visible (UV-Vis) spectroscopy. This increases sensitivity and precision of the measurement of an IC_{50} value. However, aggregation can still occur, especially with multivalent ligands, and IC_{50} values determined by solid-phase methods are still not an accurate measure of affinity constants.^[13]

Other techniques have been developed to measure protein-carbohydrate interactions, such as surface plasmon resonance (SPR),^[34] but isothermal titration microcalorimetry (ITC)^[35] provides an accurate measure of affinity and thermodynamic data in one experiment. The calorimeter is capable of measuring extremely small quantities of heat and directly provides the association constant, K_A , stoichiometry, and the molar enthalpy of binding as calculated by the software provided with the instrument. Entropic contributions are calculated using equations 2 and 3 (Page 3). This technique is extremely sensitive and precise but requires a significant amount of protein receptor. Under ideal circumstances, the receptor can be re-purified and recovered free of titrated ligand.

1.4. Description of the System Used in this Project

1.4.1. The *Shigella flexneri* IgG Monoclonal Antibody, SYA/J6.

A murine monoclonal antibody, SYA/J6 (IgG3, κ) was generated by the hybrid-myeloma method.^[30] It recognizes the hetero-polysaccharide repeat from the lipopolysaccharide (LPS) of *Shigella flexneri* variant Y (with the letters A to D representing the residues of the repeat):



S flexneri is a gram-negative non-motile opportunistic pathogen most commonly found in developing countries and causes violent, bloody enteritis and diarrhea. Vaccine research for protection against this pathogen has been directed at the LPS as an essential component, because a major humoral response is comprised of LPS specific antibodies.^[36] It has been estimated that the LPS covers about 45% of the surface of the bacterium.^[37] As such, studies from the Bundle group and its collaborators have focused on the molecular events of the binding process.^[38-42]

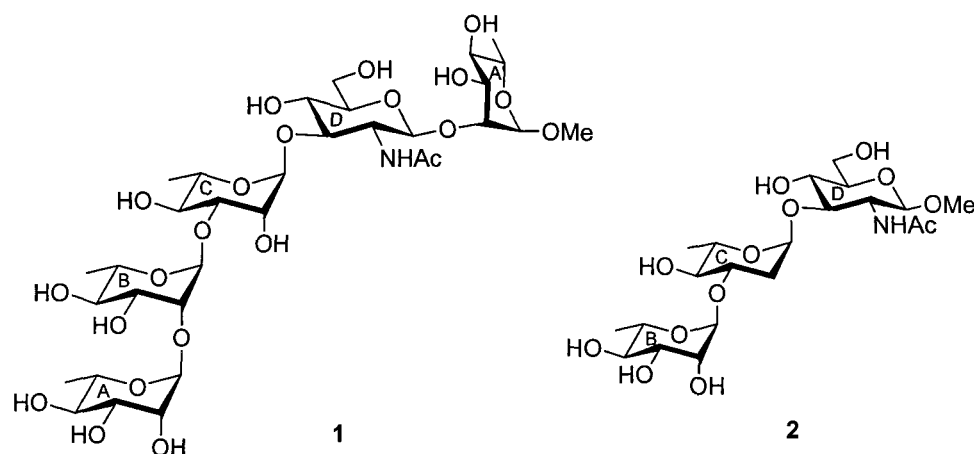
Initial recognition studies investigating the structure of this polysaccharide epitope. They used a series of synthetic frame-shifted conjugates, incorporating tetra- to heptasaccharides, in conjunction with enzyme inhibition assays.^[43-45] These studies demonstrated that the antibody recognized an internal segment of the *O*-polysaccharide. Although the affinity of the larger pentasaccharide was less than the smaller trisaccharide haptens, ITC showed that unfavorable entropic contributions to binding increased as the oligosaccharide was lengthened.^[46] This is consistent with steric interaction of the protein surface at, or just beyond the binding site, possibly disrupting water molecules. Using crystal structure data along with chemical mapping studies, the optimum epitope was identified as the BCD trisaccharide.^[47]

1.4.2. Crystal Structure of the SYA/J6 Antibody.

In the last two decades, a number of antibody crystal structures have been reported detailing bound oligosaccharides in the combining site. Two of these are murine antibodies towards human carbohydrate structures; an anti-Lewis x Fab fragment,^[48] and

a murine antibody, Ab BR96, against tumor cells,^[49] and a structure of a human Fab complexed to gp120 oligosaccharides from human immunodeficiency virus.^[50] A number of crystal structures of anti-bacterial antibodies have been solved including an anti-LPS antibodies against *Vibrio cholerae*,^[51] the family *Chlamydiaceae*,^[52] and *Salmonella* serogroup B.^[53]

SYA/J6 was amenable to proteolytic treatment for the generation of a fragment with antigen binding (Fab) and subjected to crystallization studies, although chemical mapping studies were at an advanced stage.^[40-42, 54] A co-crystallized structure was solved and shows the electron densities for a variant form of the internal BCD trisaccharide, and an ABCDA' pentasaccharide (1).^[54] These crystal data were later refined and solved to afford higher resolution: 2.5 Å for pentasaccharide 1 and 2.3 Å for the deoxygenated BCD trisaccharide 2 (Figure 1.2).^[46, 55] The antigen-combining site is a groove approximately 25 Å long by 10 Å deep and 12 Å wide. It runs parallel to the V_H and V_L domains and contains both hydrophobic and polar residues, with the latter predominantly having charged carboxylate residues. Initial comparison of the bound oligosaccharides shows the 2'-hydroxyl of the pentasaccharide points directly toward the bottom of the binding site.



Compound	K_A (M^{-1})	ΔG ($kcal/mol$)	ΔH ($kcal/mol$)	$-T\Delta S$ ($kcal/mol$)
1	2.5×10^5	-7.4	-1.5	-5.9
2	2.5×10^6	-8.5	-8.1	-0.5

Figure 1.2: ABCDA' pentasaccharide (1), 2'-deoxy BCD trisaccharide (2) and their calorimetric binding parameters.

The 2'-deoxygenated trisaccharide **2** has more intimate contact with the binding site as it sinks deeper into the groove, making more intimate contact with the protein. A slight rotation of the ψ angle of the Rha-GlcNAc linkage accommodates this change in binding mode. Inspection of the structures clearly indicates that in both cases, the Rha C residue is completely buried in the binding site, while the GlcNAc D ring oriented such that 75-80% of its surface area is inaccessible to bulk solvent. The Rha B residue was the most exposed of the three BCD residues, being approximately 70% exposed to bulk solvent.

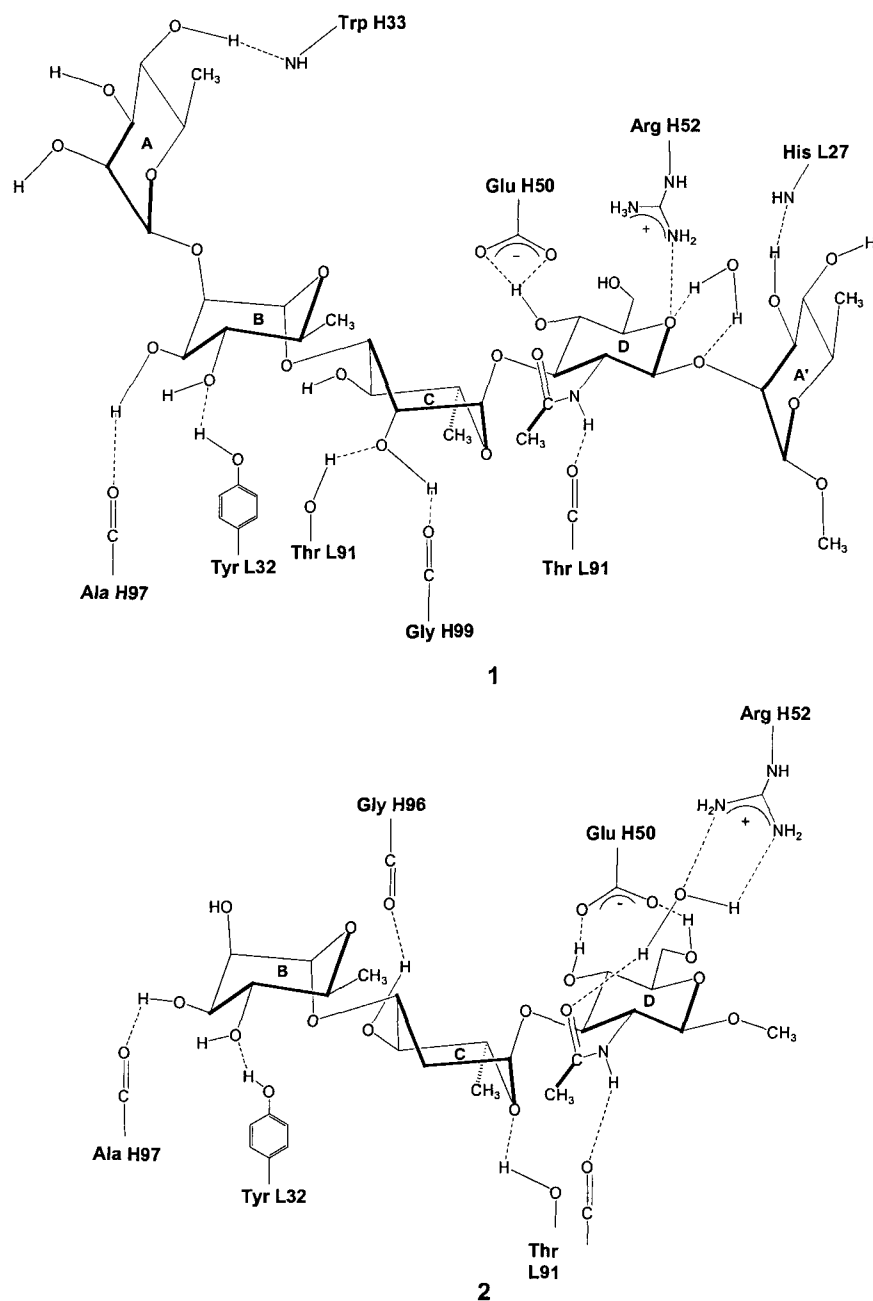


Figure 1.3: *Hydrogen bond map for 1 and 2.*

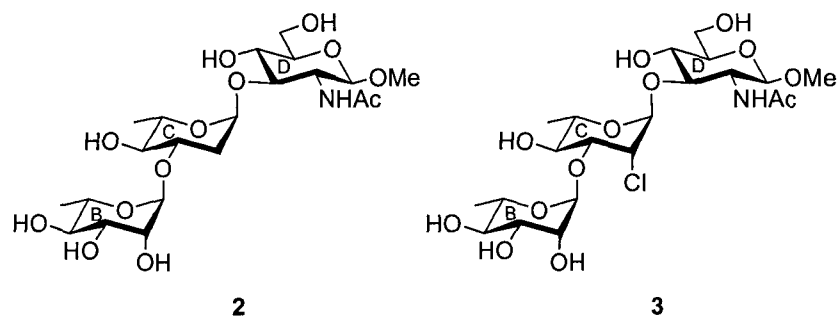
Of the 74 contacts pentasaccharide 1 makes with the binding site ($K_A = 2.5 \times 10^5$), eight are hydrogen bonds, none being water-mediated. Each residue contributes to these contacts, with the flanking A and A' residues contributing one hydrogen bond each. The

remainder of the contacts are hydrophobic ($<4 \text{ \AA}$). The 2'-deoxy trisaccharide **2** has also has a similar number of contacts, totaling 75, and makes eight hydrogen bonds plus an additional water mediated contact not seen for the pentasaccharide/SYA/J6 complex. This deoxygenated BCD derivative fits more intimately in the binding site, and makes more hydrophobic contacts per residue than the pentasaccharide. Figure 1.3 depicts the hydrogen bonding maps for both the BCD portion of pentasaccharide **1** and trisaccharide **2**.^[46, 56]

1.4.3. Increased Affinity *via* Functional Group Modification.

Chemical mapping studies identified a number of congeners of the BCD trisaccharide that bound to SYA/J6 with higher affinity than the native trisaccharide. The aforementioned 2'-deoxy derivative **2** exhibited an approximate 25-fold increase in affinity. The majority of the free energy changes were enthalpic in nature, indicating intimate contact with the protein surface, and re-enforcing the observations from the crystal structure data.

An additional trisaccharide derivative was synthesized, also modified at the 2'-position of the Rha C ring. The replacement of this hydroxyl by a chlorine atom while retaining the *rhamno*- configuration gave a tighter binding congener (**3**, Figure 1.4), exhibiting an approximate 10-fold increase in affinity over the BCD trisaccharide.^[40, 42] It is postulated that **3** binds in a similar mode to the methyl glycoside of the native BCD trisaccharide, as their size and electronegativity are similar.^[57] If these assumptions are correct, a π -halogen stabilization may account for the primarily enthalpic increase in free energy.^[58-60]



Compound	K_A (M^{-1})	ΔG ($kcal/mol$)	ΔH ($kcal/mol$)	$-T\Delta S$ ($kcal/mol$)
1	2.5×10^5	-7.4	-1.5	-5.9
2	2.5×10^6	-8.5	-8.1	-0.5
3	1.1×10^6	-8.1	-6.3	-1.8

Figure 1.4: BCD trisaccharide derivatives **2** and **3** modified at the 2'-positions. Binding parameters were measured with isothermal titration microcalorimetry.

1.5. Intramolecular Pre-Organization of Carbohydrate Structures.

With only a few exceptions, oligosaccharide-protein interactions are of low affinity. As such, increased univalent affinity of carbohydrates for their receptors could be of great interest in therapeutic research and investigations into biological recognition and regulation. The thermodynamics of oligosaccharide binding are typically comprised of a large enthalpic contribution counteracted by an entropic penalty. Enthalpic contributions are usually attributed to hydrogen bonding and van der Waal's interactions. The circumstances surrounding unfavorable entropic penalties upon oligosaccharide immobilization are of some debate, and solvation effects and the immobilization of a flexible oligosaccharide are often attributed to this phenomenon. The penalty for freezing of glycosidic rotamers has been calculated to be as high as 0.6-2.0 kcal/mol,^[23]

^{61]} although more conservative estimates have been made (0.1-0.3 kcal mol⁻¹).^[62] Bartlett and co-workers have reported intramolecularly pre-organized phosphate analogues of an inhibitor of penicillopepsin. This work demonstrated the free energy gains realized by tethering were amongst the highest values reported for a conformational constraint and were essentially entropic in origin. Cyclic analogues showed that the effect of tethering provided an increase ranging from 0.3 to 1.4 kcal/mol per rotamer of the tether.^[63, 64]

There are two factors that could contribute to the magnitude of an entropic penalty. The *exo*-anomeric effect of glycosidic bonds restricts rotamer populations in solution, dictating a conformational bias to these flexible molecules prior to binding. Also, the release of water from polyamphiphilic protein surfaces in aqueous solutions can cause a beneficial increase in entropy. These competing factors has been termed hydrphobic effects by Lemieux.^[27, 65] Microcalorimetric measurements by Toone also support this hypothesis.^[22, 25]

Intramolecular tethers have been employed to probe the phenomenon of oligosaccharide flexibility. Residues in contact with protein are fixed *via* a short linker spanning between monosaccharide residues. The primary aspects of this methodology are tether placement and composition. The most abundant conformation of a tethered molecule is required to emulate the bound conformation of the ligand of interest. Knowledge of the epitope, or key polar groups, is used to identify functional groups oriented toward bulk solvent. This information can come from co-complexed x-ray data that give an immediate and clear picture of an oligosaccharide bound to protein. Chemical mapping, *via* methylation and deoxygenation of hydroxyl groups gives an indication of which groups are critical for recognition. Additionally, hydroxyl groups at

the periphery of the binding site can be identified when a small change of binding activity is measured. This knowledge aids in the design of the length of the tether. It must be of sufficient length not to alter the solution/bound conformation of the ligand.

1.5.1. Literature Precedent for Intramolecular Pre-Organization.

A number of groups have synthesized and evaluated conformationally pre-organized oligosaccharides. The receptors used in these examples are nucleic acids or protein from bacterial, plant, or human systems. While the activity of the ligands in the following cases were not all tested with microcalorimetry, changes in affinity ranged from detrimental to a moderate increase.

Kolb and co-workers devised a ligand based on sialyl Lewis x (sLe^x) to bind with an increased affinity to E-selectin, a protein involved in inflammation and cell rolling processes. Key polar groups were known from chemical mapping studies. Sialic acid was replaced with *S*-lactic acid, and the glucose residue was replaced with *R,R*-cyclohexane diol.^[66] A homologated fucose residue served to anchor the tether to a *talo*-configured monosaccharide, substituting for the galactose residue (**4**, Figure 1.5).^[67] The binding of this derivative was 3-fold lower than sLe^x, presumably due to the tether inducing a conformational shift in the carboxylate group, a critical recognition element.^[68, 69]

Magnusson and co-workers synthesized a macrocyclic galabiose disaccharide. This compound, as the trimethylsilylethyl glycoside, was tethered from the 2'- to the 6-position, as these groups were known not to be involved in the binding process (**5**, Figure 1.5).^[70] The span of the tether was only one methylene unit, and biological assays showed a significant but reduced activity, presumably due to a slightly altered conformation.^[71]

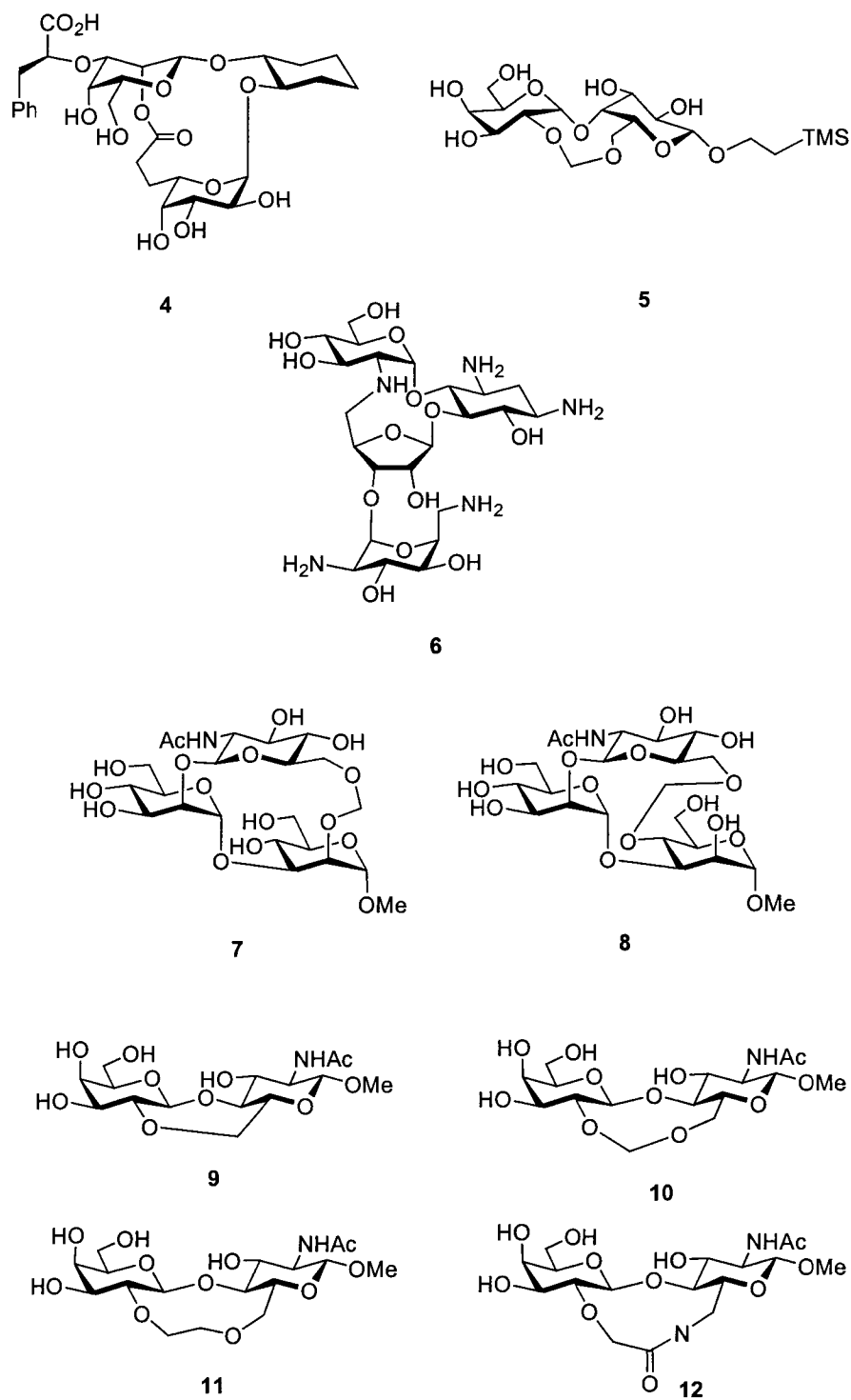


Figure 1.5: Examples of conformationally pre-arranged oligosaccharides.

Pre-organized aminoglycosides were synthesized and tested by Tor and co-workers.^[72] It was thought that by pre-organizing these highly polar derivatives that their binding specificity could be increased for ribonucleic acids (RNA). Though unclear, it was determined that one of the target RNA sequences was more discriminating, and bound the constrained amino glycoside (**6**, Figure 1.5).

Boons and co-workers have investigated a conformationally constrained fragment of a biantennary glycan recognized by Concanavalin A. Using methylene tethers to simulate postulated intramolecular hydrogen bonds, two derivatives were synthesized (**7** and **8**, Figure 1.5).^[73] Microcalorimetry measurements indicated that while the free energies of the tethered and native trisaccharides were similar, an increase in the entropic binding component was offset by a compensating reduction in enthalpy. In separate work, a β -D-Gal-(1 \rightarrow 4)- β -D-GlcNAc (LacNAc) scaffold was used to probe acceptor flexibility toward an α -2,6-sialyltransferase and human α -1,3-fucosyltransferase V (**9-12**, Figure 1.5).^[74, 75] It was known through chemical mapping that the 2'- and 6-positions are not crucial for binding and incur only a small binding penalty when modified.^[76] While **11** and **12** were superior substrates for the sialyltransferase, compounds **9-12** could not match the transfer rates as with the native trisaccharide and fucosyltransferase V.

The research of Bundle and co-workers has focused on a number of systems in which ligands were pre-organized to probe molecular interactions. The first instance dealt with the pre-organization of the H-type II trisaccharide (α -L-Fuc-(1 \rightarrow 2)- α -D-Gal-(1 \rightarrow 4)- β -D-GlcNAc-OMe) and its binding to *Ulex europaeus* I (UE-I)^[77] and *Phosphocarpus tetragonolobus* (winged bean agglutinin).^[78] Extensive chemical mapping of the H-type II trisaccharide with each protein identified two patterns of recognition.^{[79-}

^{82]} Using crystal structure data, the H-type II trisaccharide was docked in the binding site of UE-I. This reinforced chemical mapping data, as it was apparent that the 6'- and 3-positions of the trisaccharide were in solvent exposed regions. The most successful derivative was tethered at these positions using a propyl ether (**13**, Figure 1.6).

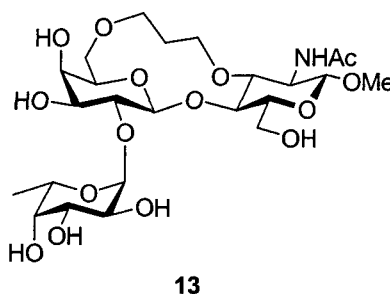


Figure 1.6: *Conformationally restricted H-Type II trisaccharide derivative 13.*

The binding affinity, measured with an enzyme-linked immunosorbent assay (ELISA) of this congener was approximately 3-fold weaker for *Ulex europaeus* I indicating pre-organization had, for the most part, preserved the bioactive conformation of the ligand. The binding affinity of **13** was 250-fold weaker for the *Phosphocarpus tetragonolobus* II lectin.^[83] Clearly, **13** binds differently to each lectin and the tether had a significant detrimental impact for interactions with WBA II.

A monoclonal IgG antibody, Se155.4, that binds the *O*-polysaccharide of *Salmonella essen* was isolated and studied by Bundle *et al.* Fab and single chain variable fragments (ScFv) were crystallized with and without bound ligand.^[53, 84] The molecular interactions detailed the electron density for a trisaccharide portion (α -D-Gal-(1 \rightarrow 2)-[α -D-Abe-(1 \rightarrow 3)]- α -D-Man-OMe) of the repeating unit of the polysaccharide (Abe = abequose = 3,6-dideoxy-D-xylo-hexopyranoside). Crystal structure data indicated the possibility of intramolecular hydrogen bonds between the 2-OH of Abe and the Gal O-2

and Man O-4 positions. Synthetic derivatives connecting these positions using methylene acetals were prepared (**14** and **15**, Figure 1.7).^[85] Also, x-ray data showed the 6- and 6'-positions of the Man and Gal residues were oriented towards bulk solvent. A series of four trisaccharides were synthesized utilizing tethers of various length and composition to effect pre-organization (**16-19**, Figure 1.7).^[85, 86]

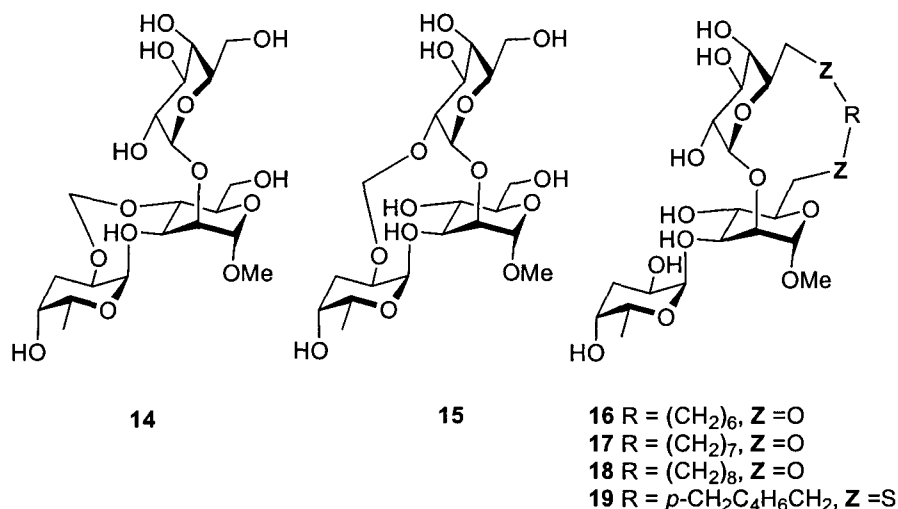


Figure 1.7: Pre-organized derivatives of the mAb Se155.4 epitope.

Methylidene-tethered **14** and **15** had no activity towards Se155.4 due to the geometry the short tethers imposed on their conformation, and this was verified by molecular dynamics calculations. Isothermal titration microcalorimetry was performed on the remainder of the trisaccharides and only **19** exhibited a free energy of binding greater than the native trisaccharide. Compounds **16** through **18** bound with a slightly reduced free energy compared to the non-tethered structure.

1.5.2. Pre-Organization of the *S. flexneri* LPS BCD Trisaccharide.

Details of the co-complexed crystal structure of monoclonal antibody SYA/J6 and **1** were exploited to design a pre-organized BCD trisaccharide derivative. Because it is primarily the BCD trisaccharide that fills the binding groove and contributes the bulk of the free energy of binding, this segment of **1** was the focus of a conformationally restricted congener. The methyl groups at C-6" and the acetamido of the GlcNAc D residue are in a bound arrangement where they face not only each other, but also point away from the combining site into bulk solvent (Figure 1.8). They do not make apparent van der Waal's contacts with the protein surface and the distance between them is approximately 4.5 Å. Previous mapping studies of the CD disaccharide portions found that substitution of the acetamido (NHAc) for a trifluoroacetamido or 2,2,2-trimethylacetamido produced derivatives with significantly reduced activity. This implies proximity of the protein surface since significant changes in steric bulk or electronegativity have a profound effect on binding. However, introduction of a propionamido group gave a disaccharide congener with a slightly enhanced activity.^[41] Thereby enforcing the notion that there is steric access to the methyl group of the acetamido moiety and hence attachment of an intramolecular tether at this point.

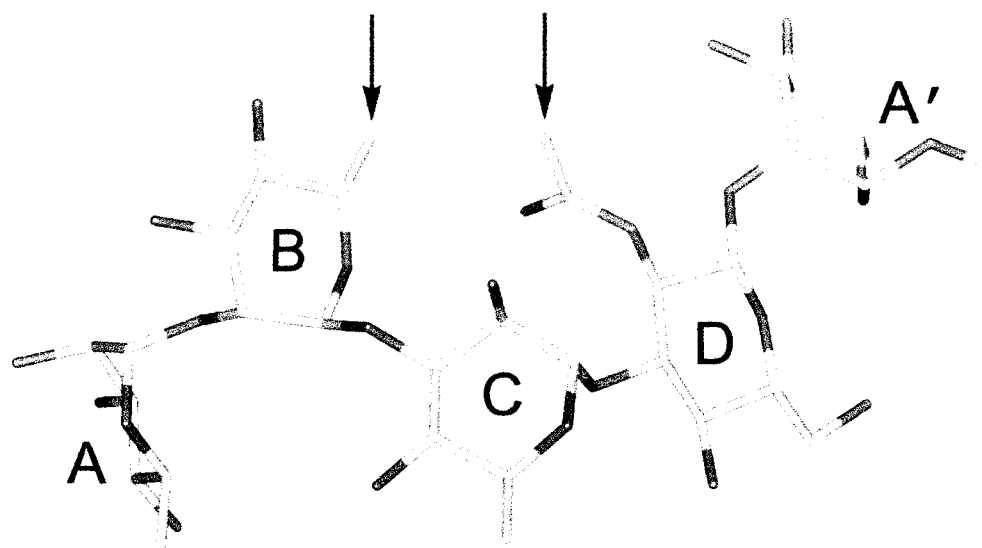
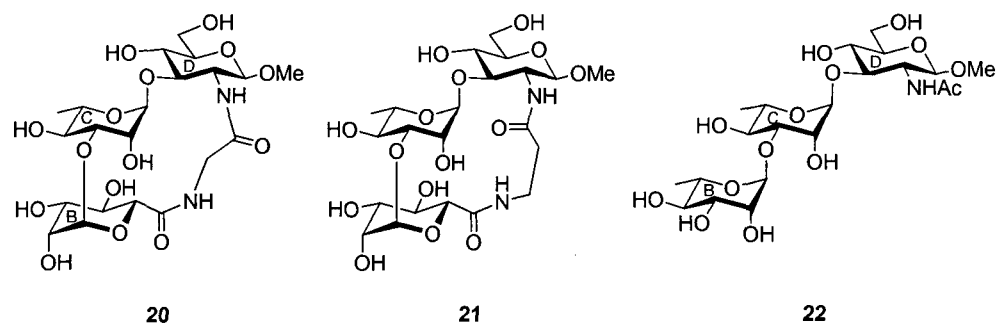


Figure 1.8: *The bound ABCDA' pentasaccharide 1. Arrows point to the methyl groups to which the tether was attached. These groups are 4.5 Å apart, and are close to the outside of the binding site. The rest of 1 contacts protein.*

A reported synthesis details pre-organized derivatives containing a β -glycinyll (**20**) and β -alanyl tether (**21**) spanning these two methyl groups.^[87] This preparation used the methyl glycoside of the BCD trisaccharide (**22**) as a scaffold for these macrocyclic congeners, except L-mannose was used in place of L-rhamnose for the Rha B ring to facilitate chemical ligation of the tether. Molecular dynamics calculations indicated that the drastically reduced binding activity of glycinyll-tethered **20** was due unfavorable conformational restraint imposed by the short tether. Conversely, calorimetry measurements of **21** demonstrated a 15-fold increase in affinity for SYA/J6 and also demonstrated a significant increase in the entropic contribution of binding (Figure 1.9).^[87]



Compound	K_A (M^{-1})	ΔG ($kcal/mol$)	ΔH ($kcal/mol$)	$-T\Delta S$ ($kcal/mol$)
1	2.5×10^5	-7.4	-1.5	-5.9
2	2.5×10^6	-8.5	-8.1	-0.5
3	1.1×10^6	-8.1	-6.3	-1.8
20	N/A			
21	$1.5 \pm 0.05 \times 10^6$	-8.3 ± 0.1	-4.2 ± 0.05	-4.1 ± 0.05
22	1.1×10^5	-6.8 ± 0.2	-3.9 ± 0.1	-2.9 ± 0.1

Figure 1.9: Glycinyl- (**20**) and β -alanyl-tethered (**21**) with native trisaccharide **22**. The Man B residue (formerly Rha) is depicted with a conformational rotation about the B and C residues. Values with standard deviations are the result of two measurements.

1.6. Scope of Project. The objective of this project is to design high-affinity trisaccharide derivatives toward monoclonal antibody SYA/J6. To this end, our efforts were focused on the synthesis of two main types of trisaccharides. The first was to validate the β -alanyl tether methodology by synthesizing non-macrocyclic control compounds based on this successful macrocycle. Two isomeric derivatives with “cut” tethers in isomeric positions (**23** and **24**) will retain similar atom arrangements as **21**, especially with respect to the non-natural amide at the C-6'' position of the Man B residue. Analysis of the binding of these compounds should determine whether the tether is solely responsible for the 15-fold affinity gain of **21** over the native trisaccharide **22** (Figure 1.10).

modifications with intramolecular pre-organization demonstrated for **21**^[56] to achieve this goal. As seen earlier, 2'-deoxygenation and 2'-chloro-2'-deoxygenation gave trisaccharide congeners (compounds **2** and **3**, respectively), each with an order of magnitude increase in free energy of binding with SYA/J6. By combining these functional group modifications with the β -alanine tethering methodology (**25** and **26**, Figure 1.12), we aim to deduce whether free energy gains of these modifications are additive. If so, they would prove a concept that could lead to the successful design of univalent ligands with very high affinity, as such carbohydrate-based molecules are rare.

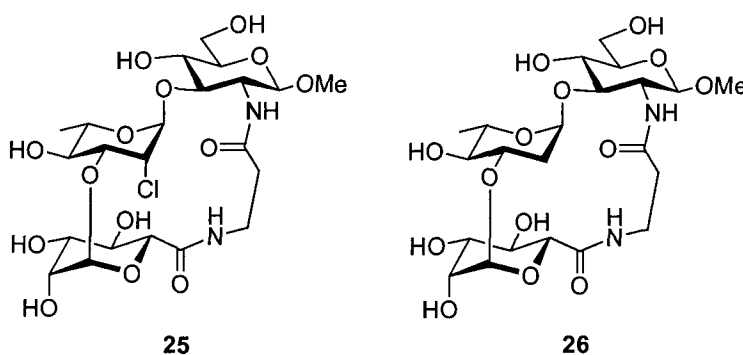


Figure 1.12: *Macrocyclic BCD trisaccharide targets 25 and 26.*

The following chapters describe the synthesis of **23** through **26** and evaluation of their binding via ELISA and ITC. To explain the results of binding assays, molecular dynamics calculations and simple ligand docking are performed. Saturation transfer nuclear magnetic resonance (STD-NMR) spectroscopy is described for all trisaccharides related to this work, and is used to explain binding results by qualitatively measuring the degree of contact of a ligand with SYA/J6.

Chapter 2

The Syntheses of Target BCD Trisaccharides.

2.1. Stereic and Electronic Factors in Glycosylation Chemistry.

2.1.1. The Anomeric Effect.

The most prominent feature of carbohydrate synthesis is the contribution of the pyranosyl oxygen in glycosylation chemistry. Termed the *endo*-anomeric effect, a lone pair from this atom can overlap with an antibonding orbital of the axially linked C₁-X bond (typically called an α linkage) and is more pronounced for increasingly electronegative X substituents. An ionic resonance structure can be drawn for this type of interaction (Figure 2.1). As a consequence, this orbital stabilization favors an axially linked product that is kinetically preferred upon activation of a leaving group at the anomeric center. The anomeric effect contributes to the free energies of many pyranoid compounds and thus contributes to a preferred conformation. The effect of this stabilization is dampened in solvents with a high dielectric constant, and decreasing electronegativity of X.^[88] It has been demonstrated via x-ray crystallography that the O-5/C-1 bond length of anomeric acetals in both α - and β -linked sugars shortens by approximately 0.03 Å. Additionally, the *exo*-anomeric effect is a stabilization involving a lone pair from the glycosidic oxygen (O-1). This stabilization thus imparts a conformational preference about the ϕ angle of the glycosidic bond. This phenomenon results in a slightly shorter C-1/O-1 bond length (0.04-0.05 Å) that is more pronounced

for the β -anomer. This arises due to the fact that for equatorially oriented aglycons the *exo*-anomeric effect does not compete with the *endo*-anomeric effect, whereas, for axially oriented aglycons the *endo*- and *exo*-cyclic oxygen atoms are involved in electron delocalization with the anomeric carbon atom. ^[89]

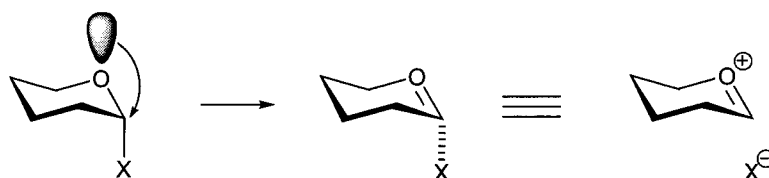
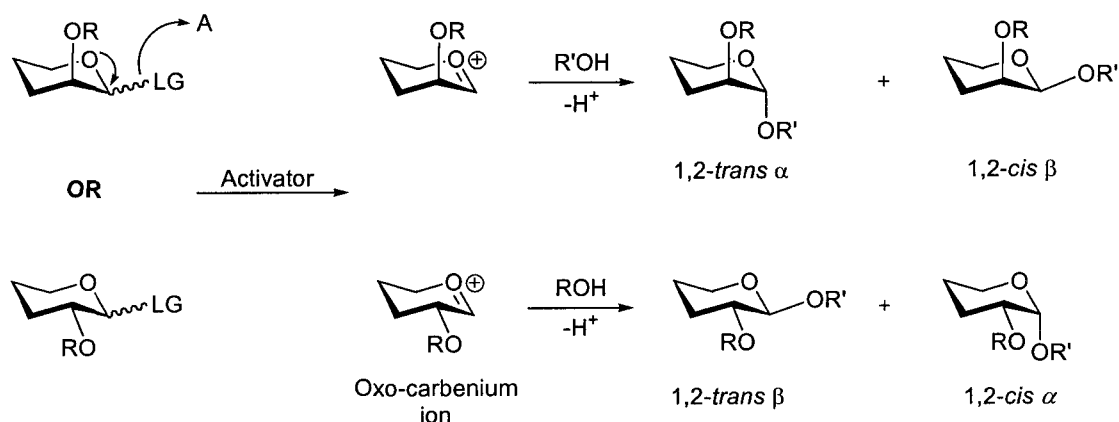


Figure 2.1: *Orbital overlap that leads to the anomeric effect.*

2.1.2. Substituents at C-2 and Neighboring Group Participation.

During glycosylation, an anomeric leaving group is activated and expelled via the ring oxygen to form an oxocarbenium ion. Attack from an incoming nucleophile, such as ROH in the case of glycosylation, can then occur at both faces of this ion. Besides the anomeric effect, the steric and electronic properties at C-2 have a great influence on the ratio of resultant anomers. Taking into account the stereochemistry of the C-2 group, there are four possible 1,2- configurations following reaction at the anomeric center (Scheme 2.1). The two easier isomers to synthesize are the *trans* configured molecules. Sterics is thought to play a large role in this outcome, with the α -linked isomer aided by the anomeric effect. The remaining two isomers have an increased steric repulsion between the 1,2-disubstituted groups due to their *cis* relationship. Again, the 1,2-*cis* α linkage is stabilized by the ring oxygen, with the 1,2-*cis* β linkage having little, if any, stabilizing forces to aid in its construction.

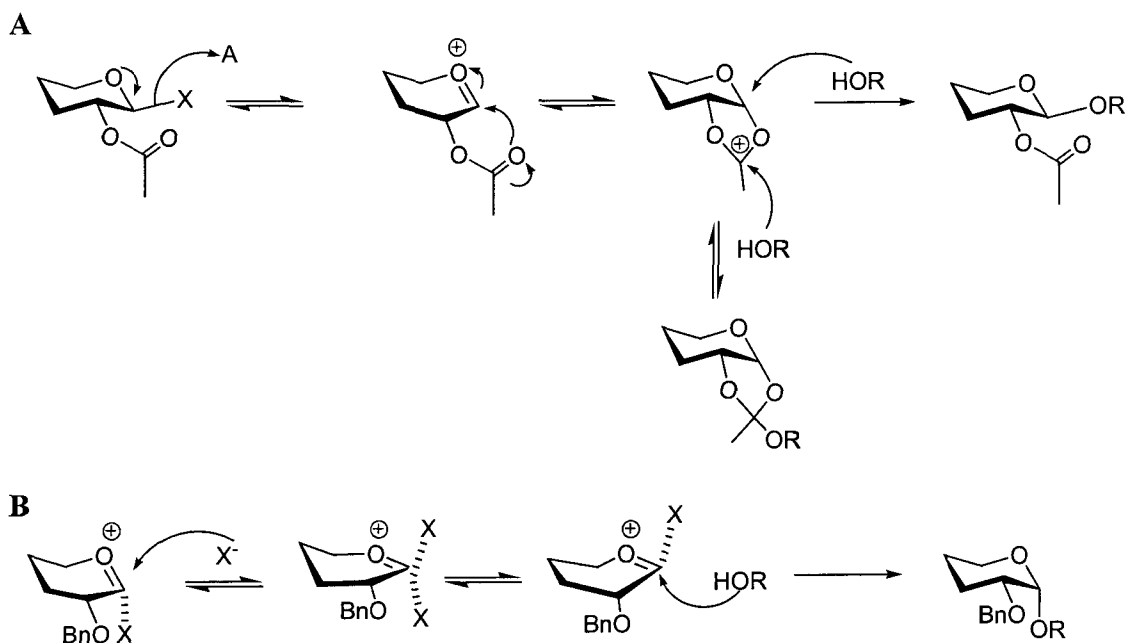


Scheme 2.1: A general glycosylation pathway showing the four possible configurational outcomes for standard pyranoses.

Trans glycosidic linkages are typically synthesized by employing an acyl group at the C-2 position to effect neighboring group participation. Once the anomeric group has been activated, usually under slightly acidic conditions, the carbonyl oxygen can attack the α -face of the oxocarbenium ion to produce an acetoxonium ion (Scheme 2.2). The incoming alcohol nucleophile can be trapped at this stage affording the corresponding orthoester. Under acidic conditions, the alcohol can rearrange to the β -glycoside as the acetoxonium ion shields the α -face. In a series of papers in 1975, Lemieux and co-workers described the first reliable synthesis of α -linked glycosides having an equatorial non-participating substituent, termed the halide-ion method.^[90-93] A variant of the Keonigs-Knorr glycosylation,^[94, 95] anomeric α -bromides were treated with tetraethylammonium bromide to initiate an equilibrium that produced the more reactive β -bromide, or an ion pair derived from it. Incoming alcohol nucleophiles would displace this bromide to afford the α -glycosides (Scheme 2.2). More recently, Boons and co-workers have developed a chiral sulfide containing O-2 protecting group that exploits

conformational aspects of *trans* decalins to block the β -face of an oxocarbenium ion to afford the α -glycoside.^[96]

Recently, a protocol for the efficient generation of β -manno- and β -rhamnosides, via glycosyl triflates, was reported.^[97] This linkage is the most difficult to synthesize, as the α -linked isomer is heavily favored by steric and electronic effects.



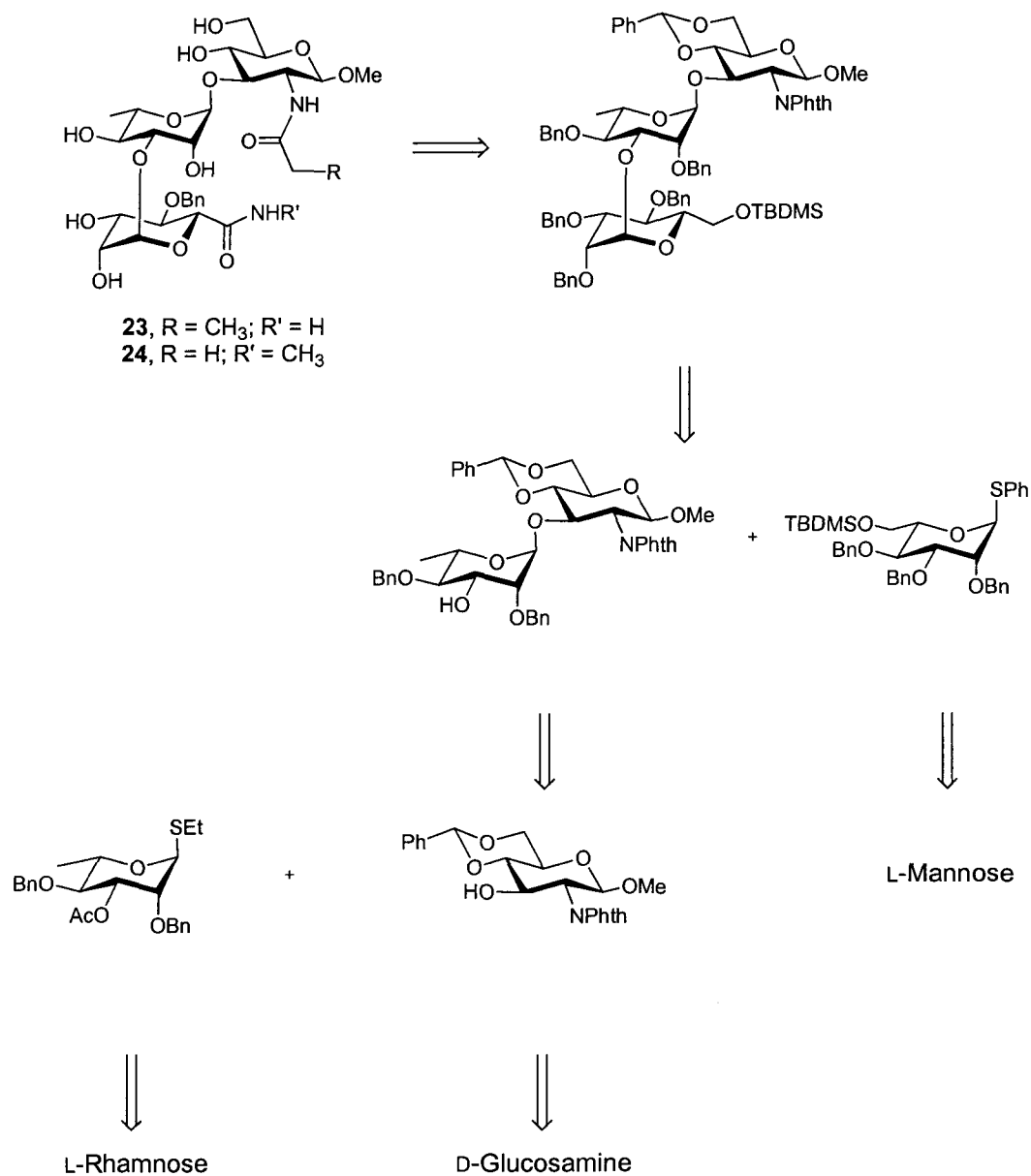
Scheme 2.2: *Neighboring group participation (A) and the halide-ion method of glycosylation (B) that blocks the β -face of an oxocarbenium ion to afford the α -glycoside.*

2.2 Acyclic BCD Trisaccharide Variants.

2.2.1. General considerations and Retrosynthetic Analysis.

The synthesis of the acyclic BCD trisaccharide derivatives (**23** and **24**) was similar to cyclic **21** and followed an analogous route, employing a linear assembly of monosaccharide donors to afford protected core structure **41**.^[87] Persistent protecting groups such as benzyl ethers and a benzylidene acetal gave the required orthogonality to

perform manipulations on the trisaccharide core in basic media. L-Mannose was used in place of L-rhamnose to facilitate chemical manipulation at the 6''-position at the trisaccharide stage.

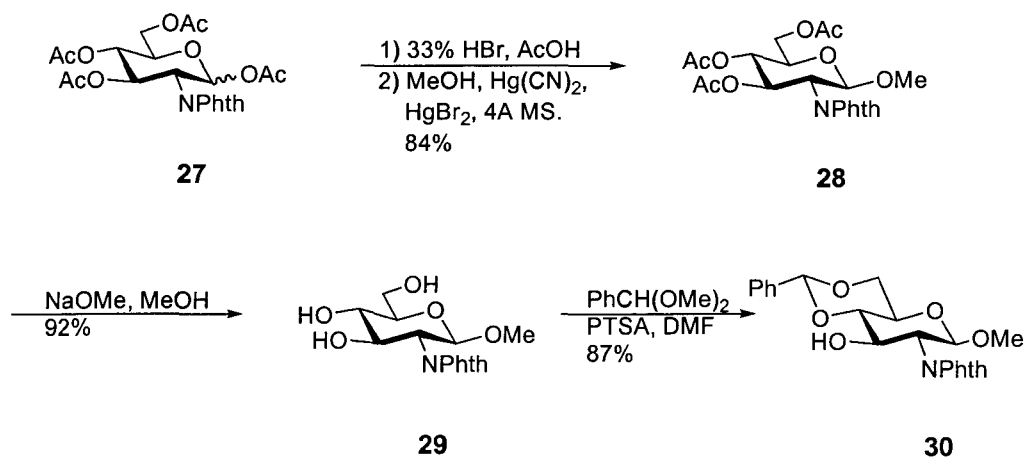


Scheme 2.3: Retrosynthetic analysis of acyclic BCD trisaccharides.

Retrosynthetic analyses of protected **23** and **24** (Scheme 2.3) show that the deprotected bis-amides are available from the fully protected trisaccharide, orthogonally blocked at the glucosamine nitrogen and the 6''-position of the L-mannose ring.^[56, 87] This trisaccharide is available from the glycosylation of glucosamine acceptor by a suitably protected rhamnosyl thioglycoside donor, followed by a selective deprotection of a 3'-acetate protecting group and subsequent glycosylation by an L-mannosyl thioglycoside donor. The monosaccharide components are all available commercially as unprotected reducing sugars.

2.2.2. Synthesis of Monosaccharide Components.

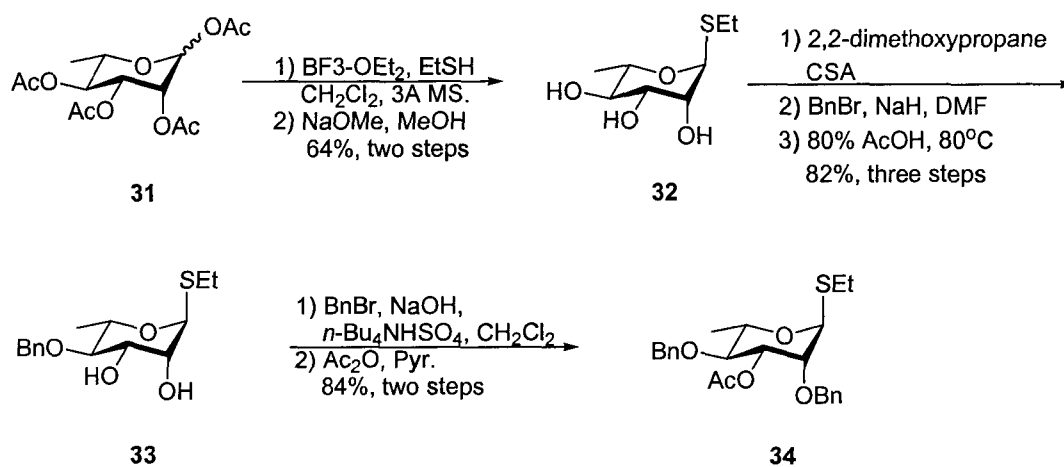
Synthesis of the glucosamine acceptor **30** was carried out as described previously, starting with a sequence that installs the phthalimido and acetyl groups in a step-wise, one-pot manner to give **27** (Scheme 3.2). Bromination of the anomeric carbon with hydrogen bromide in acetic acid and ensuing glycosylation of methanol under classic Helferich conditions furnished the methyl glycoside **28**.^[95, 98, 99]



Scheme 2.4: Synthesis of *N*-Phthalimido protected glucosamine acceptor **30**.

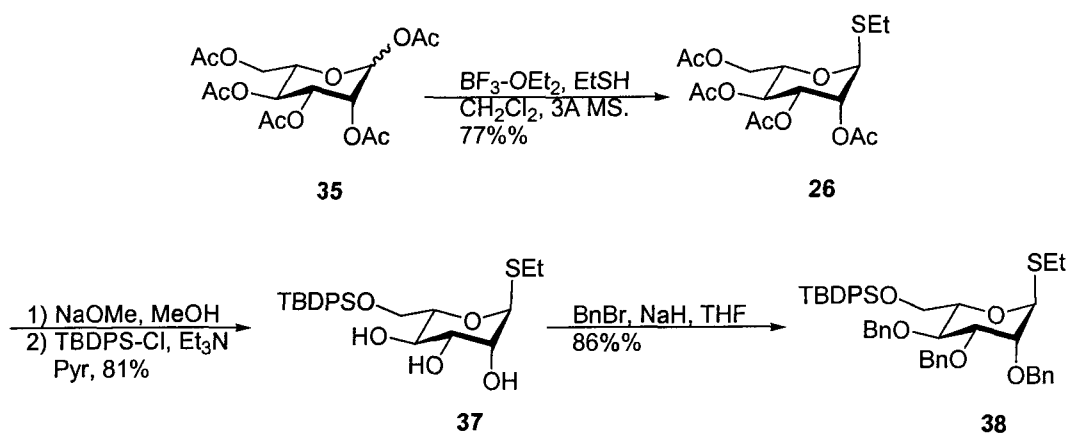
Zemplén transesterification gave the triol **29**, and subsequent benzylidenation with benzaldehyde dimethylacetal and *p*-toluenesulfonic acid gave **30** in yields comparable to literature precedent (Scheme 2.4).^[100]

Synthesis of the rhamnosyl thioglycoside was performed as described in the literature.^[101] Lewis acid promoted thioglycosidation of peracetylated L-rhamnose (**31**) followed by transesterification gave the thioglycoside triol **32**.^[102] The 4-*O*-benzyl rhamnosyl thioglycoside was prepared in a three-step sequence initiated by isopropylideneation with 2,2-dimethoxypropane and camphorsulfonic acid. Subsequent anionic benzylation of the 4-OH using benzyl bromide and sodium hydride followed by acid hydrolysis of the acetal gave **33** in high yield. Selective phase-transfer catalyzed benzylation^[103] using benzyl bromide, aqueous sodium hydroxide, and tetra-*n*-butyl ammonium hydrogen sulfate in dichloromethane afforded the 2,4-di-*O*-benzyl derivative **34** that was subsequently acetylated with acetic anhydride and pyridine (Scheme 2.5)



Scheme 2.5: Synthesis of rhamnosyl thioglycoside donor **34**.

The L-mannosyl donor was synthesized according to a previous protocol^[87] that involved boron trifluoride diethyl etherate promoted glycosylation of ethanethiol with peracetylated L-mannose to afford **35**.^[104] Subsequent transesterification and selective silylation of the 6-position with *t*-butylchlorodiphenylsilane and imidazole furnished triol **37** in 81% yield. Exhaustive benzylation with benzyl bromide and sodium hydride produced donor **38** (Scheme 2.6).^[56, 87] The identity and confirmation of the structure of all three monosaccharide components (**30**, **34**, and **38**) were confirmed by ¹H and ¹³C NMR coupled with mass spectroscopic analysis.

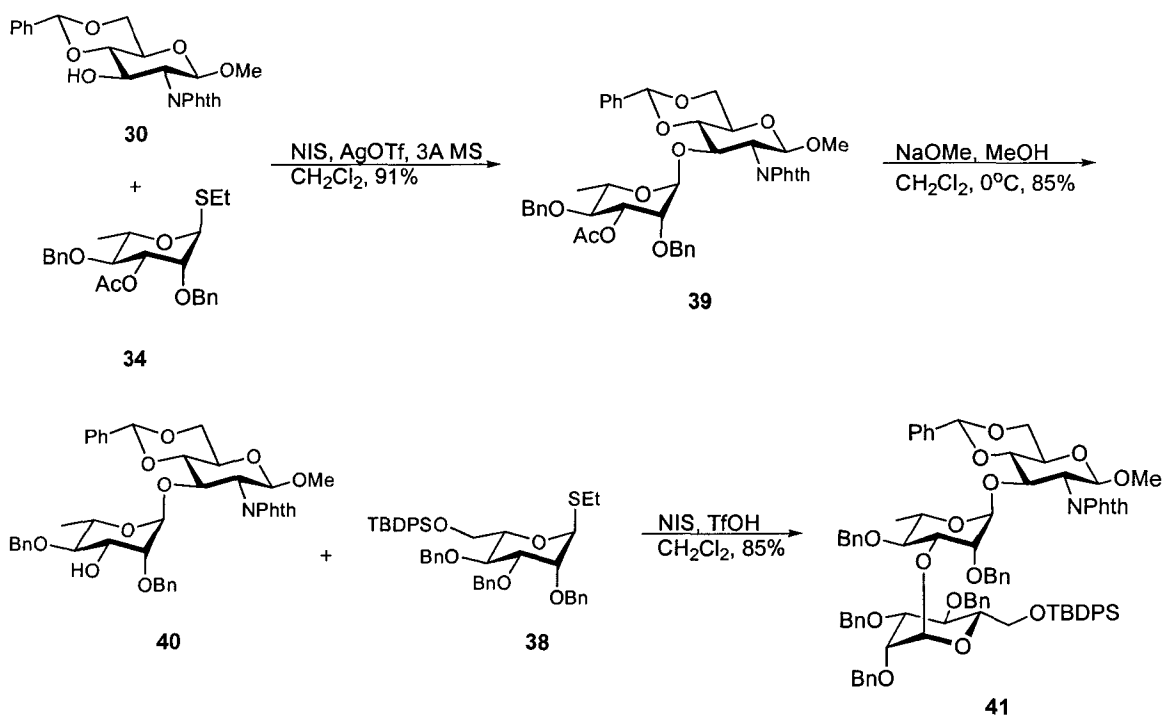


Scheme 2.6: *Synthesis of the L-mannosyl thioglycoside donor 38.*

2.2.3. Assembly of the Acyclic Trisaccharides

The synthesis of the core trisaccharide followed a linear route as depicted in the retrosynthetic analysis (Figure 2.3). Acceptor alcohol **30** was coupled with donor **34** using *N*-iodosuccinimide (NIS) and silver trifluoromethanesulfonate (AgOTf) to afford protected disaccharide **39** in 91% yield (Scheme 2.7). Subsequent deacetylation with sodium methoxide was performed at low temperatures to avoid nucleophilic opening of the phthalimido ring. Dichloromethane was used as a co-solvent to increase solubility of

the starting material. Glycosylation of this disaccharide alcohol with L-mannosyl thioglycoside **38** using NIS and catalytic trifluoromethanesulfonic acid (TfOH) gave the fully protected trisaccharide **41** in 85% yield (Scheme 2.7).

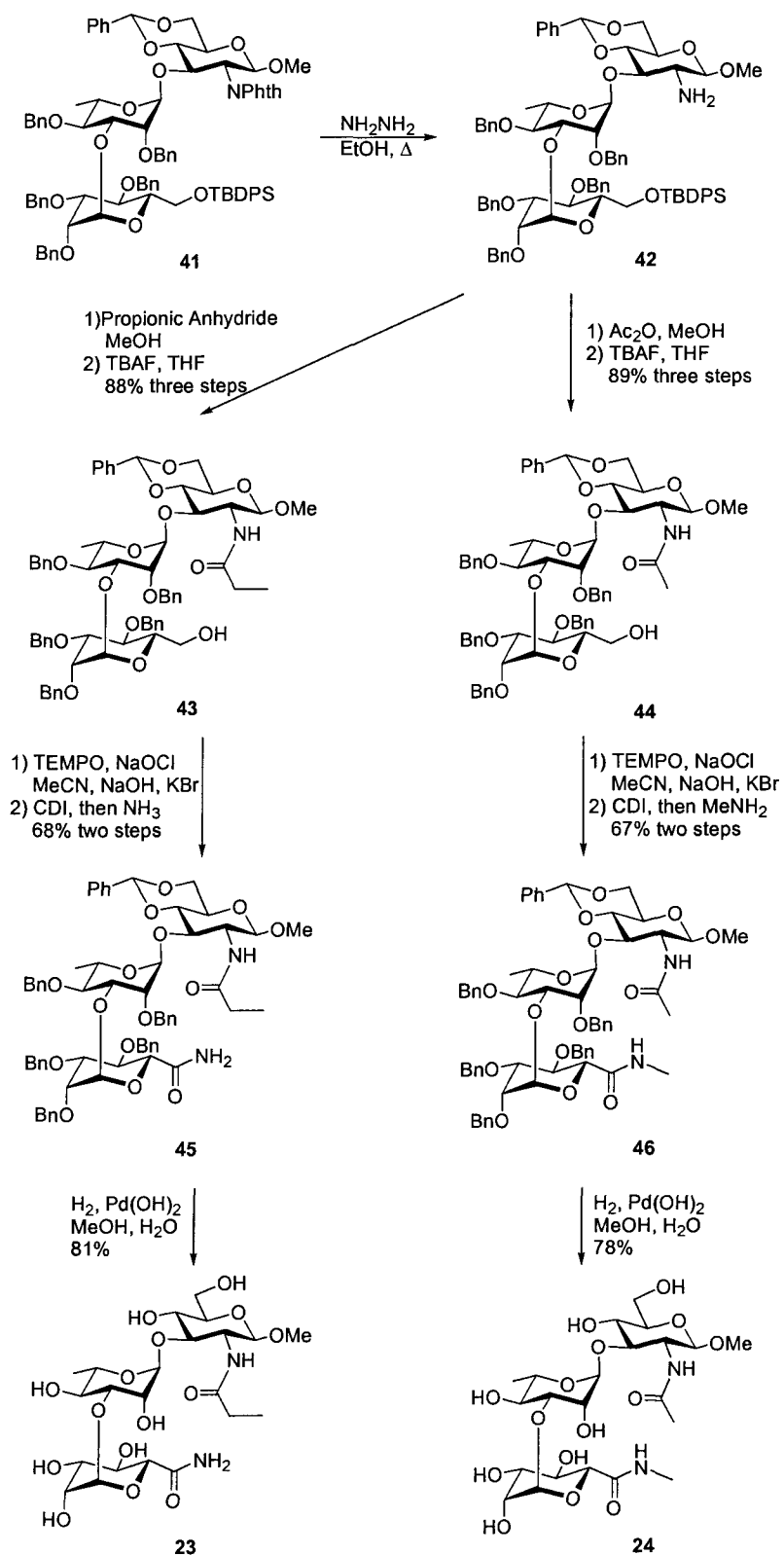


Scheme 2.7: Assembly of the protected core trisaccharide **41**.

The $^3J_{\text{H1-H2}}$ values of α - and β -linked mannose and rhamnose compounds are, in many cases very similar, and are frequently close to zero or 1 Hz. Therefore, interpreting these data by employing the Karplus relationship^[105, 106] cannot be used to identify the stereochemistry about the anomeric center. One-bond carbon-proton coupling constants ($^1J_{\text{H1-C1}}$) were measured employing HMQC NMR. The magnitude of this coupling constant for α -linked pyranose residues ranges from 165-175 Hz while the β anomers are usually within 155-165 Hz.^[107] The α -anomer was formed for each glycosylation reaction

in this synthesis and HMQC spectra of the protected trisaccharide have values of 167.3 Hz ($^1J_{\text{H1}'\text{-C1}'}$) and 171.1 Hz ($^1J_{\text{H1}''\text{-C1}''}$).

Removal of the phthalimido group with refluxing hydrazine hydrate in ethanol provided the free amine that was reacted without purification with acetic or propionic anhydride to branch the synthesis en-route to final trisaccharides **23** and **24**. The amides were then reacted with tetra-*n*-butylammonium fluoride (TBAF) to afford the 6''-alcohol in high yield.^[108] The primary alcohols of **43** and **44** were oxidized with 2,2,6,6-tetramethyl-1-piperidiny-*N*-oxide (TEMPO) using sodium hypochlorite (NaOCl) as co-oxidant to afford the corresponding carboxylic acids.^[109] Reaction of the crude acids with excess carbonyldiimidazole followed by quenching the mixed anhydrides with the respective amines (ammonia or methylamine) gave the isomeric bis-amides **45** and **46** (Scheme 2.8). These trisaccharides were deprotected using hydrogenolysis with Pearlman's catalyst (Pd(OH)₂).



Scheme 2.8: Final synthesis of acyclic BCD derivatives **23** and **24**.

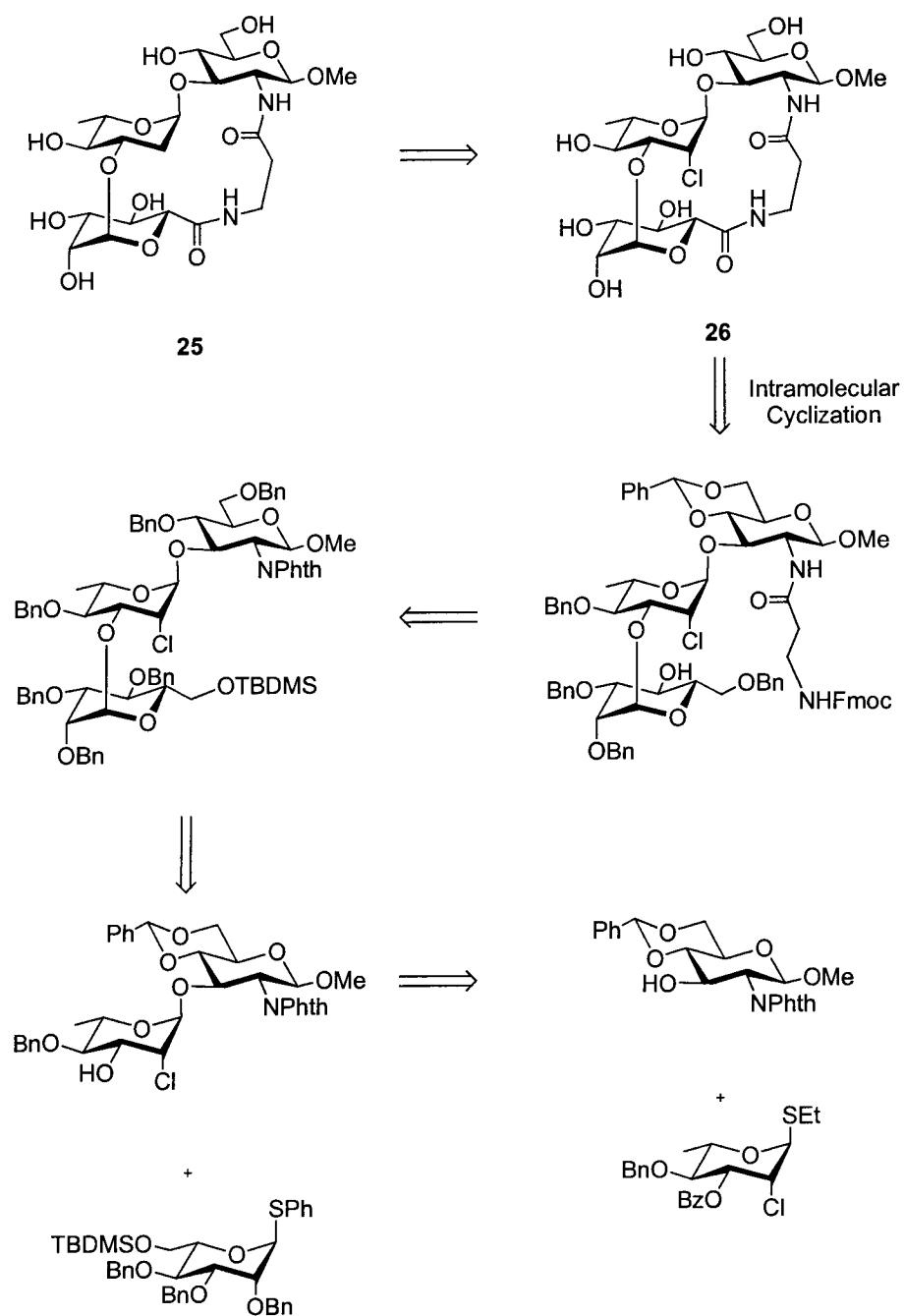
2.3 Macrocyclic BCD Trisaccharides Containing Functional Group Modifications

2.3.1. Synthesis of a 2'-chloro-2'-deoxy Rhamnosyl Donor and L-Mannosyl Donor

The same strategy used for the synthesis of **21** was envisioned for the preparation of the cyclic-chloro trisaccharide **25** derivative. Synthetic disconnection at the deprotected macrolactam demonstrates that a linear sequence of monosaccharide assembly followed by modifications at the B and D residues and subsequent cyclization provides the target trisaccharides (Scheme 2.9).

This approach required the preferential installation of an axial chlorine atom at the 2-position of the C residue to give the *rhamnose* (6-deoxy-L-mannose) over the *quinovose* (6-deoxy-L-glucose) configuration. This goal was visualized to occur at the monosaccharide stage from a suitable starting material. One possible solution arises from an inversion of the 2-position of a quinovoside with a suitable leaving group at this center. However, the synthesis of this hexose would ultimately have to start from a rhamnose derivative leading to a long chemical synthesis.

A shorter, alternative route was to begin with a suitably protected rhamnol (glycal, a cyclic enol-ether) derivative. The addition of an electrophilic chlorine atom would occur at the 2-position followed by concomitant nucleophilic addition to the anomeric center. Such a nucleophile would need to allow the elaboration of the monosaccharide to an activated donor in a minimum number of chemical steps. Chloro-methoxylation has been reported for 3,4-di-*O*-acetyl-L-rhamnol, using chlorine gas in methanol.^[42] Silver acetate

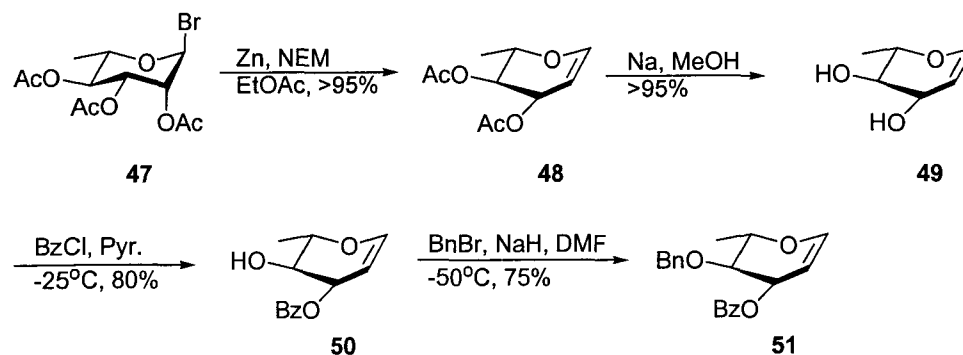


Scheme 2.9: Retrosynthetic analysis of cyclic 25 and 26.

was used to activate any anomeric chloride formed as a result of nucleophilic addition of chloride to a 1,2-chloronium ion, allowing methanol to attack the anomeric center. This reaction suffered from poor diastereofacial selectivity producing α/β mixtures of both *rhamno*- (minor) and *quinovo*- (major) configured compounds. The desired isomer was formed in a low yield of 25%.

It was envisioned that a hydroxy or acetoxy nucleophile could be delivered to the chloronium ion resulting from the addition of chlorine gas to a rhamnol derivative that was orthogonally protected to afford base-labile access to the 3-position later in the synthetic route. Lewis acids were also used to activate any 1,2-dichlorides for reaction with acetic acid or water. The synthesis of protected rhamnol, 1,5-anhydro-3-*O*-benzoyl-4-*O*-benzyl-2,6-dideoxy-L-*arabino*-hex-1-eneitol (**51**), was done as previously reported.^[54] L-Rhamnol was generated from the reductive elimination of acetobromorhamnose (**47**), after subsequent transesterification (Scheme 2.10).

The 3-position is more nucleophilic as attempts to selectively alkylate or acylate the diol prefer this position. Under optimal conditions, benzylation of the 3-position was accomplished using benzoyl chloride in pyridine at $-25\text{ }^{\circ}\text{C}$ (80% yield). Subsequent benzylation of the 4-position was performed using sodium hydride and benzyl bromide. Typically, under these conditions, acyl protecting groups can migrate to adjacent alcohols or be removed via attack of hydride. The migratory aptitude of this benzoyl group is lessened due to the trans relationship of the 3,4-diols and benzylation at low temperature using an inverse addition method (benzyl bromide, then sodium hydride) was effective, giving the orthogonally protected L-rhamnol derivative **51** in 75% yield (Scheme 2.10).



Scheme 2.10: *Synthesis of protected L-rhamnol derivative 51.*

Attempts to chlorinate the glycal, followed by attack of hydroxy or acetoxy nucleophiles at the anomeric carbon, were made using a variety of conditions in which the quinovose isomers were predominant (Table 2.1). It had been demonstrated that the dielectric constant of the solvent used during chlorination of D-glucal triacetate can effect a *cis*- or *trans*- addition to the olefin, and influences facial selectivity.^[110] It was found that exceptional diastereofacial selectivity for the production of both *rhamno*- and *quinovo*- configurations could be achieved for the chlorination of **51** using carbon tetrachloride and propylene carbonate (PC), respectively, without an additional nucleophile. This unexpectedly high selectivity gave, after a one-pot glycosylation of acetic acid, the *quinovo*- and *rhamno*- 2-chloro acetates (**54** and **55**) in unprecedented yields. It had been previously shown that 2-chloro-2-deoxy rhamnosyl thioglycosides act as an efficient glycosylating agent, therefore the anomeric acetate was reacted with ethanethiol and boron trifluoride diethyletherate to give donor **56** (Scheme 2.11).^[42]

Conditions	Yield	Target	Major Isomers
Cl ₂ , Ag ₂ CO ₃ , THF, H ₂ O	~70	A	qui
Cl ₂ , Ag ₂ CO ₃ , H ₂ O	~75	A	~1:1 qui: rha
Cl ₂ , AcOH, Ac ₂ O, AgOAc	~50	B	mainly qui
Cl ₂ , AgOAc, Et ₄ NOAc, DME	~80	B	~3:2 qui: rha

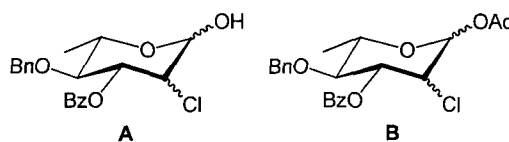
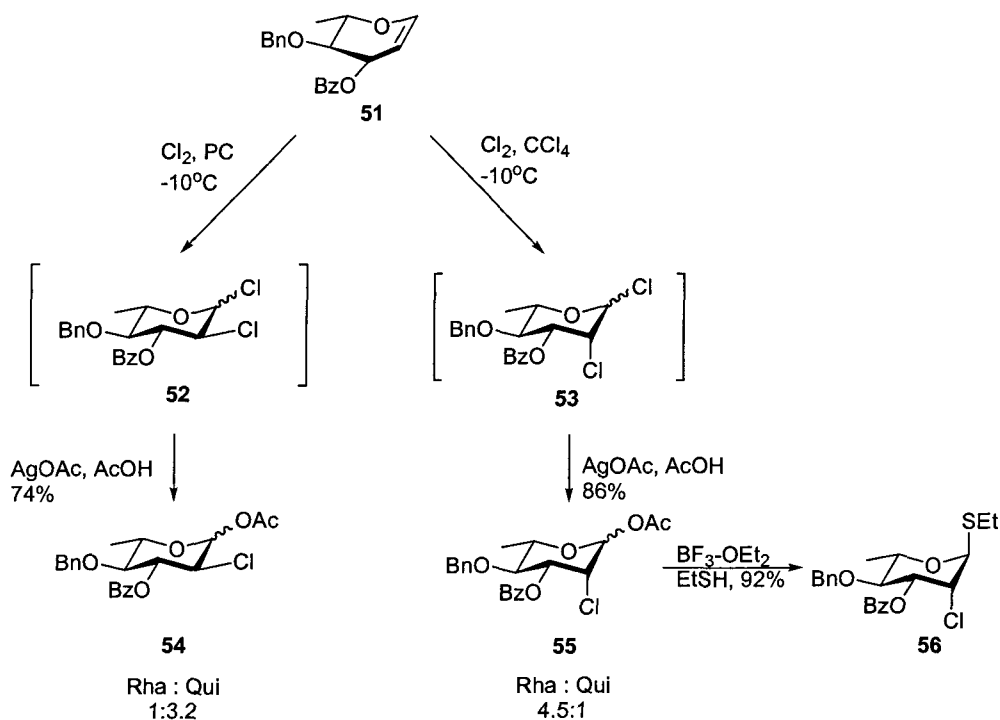
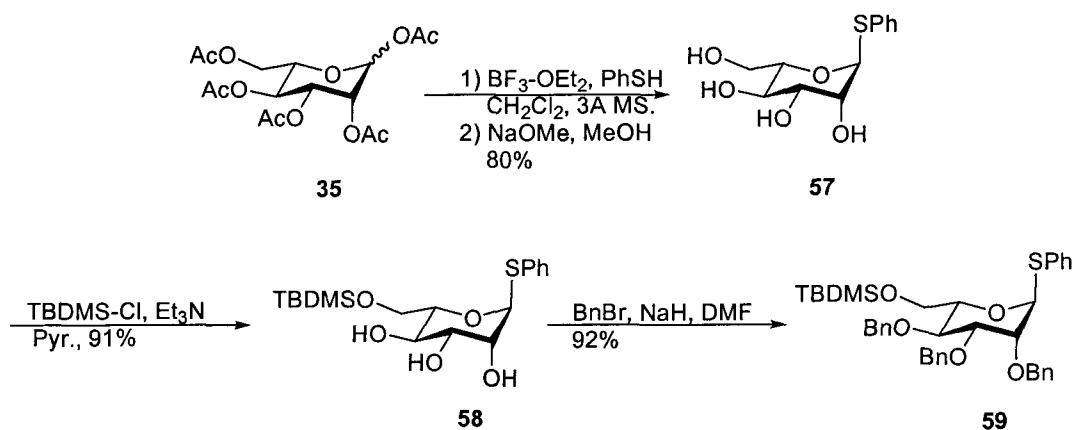


Table 2.1: Conditions attempted for the chlorination of *L*-rhamnol derivative **51**.



Scheme 2.11: Successful chlorination of protected rhamnol derivative **51** and its elaboration to thioglycoside donor (**56**). PC refers to 1,2-propanediol cyclic carbonate.

In addition, another L-mannosyl thiophenyl donor was synthesized for maximum flexibility of activation conditions. While thioglycosides are activated under a variety of conditions,^[111] hydrolysis of the resulting hemiacetal with trichloroacetonitrile and 7,11-diazabicyclo[5,4,0]undec-11-ene (DBU) provides access to a trichloroacetimidate donor.^[112] Additionally, oxidation to the sulfoxide provides another class of donors.^[113] Known thiomannoside tetraol **57**^[104] was selectively silylated using *tert*-butylchlorodimethyl silane (TBDPS-Cl) and the resultant triol **58** was exhaustively benzylated (Scheme 2.12).

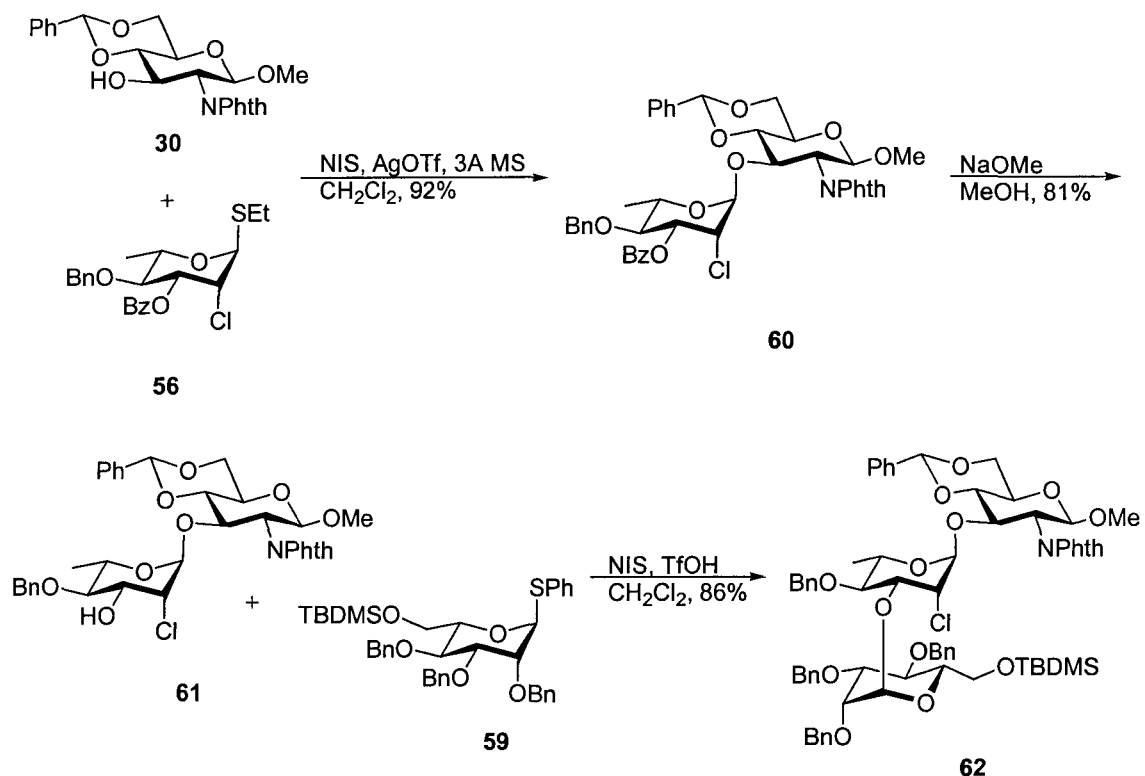


Scheme 2.12: Synthesis of L-mannosyl thioglycoside **59**.

2.3.2. Assembly of Macrocyclic Trisaccharides **25** and **26**.

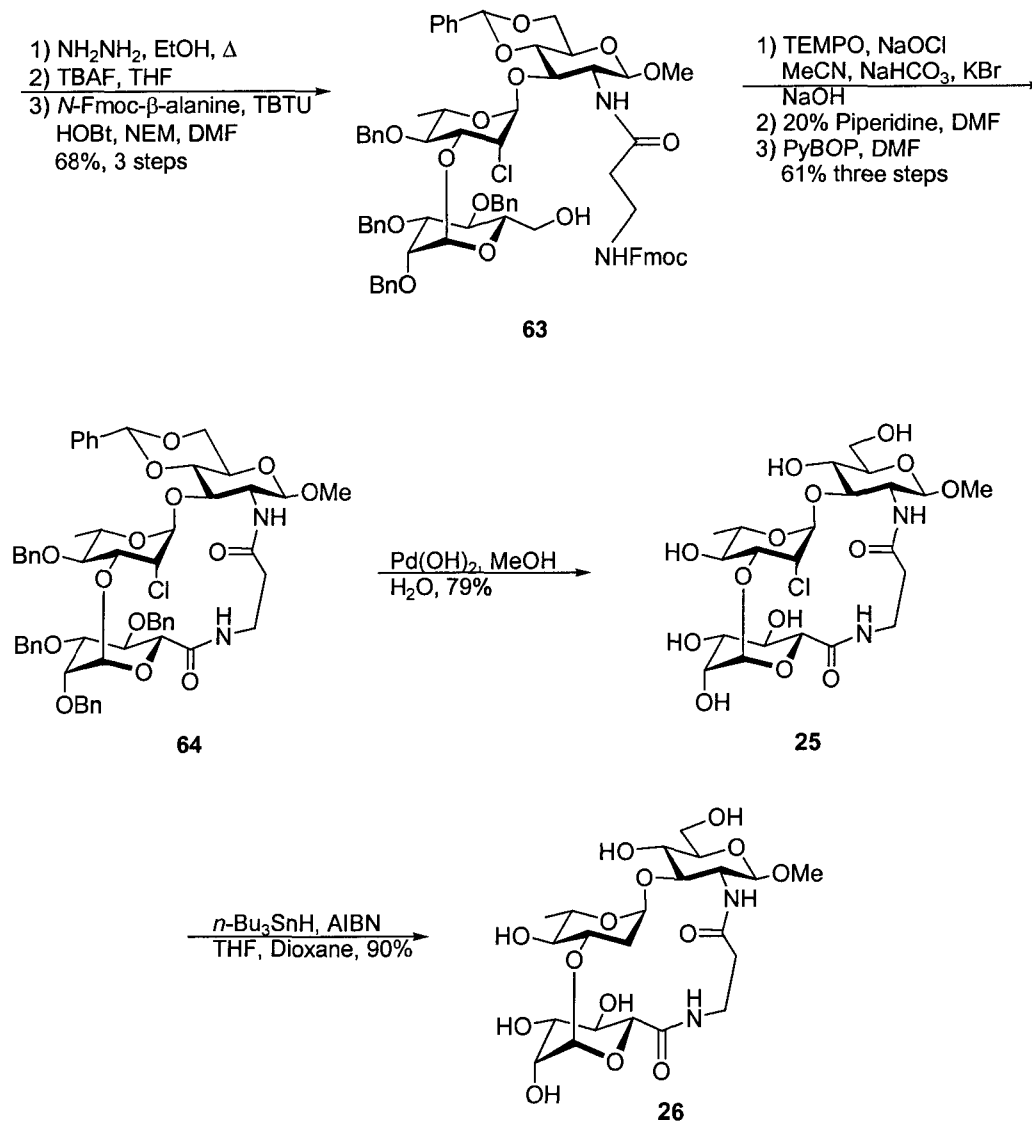
Glycosylation of glucosamine acceptor **30** using rhamnosyl thioglycoside **56**, NIS and AgOTf proceeded smoothly and rapidly to afford the protected disaccharide **60** in 92% yield with no detectable trace of the β -anomer (Scheme 2.13). The anomeric configuration of the newly formed rhamnosyl linkage was determined by HMQC ($^1J_{\text{C1-H1}} = 173.2$ Hz). Transesterification of the 3'-*O*-benzoate gave disaccharide acceptor **61**, which was subsequently glycosylated by **59** in 81% yield. Initial attempts using

NIS/AgOTf to promote glycosylation gave only a small portion of the correct trisaccharide product, but use of NIS/TfOH as promoter furnished **62** in 86% yield. HMQC experiments confirmed the assignment of the linkage as α ($^1J_{\text{C1-H1}} = 169.8$ Hz) and, as expected for a 2-*O*-benzyl-mannosyl donor, the undesired β -anomer was formed in approximately 5% yield.



Scheme 2.13: Synthesis of protected trisaccharide **62**, containing the 2'-chloro-2'-deoxy modification.

The transformation of protected trisaccharide **62** to **63** was accomplished by performing two selective deprotections followed by amide bond formation. The phthalimido group was removed using hydrazine hydrate, followed by TBAF to remove the 6''-*O*-TBDMS ether. The amino-alcohol intermediate was treated with *N*-Fmoc- β -



Scheme 2.14: *Synthesis of macrocyclic 25 and 26.*

alanine-OH under peptide coupling conditions *O*-(benzotriazol-1-yl)-*N,N,N',N'*-tetramethyluronium tetrafluoroborate (TBTU) and 1-hydroxybenzotriazole (HOBt)^[114] to afford **63** in 68% over 3 steps. The primary alcohol was oxidized using TEMPO/NaOCl, filtered through a short pad of silica gel and treated with standard Fmoc deprotection conditions (20% piperidine in DMF). Initial attempts at macro-lactamization using the

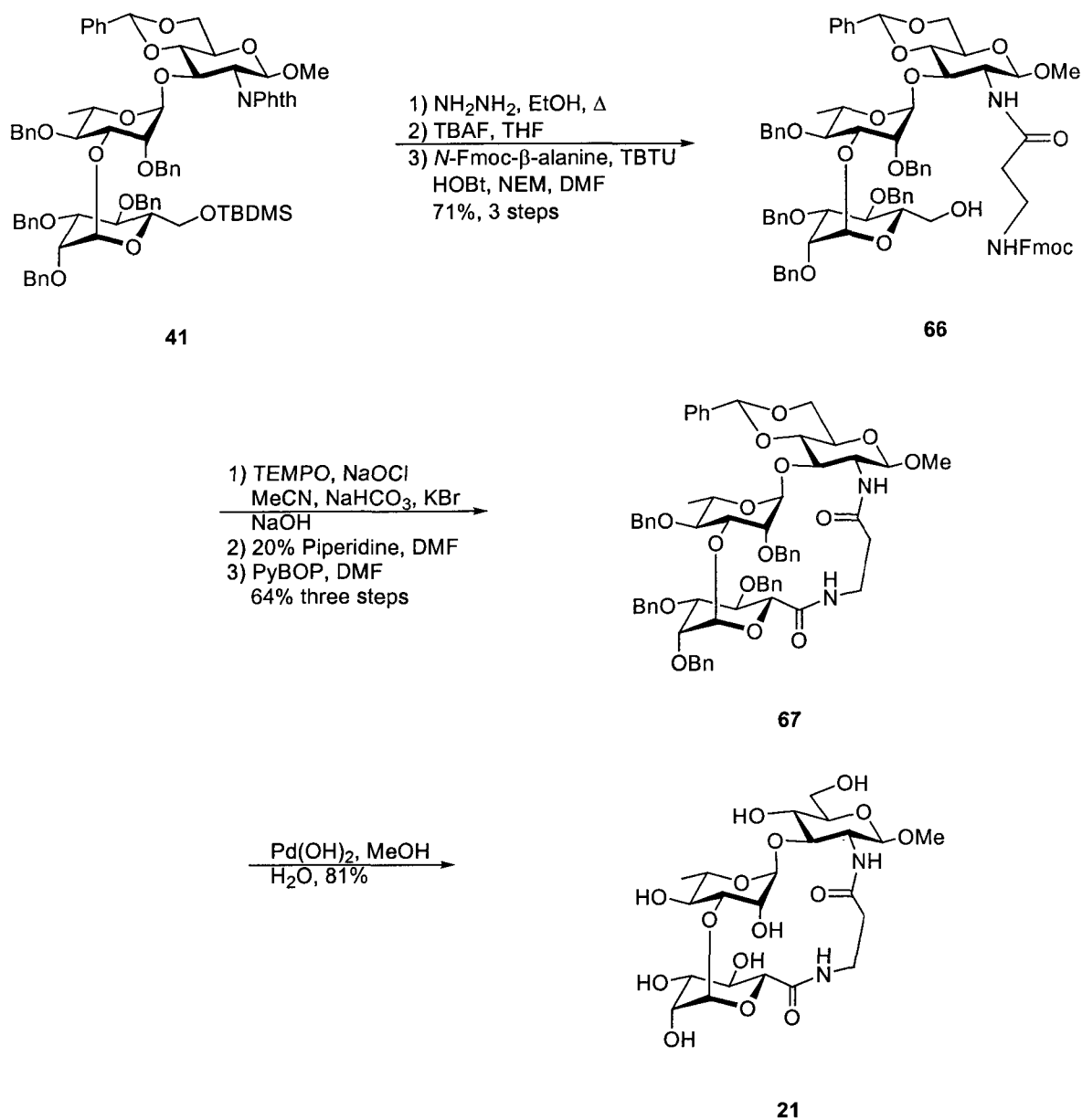
TBTU/HOBt combination resulted in a large amount of unreacted activated ester, although some product was obtained in poor yield after chromatography. Employing a single component coupling system of (benzotriazol-1-yloxy)tripyrrolidinophosphonium hexafluorophosphate (PyBOP)^[115] in DMF at high dilution (1 mg/mL) afforded the protected lactam **64** (91% for the cyclization from the acid, 61% from **63**), indicating that an intermediate OBt ester is not an active species, nor is it required, for this reaction. Protected macrocycle **64** was hydrogenated over Pd(OH)₂ to afford deprotected **25** in 79% yield (Scheme 2.14).

The one and two dimensional proton NMR spectra of protected cyclic trisaccharide **64** indicated that tethering had restricted the solution conformation of the molecule. Resonances corresponding to the methylene protons of the tether had sharpened into diastereotopic signals with defined line structure. As expected, this fine structure was not present for acyclic precursor **63**, as rotamer conformations about the amide linkage averaged and broadened a number of signals in the spectrum. The gradient-enhanced COSY spectra (GCOSY) of **64** exhibited long-range intra-residue coupling (up to ⁵J_{H-H}) within the *rhamno*- and *manno*-ring systems. The deprotected compounds **25** and **26** also exhibited this long-range scalar coupling. The protected derivative **64** also exhibited ⁴J_{H-H} inter-residue coupling for both H-1'' and H-1' across the glycosidic bonds. While these extended coupling pathways have very small values and are only observed in two-dimensional spectra of α-linked sugars, they were not observed for the less restricted open chain molecules.^[116]

Initially, it was intended to acetylate cyclic **25**, effect reduction of the chloride with tri-*n*-butyltin hydride (TBTH)^[117] and deacetylate to get cyclic deoxygenated **26**.

Standard acetylation conditions (acetic anhydride, pyridine) produced a mixture of hexa- and hepta-acylated compounds. Although it is rarely observed that a lactam nitrogen is acetylated under these conditions it is the only available site for over-acetylation.^[118, 119] Reduction of this mixture with TBTH and 2,2-azo-bis-isobutyronitrile (AIBN) as a radical initiator in toluene, followed by Zemplén transesterification produced low yields of cyclic-deoxy derivative **26** along with recovered **25** after HPLC purification. The solubility of cyclic **25** was acceptable in a refluxing mixture of 3:1 dioxane:THF and direct reduction of the chloride was performed with TBTH/AIBN to give cyclic-deoxygenated derivative **26** in excellent yield with little or no starting material detectable by HPLC (Scheme 2.14).

Because native trisaccharide **22** and its cyclic analogue **21** were required for comparative binding analysis and NMR measurements they were re-synthesized based on literature protocol.^[40, 87] Cyclic **21** was synthesized *via* a more efficient route similar to cyclic chloro **25**. Multi-step reactions could be carried out in a “one-pot” fashion in contrast to their original description.^[56, 87] Starting with protected trisaccharide **41**, a three-step sequence was used to give the precursor for macrocyclic tethering. The phthalimido group was removed using hydrazine in boiling ethanol and the 6'-alcohol was exposed using TBAF to deprotect the 6'-silyl group. The coupling of *N*-Fmoc protected β -alanine with TBTU, HOBt and *N*-ethylmorpholine produced the partially protected trisaccharide **65**, in 74% from fully protected **64** (Scheme 2.15).



Scheme 2.15: Synthesis of macrocyclic 21.

Oxidation was facilitated using TEMPO to afford the carboxylic acid intermediate. With only a simple filtration through silica gel, this compound was treated with 20% piperidine in DMF to remove the Fmoc protecting group, before thorough evaporation from toluene (three times). The intermediate amino acid was dissolved in

dimethylformamide at high dilution (approx. 1 mg mL^{-1}) and treated with PyBOP to effect macrocyclization. This three-step process gave protected cyclic **67** (64% yield from **66**, Scheme 2.15).

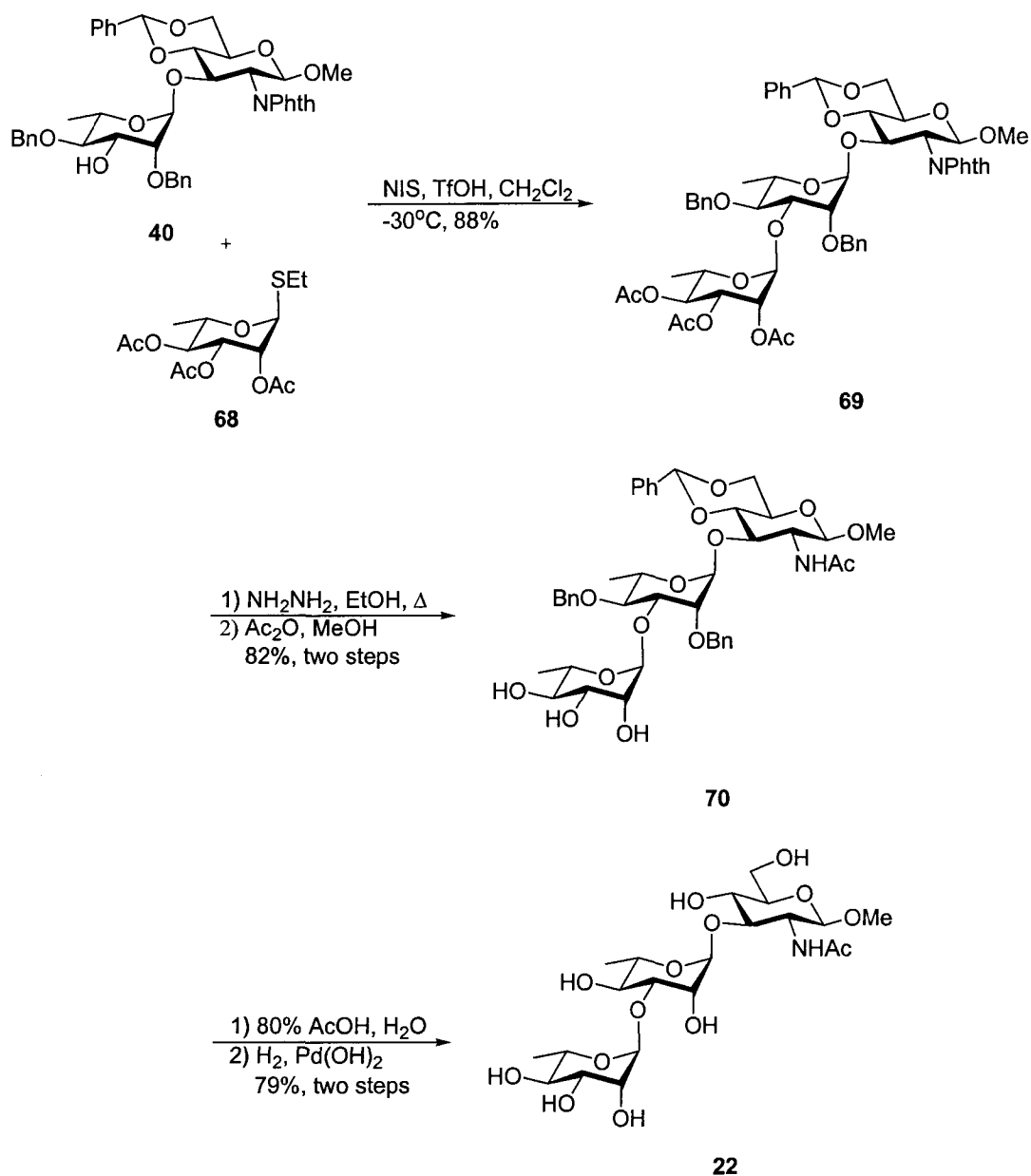


Figure 2.16: *Synthesis of the native BCD trisaccharide.*

The synthesis of the native trisaccharide utilized the common disaccharide alcohol acceptor **40**, and it was glycosylated by ethyl 2,3,4-tri-*O*-acetyl-1-thio- α -L-rhamnopyranoside^[102] (**68**) using NIS and catalytic TfOH in 86% yield. Treatment with hydrazine in boiling ethanol removed the phthalimido group and three acetate groups on the Man B residue. Exhaustive evaporation to remove excess hydrazine was followed by treatment with acetic anhydride in methanol to give amide **70** in 82% yield. There were trace amounts of acetate group containing by-products that mass spectrometry identified as over acetylated products. Hydrogenolysis was attempted using Pearlman's catalyst but no desired product was formed. Because the partially protected starting material was not particularly soluble in the aqueous methanol conditions, the benzylidene acetal was removed with 80% aqueous acetic acid at 40 °C. The aforementioned hydrogenolysis conditions were successful in removing the remaining benzyl groups to give the deprotected native trisaccharide **22** in 79% after purification using high-performance liquid chromatography (Figure 2.16). The physical and spectroscopic characteristics of both cyclic **21** and the native trisaccharide **22** matched previously reported values.^[40, 87]

Chapter 3

Analysis of the Binding of Synthetic Ligands to Monoclonal Antibody SYA/J6

3.1. Initial Binding Assessment Using ELISA.

3.1.1. The ELISA Protocol.

The enzyme-linked immunosorbent assay (ELISA) is a versatile and sensitive assay for the detection and quantification of antigen/antibody interactions. The specific reactions are assayed in a solid-phase assay in which one of the binding components, either the antigen (often as a conjugate) or antibody, is immobilized to a support such as the well of a microtitre plate. Unbound materials can be washed away, and the bound antigen/antibody complex can be detected and amplified using an enzyme-conjugate and chromogenic substrate.

Numerous variations of ELISA procedures have been developed for the detection and quantification of antigen/antibody interactions. Among them, the competitive ELISA is very useful for measuring the binding of a soluble antigen to an antibody. In this assay, antibody is adsorbed to the plates, and a ligand is added. The competition arises when a second soluble ligand is added to the reaction. Quantification of the assay requires one of the two ligands to be amenable to labeling.

There are two main ELISA assay formats: the direct and indirect. An example of the direct ELISA uses purified antibody that is immobilized to the wells of a microtitre plate. Labeled antigen, such as a polysaccharide, is conjugated to biotin and binds to the immobilized antibody. Color is developed upon the addition of an enzyme-labeled Streptavidin. Other developing conjugates can include labels that provide a chemiluminescent or fluorescent end-point.

The indirect ELISA utilizes a secondary binding component in an additional step that provides signal amplification and increases the overall sensitivity of the assay. This assay format typically has antigen conjugate adsorbed to the plate and primary antibody is added. A secondary antibody conjugated to a label is added to the mixture. This second antibody is directed at the species from which the primary antibody was generated. If the primary antibody was murine, the appropriate secondary antibody could be a goat anti-mouse immunoglobulin, for example.^[28, 120]

The specific protocol for measurement of the SYA/J6 system was developed by Bundle *et al.* and is a competitive direct ELISA (Figure 3.1).^[43, 44] A fixed concentration of purified SYA/J6 was non-covalently attached to the wells of microtitre plates. Biotinylated samples of *S. flexneri* LPS are then added.^[44] The soluble inhibitor to be assayed is then added to the wells in serial dilution. After incubation and washing steps a streptavidin-horseradish peroxidase (HRP) conjugate is introduced. Streptavidin binds to biotin with an extremely high-affinity association constant of approximately 10^{14} .

To initiate the colorimetric response, 3,3',5,5'-tetramethylbenzidine is added and oxidized by HRP to produce a blue color. Quenching the reaction with phosphoric acid produces a yellow color that is measured spectrophotometrically at 450 nm. As the

concentration of soluble inhibitor increases, a decrease in the intensity of color is observed. The absorbance readings from the wells are corrected to a control and the data are plotted in a semi-log format as % inhibition vs. \log_{10} of the ligand concentration. The midpoint of this curve denotes the IC_{50} , which is the concentration of soluble ligand required to give 50% inhibition (Figure 3.2 and 3.3). Often, the IC_{50} approximates the K_D of the ligand.

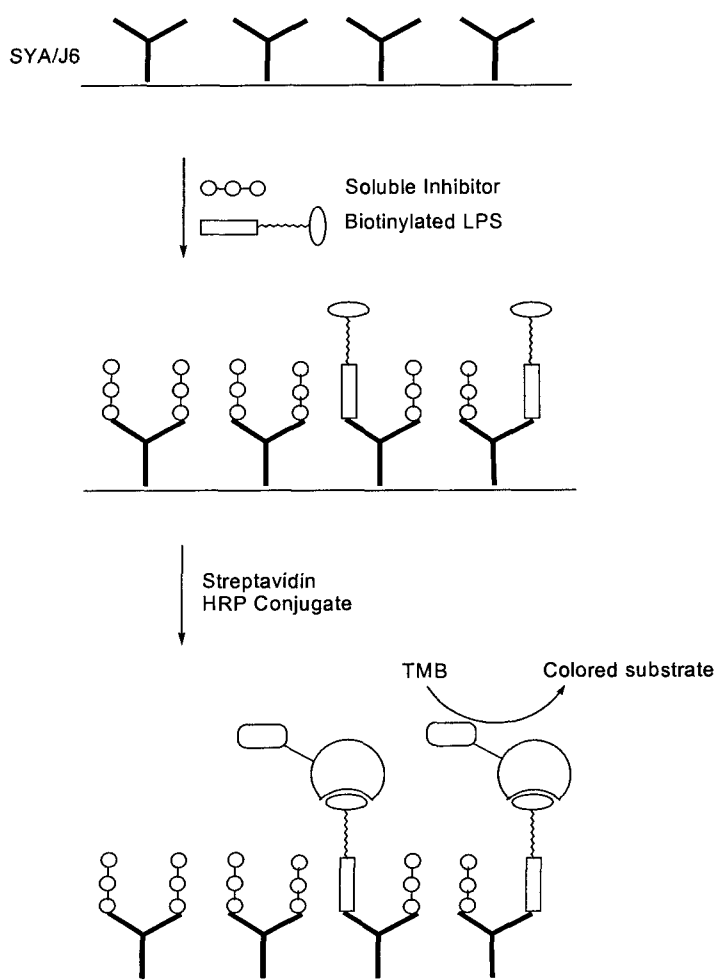


Figure 3.1: *The general ELISA protocol for the evaluation of ligands with SYA/J6.*

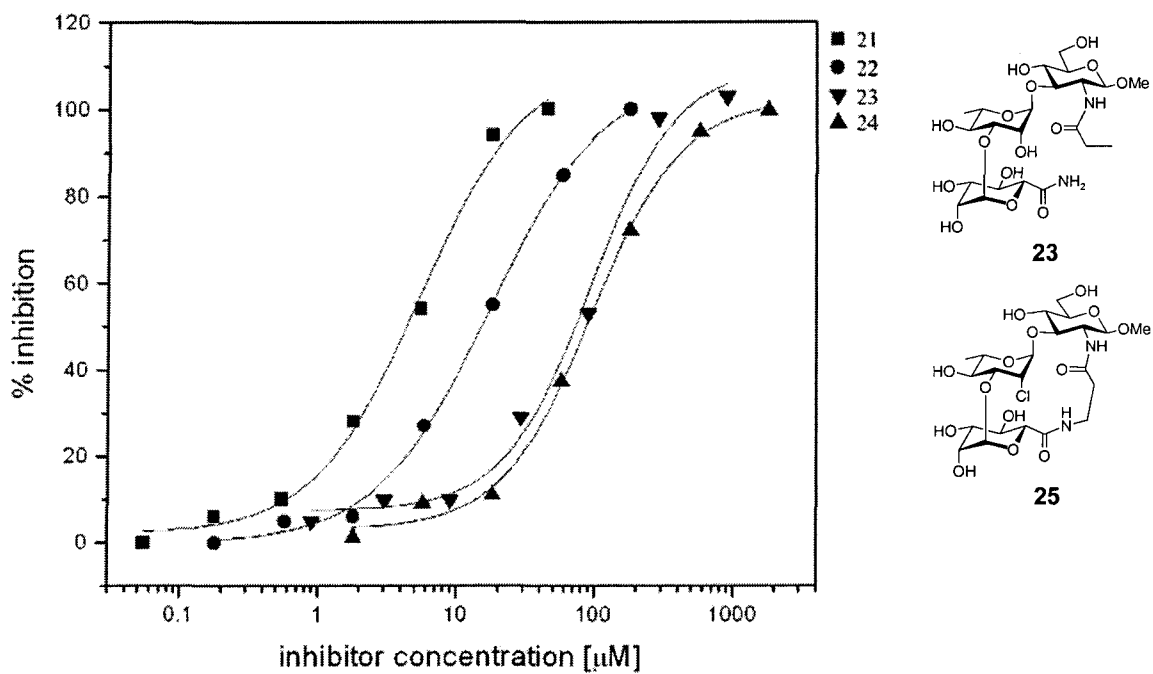


Figure 3.2: *ELISA results for acyclic control 23 and cyclic-chloro 25.*

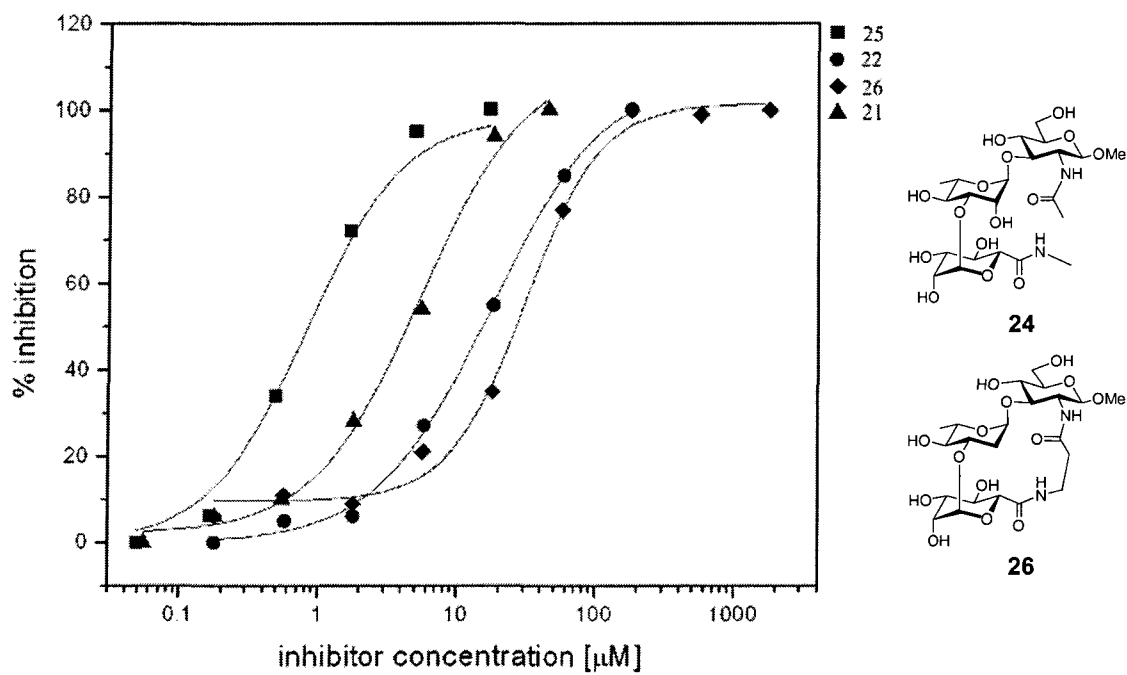


Figure 3.3: *ELISA results for acyclic control 24 and cyclic-deoxy 26.*

Compound	IC ₅₀ (μ M)
21	5
22	17
23	94
24	92
25	0.82
26	30

Table 3.1: Measured IC₅₀ values with their corresponding structures for targets **23-26**. Values for native trisaccharide **22** and cyclic **21** are included for comparison.^[56, 87]

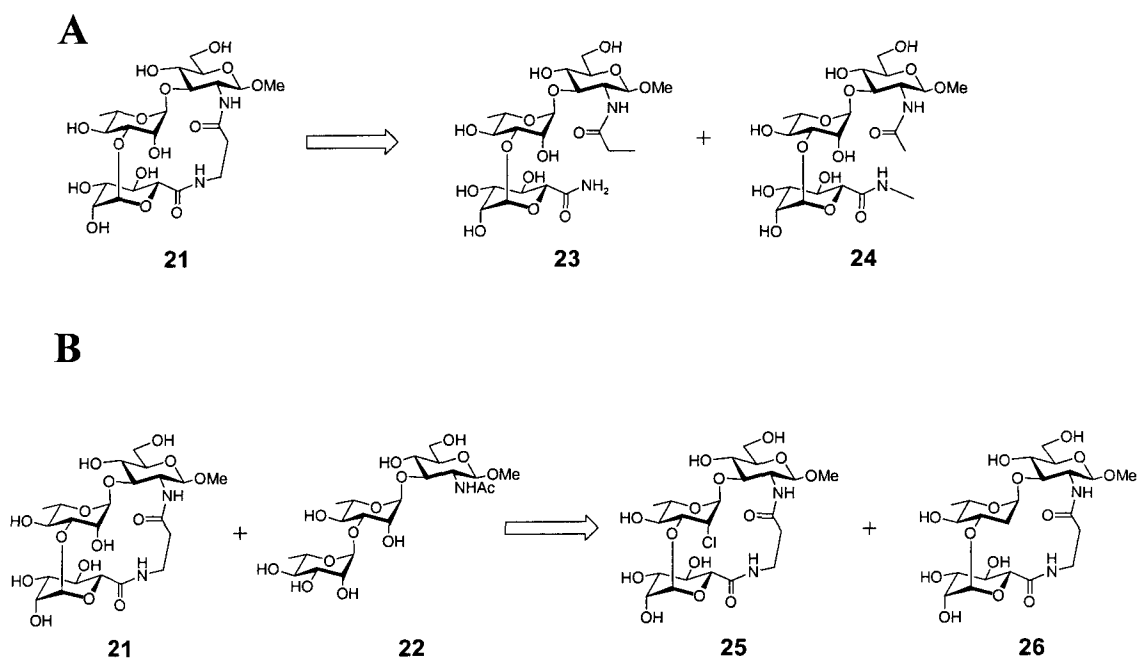


Figure 3.4: Ligands grouped based on structural similarities to compare with ELISA binding data.

ELISA assays were used to provide a rapid indication of the biological activities of our ligands. The experiment uses much smaller amounts of protein than isothermal titration microcalorimetry (ITC). The association constants of these ligands could be

qualitatively estimated from IC_{50} because accurate values of K_A for cyclic **21** and the native trisaccharide **22** were previously known.^[46, 56, 87]

Certain structural features were directly compared with the ELISA binding data. Investigation of the influence of tethering involved comparison of cyclic control compounds containing the 'cut' β -alanyl tethers (**23** and **24**) and cyclic **21** (A, Figure 3.4). The acyclic compounds were found to have with an approximate 20-fold reduction of inhibitory activity relative to their cyclic counterpart (**21**) and a six-fold reduction compared to native trisaccharide **22** (Figure 3.2, Table 3.1). This indicates it is indeed the intact tether that accounts for the increased activity of **21**, and not fortuitous polar contacts arising from the non-natural substitution of an amide for a methyl group at the 6'-position of the Rha B residue. The reduction in activity of acyclic derivatives **23** and **24** is not surprising because it is known that substitution at this position can cause an adverse effect to binding.^[45]

A comparison of the ELISA data for the tethered ligands **21**, **25** and **26** showed their relative inhibitory power (B, Figure 3.4, Table 3.1). The cyclic-chloro derivative **25** exhibited the highest activity ($IC_{50} = 0.82 \mu\text{M}$) of all ligands tested. This implies that there is a combined effect of pairing the 2'-chloro-2'-deoxy functional group modification with the intramolecular pre-organization.

Surprisingly, cyclic-deoxy analogue **26** exhibited a reduction in inhibitory capability ($30 \mu\text{M}$) when compared to the native trisaccharide ($17 \mu\text{M}$) or cyclic **21** ($5 \mu\text{M}$ Figure 3.3). Clearly, an incompatibility with pairing the 2'-deoxy functionality with the tethering methodology was detected. Because the IC_{50} is only a relative measure of

biological activity, ITC was used to derive more accurate figures of affinity, along with the thermodynamic parameters of binding.

3.1.2. Thermodynamic Binding Analysis by Isothermal Titration Microcalorimetry.

The advent of modern isothermal titration calorimetry offers an extremely sensitive method to directly and accurately measure the heat evolved or consumed during a binding event.^[121, 122] In the case of monoclonal antibody SYA/J6, all binding partners are exothermic. The magnitude of heat liberated upon binding depends on concentration and the molar enthalpy of reaction of the binding partners. The association constant (K_A), the stoichiometry (n), and the progress of the titration also affect how much heat is evolved.

A Microcal VP-ITC calorimeter (Northampton, MA) was used for the ITC analysis of synthetic ligands binding to SYA/J6. The computer and on-board software (Microcal Origin) integrate the quantities of heat generated, and plots a curve of kcal mol^{-1} of injectant *versus* molar ratio of ligand added. Solving this isotherm using non-linear regression affords K_A that is correlated to ΔG and ΔS using equation 3 (Page 3).

The calorimeter has a sample and reference cell that are approximately 1.4 mL in volume. Each is equipped with an active heating device, but are only able to cool *via* the use of an adiabatic jacket. The reference cell is loaded with high-purity water. During the experiment, the cells are heated to the same temperature and ligand is titrated into the cell from a syringe with a mixing paddle spinning at around 400 rpm to ensure homogeneity. The difference in temperature between the cells after an injection is

quantified by the amount of power required to heat the reference cell to the new temperature. Even though the technique is not perfectly isothermal, the difference in temperature from the beginning to the end of the experiment raises by no more than 0.15 °C. A typical experiment consists of 30 to 35 injections of 20-fold concentration excess of ligand added in 8 μL aliquots with approximately five minutes between injections.^[35]

ITC is useful to measure systems when the association constant ranges from 10^3 to 10^8 M^{-1} . For interactions below 10^3 , a full titration curve cannot be measured unless concentrations of receptor are high in the cell. Often, the availability of material or its solubility become an issues. In high-affinity instances, the shape of the binding isotherm can be too steep, due to sensitivity issues with the calorimeter and limitations of the software for fitting a steep curve. The constant c is the product of initial protein concentration multiplied by the association constant. Values should be in the range of 1 to 500 to give data that are amenable to treatment by the software. Calorimetry results for compounds **22** through **26**, along with measured and calculated parameters, are presented in Figures 3.4 and 3.5

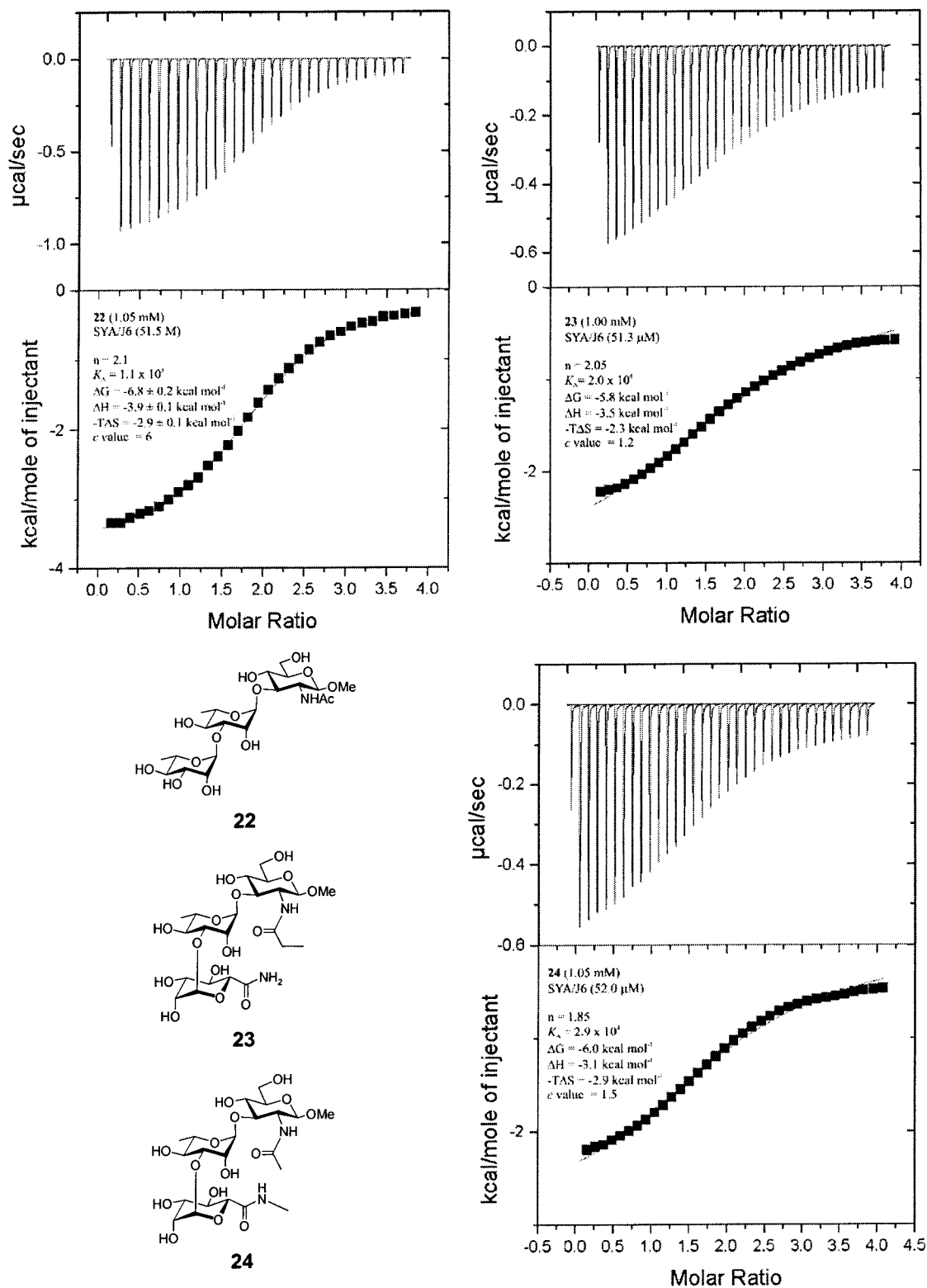


Figure 3.5: ITC results for native trisaccharide **22** and acyclic compounds **23** and

24.

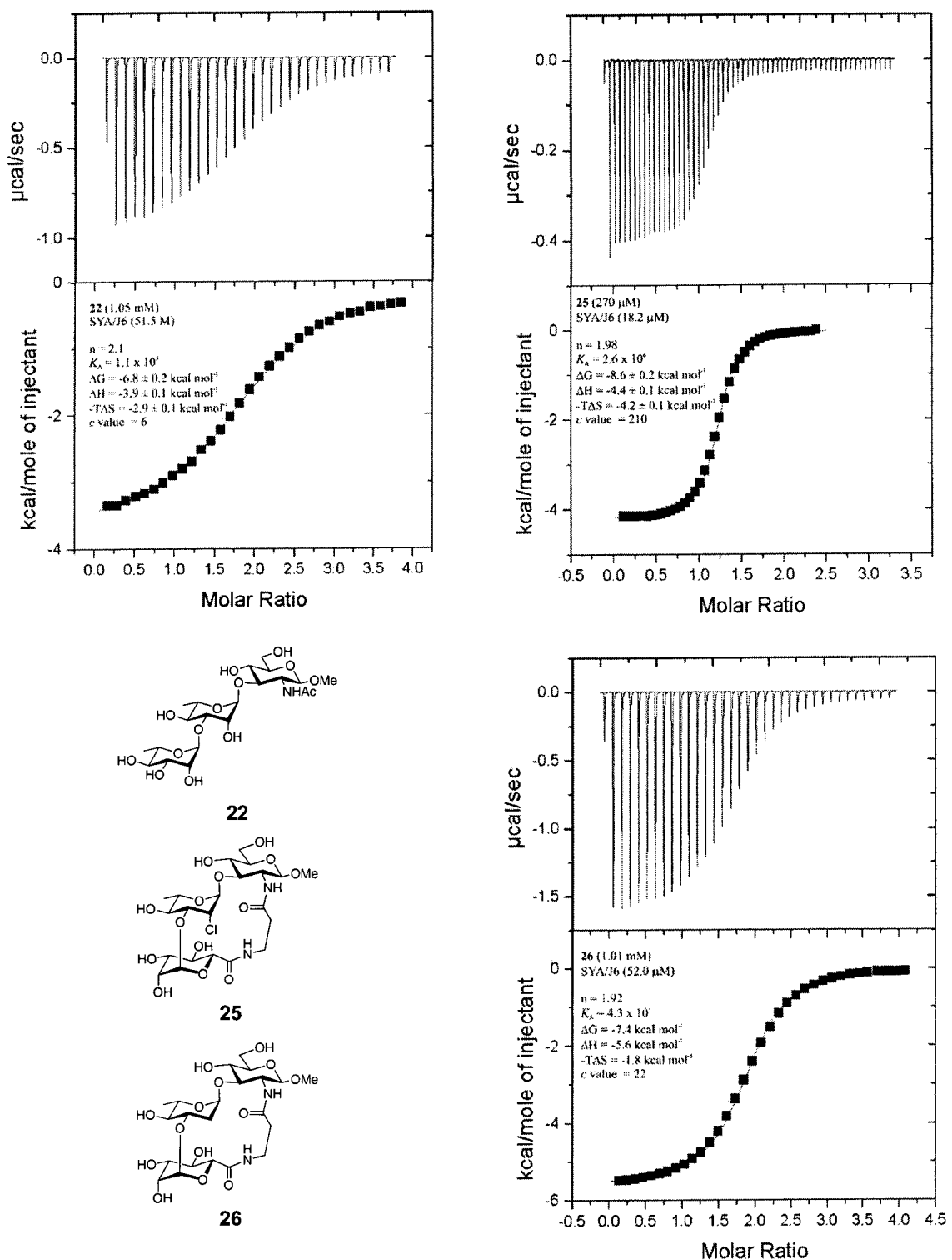


Figure 3.6: ITC results for native trisaccharide **22** and acyclic compounds **25** and

26.

3.2. ITC Analysis for Ligands Used in This Study.

Microcalorimetry was performed on all cyclic and acyclic compounds related to this study (**21** to **26**). Authentic samples of the 2'-deoxy **2** and 2'-chloro-2'-deoxy **3** trisaccharides were available to perform comparative ITC measurements. The experiments were run at 293 °K and the results are summarized in Table 3.2.

Compound	K_A (M^{-1})	ΔG (kcal/mol)	ΔH (kcal/mol)	$-T\Delta S$ (kcal/mol)
2	2.5×10^6	-8.5	-8.1	-0.5
3	1.1×10^6	-8.1	-6.3	-1.8
21	$1.5 \pm 0.05 \times 10^6$	-8.3 ± 0.1	-4.2 ± 0.05	-4.1 ± 0.05
22	1.1×10^5	-6.8 ± 0.2	-3.9 ± 0.1	-2.9 ± 0.1
23	2.0×10^4	-5.8	-3.5	-2.3
24	2.9×10^4	-6	-3.1	-2.9
25	2.6×10^6	-8.6 ± 0.15	-4.4 ± 0.1	-4.2 ± 0.05
26	4.3×10^5	-7.4	-5.6	-1.8

Table 3.2: Microcalorimetry results from measurement with each ligand and mAb SYA/J6. Standard deviations were calculated from duplicate experiments. Errors in the determination of ΔH are $\pm 2.5\%$.

Acyclic control compounds **23** and **24** were found to bind with an approximate 60-fold reduction in binding affinity compared to the previously described macrocyclic **21** (Table 3.2).^[56, 87] Considering that they contain essentially the same atom configuration as the pre-organized parent structure, these results suggest that the intact tether is responsible for the affinity gains of **21**. The acyclic compounds bind with a significantly reduced affinity compared to the native BCD trisaccharide **22**, reinforcing the notion that the intact tether prevents any steric collision of the non-natural functional

group changes (at the Man B residue 6''-position) from considerable clash with the protein surface. It is unknown why there is a small difference in the free energies of **23** and **24** ($\Delta\Delta G = 0.1$ kcal/mol). It is known that the homologation of an additional methyl group does not cause reduced affinity.^[41]

The association constants and related binding parameters of acyclic BCD derivatives modified at the 2'-position (**2** and **3**) were measured and found to bind with a similar affinity as previously reported, each with values in the low 10^6 region.^[46] As mentioned previously, binding of deoxygenated **2** was almost entirely enthalpic, whereas 2'-chloro substituted **3** had approximately 25% of its binding energy, arising from entropic factors. Each of these compounds had an increased enthalpic contribution over the native trisaccharide **22**. In contrast, the free energy of binding of cyclic **21** had approximately equal portions of enthalpy and entropy. Determining specific causes for individual increases of individual binding parameters is a difficult task, but the increase in entropy for cyclic **21** is indicative of a highly constrained structure.^[56, 87] Alternatively, displacement or reorganization of water molecules at the periphery of the binding site could contribute to this entropic gain.^[27, 123]

Cyclic chloro derivative **25** was found to bind with the highest affinity of all ligands tested. Binding with a slightly higher affinity than singly modified **21** or **3**, indicated each modification contributing to the overall free energy, but complete additivity was not realized. When comparing the native trisaccharide **22** and 2'-chloro derivative **3**, it was apparent that the functional group modification primarily contributed to enthalpic increases toward free energy. This is not the case for cyclic 2'-chloro derivative **25**, as slight increases in both enthalpy and entropic contributions were

measured. Therefore, the thermodynamic ramifications of the replacement of a hydroxyl group for chlorine has not contributed to the individual binding parameters of **25** in a similar way as **3**. It has been hypothesized that in the case of **3**, the chlorine makes a stabilizing contact with an adjacent aromatic ring.^[46] However, the tether of **25** could be imposing a mobility restriction within the binding site not allowing optimal benefits of this halogen substitution.

The cyclic 2'-deoxygenated congener **26** bound to SYA/J6 with surprisingly poor affinity. With a K_A of 4.3×10^5 , it had only slightly more affinity than the native trisaccharide, and almost an order of magnitude less than 2'-deoxy trisaccharide **2** or macrocyclic **21**. In this case, pairing of functional group modification and intramolecular tethering has produced a congener where conflicting forces have led to the trisaccharide to binding in an unexpected way. Crystal structure data shows that **2** binds in a different mode than the BCD portion of ABCDA' pentasaccharide **1**, and does so with greater than 90% of its free energy being enthalpic. Compound **26** has an increased entropic contribution to its free energy of binding. It can be rationalized that since **2** sinks deeper into the binding site than **1**, the tether may have been brought into contact with the protein surface, forcing an alteration in the binding mode of **26**. This is consistent with the observed thermodynamics of binding, which indicates less favorable cohesive contacts with the protein surface.

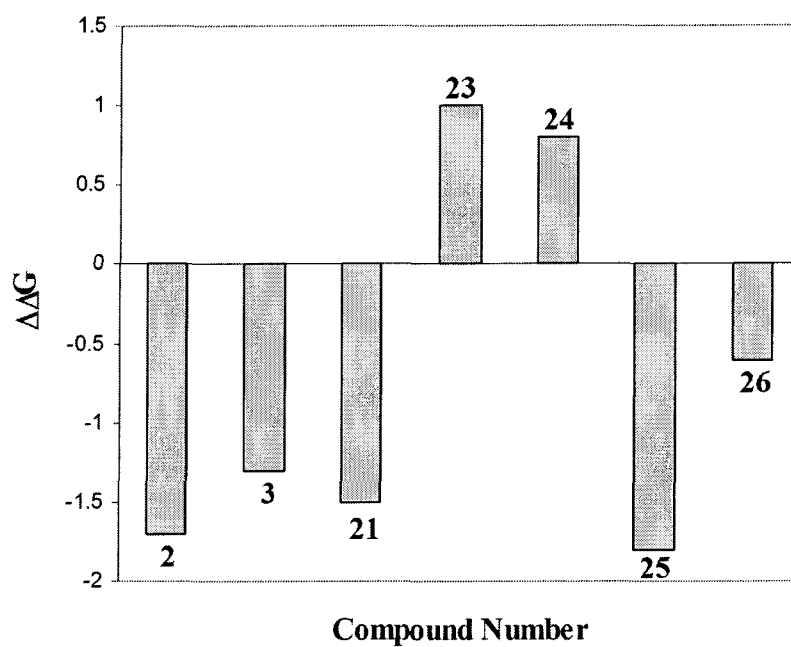
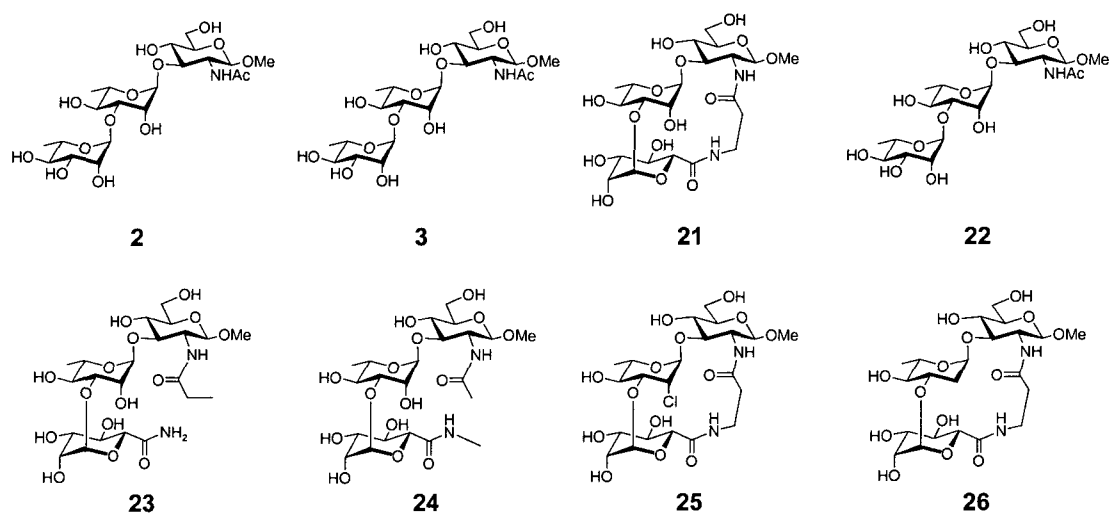


Figure 3.7: *Relative comparisons of the change in free energies of the ligands measured by ITC. Native ligand 22 is not shown as its free energy of binding represents the zero point from which the $\Delta\Delta G$ values (kcal mol⁻¹) are calculated. The differences in free energy are beneficial when negative.*

The summary of binding affinities for all the compounds measured with isothermal titration microcalorimetry is displayed in Figure 3.6. The following chapters deal with the use of molecular dynamics calculations and NMR-based methods to measure and compare the binding modes of the ligands in Figure 3.6. Foremost in this

discussion will be confirming that tethered trisaccharides are pre-organized in their bioactive conformation and do not clash with the protein surface. The flexibility of such ligands are examined by dynamics calculations.

Chapter 4

A Molecular Modeling Investigation of Ligand Flexibility to Understand Binding with Monoclonal Antibody SYA/J6.

4.1. Determining the Conformation of Oligosaccharides in Solution.

4.1.1. NMR Methods.

The overall three-dimensional shape of an oligosaccharide is important for its biological function. The diversity of monosaccharide residues coupled with steric and stereo-electronic factors such the *exo*-anomeric effect somewhat limit the conformation of oligosaccharides in solution, but not enough to allow chemists to predict a single conformation. Conformational analysis leads to an overall picture of the molecule in solution and groupings of key polar contacts of the epitope can help understand the molecular interactions involving protein-carbohydrate recognition.^[7]

Oligosaccharides are now generally regarded as non-rigid molecules.^[61] While the chair structures of individual residues may be considered more rigid due to the energy barrier of inversion, the rotamers of glycosidic bonds can be promiscuous and sample a number of low energy conformations in solution. NMR-based tools of conformational measurement include two-dimensional quantitative correlation of nuclear Overhauser effects (NOE). This technique measures dipolar couplings, and the magnitude is correlated to the average distance between protons. This technique has certain limitations

in that many inter-residue dipolar couplings cannot be quantified due to heavy spectral overlap in the 3.0-4.5 ppm region of the spectrum, leaving few relevant signals. The small size of an average oligosaccharide epitope is typically two to six residues long and the correlation times of many oligosaccharides yield little or no signal in a standard NOE spectrum. In this case rotating-frame Overhauser effects (ROE), which give similar information, can be measured.^[124] The transferred NOE effect has been exploited to give bioactive conformations of oligosaccharide ligands by using an NOE sequence in the presence of protein. As the ligand samples the binding site during the mixing time NOEs are generated and intensities of correlations can be quantified to interproton distances and generate a bound conformation.^[125] The experiment requires moderately high protein concentration, and is useful for a K_A range of 10^3 to 10^6 . Our system was not amenable to this technique, as many of the trisaccharides of interest are at the upper end of this affinity limit, and SYA/J6 readily precipitates above 100 μM

Other NMR-based methods include the association of long-range scalar coupling constants (i.e. $^3J_{\text{COCH}}$) to give an average angle across the glycosidic linkage *via* a Karplus type relationship.^[126, 127] One drawback of NMR measurement is the relatively slow time-scale inherent with the technique. Molecular movements such as rotation and flexibility occur on the nanosecond time scale, while NMR spectroscopy cannot typically measure events occurring faster than the millisecond range.

4.1.2. Molecular Modeling.

Molecular modeling provides a method for examining a calculated conformational model of an oligosaccharide at a much faster time scale, on the order of picoseconds. The software can evaluate the potential energies of an oligosaccharide as it

explores conformational space. A computational force field contains instructions for calculating such energies and includes terms and constraints for such parameters as strain and electrostatics. Several force-fields have been developed for use with carbohydrates and include AMBER,^[128, 129] CHARMM^[130], GLYCAM,^[131] and MM3,^[132] each with unique features. There is no agreement in the literature as to which one provides the most accurate results.

One method for the generation of conformational potential energies of carbohydrates is to systematically vary the angle of each bond from 0 to 360 degrees in the glycosidic linkage. The energy of each conformation is calculated and gives a surface corresponding to potential energies for pairs of dihedral angles. The program GEGOP^[133] uses a hard-sphere *exo* anomeric effect (HSEA) force field to calculate such surfaces. For our pre-organized compounds, methodical rotation of glycosidic bond angles is incompatible, as rotations around the glycosidic linkage cannot be performed due to tethering. We sought to utilize a computational method compatible with all of our ligands of interest that could give us an indication of flexibilities and conformation of our molecules.

4.2. Molecular Dynamics of Trisaccharide Ligands.

4.2.1. Definition of Torsional Angles of Oligosaccharides.

The glycosidic bond angles are dihedrals described by four atoms encompassing the glycosidic oxygen (Figure 4.1). The remainder of the chapter will refer to these angles ϕ^H (HX-CX-OX-CY) and ψ^H (CX-OX-CX-HY), where X refers to the B or C residues and Y refers to the C or D residues, respectively. For simplicity, the

abbreviations ϕ_{BC} , ψ_{BC} specify the linkage between the BC (L-Man- α -(1 \rightarrow 3)-L-Rha or L-Rha- α -(1 \rightarrow 3)-L-Rha) residues, and ϕ_{CD} , ψ_{CD} designate the dihedral of the Rha-GlcNAc linkage. The ω angle is defined as the dihedral between H5''-C5''-C6''-O6''.

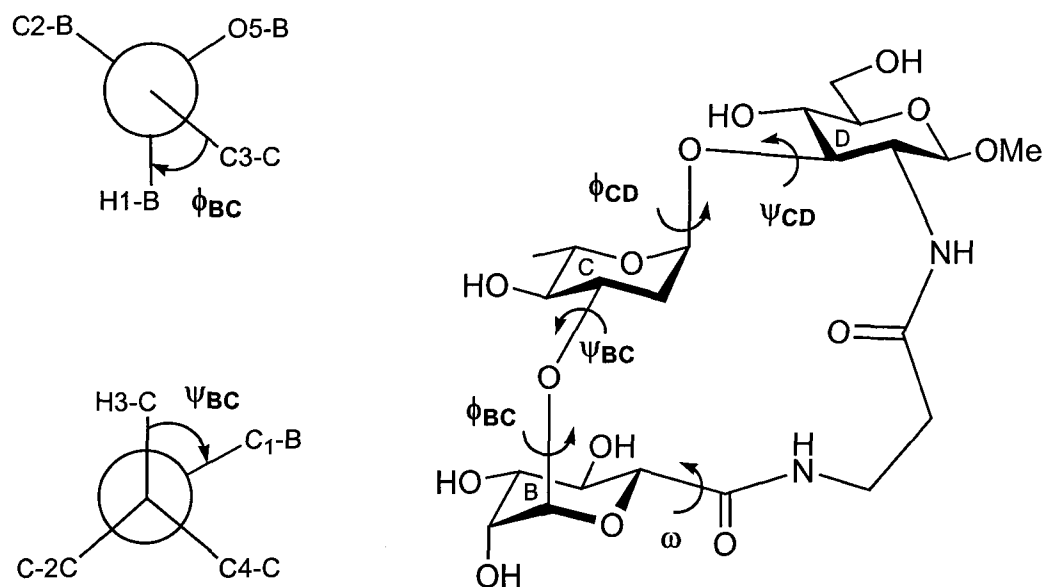


Figure 4.1: *Definitions of glycosidic torsion angles.*

4.2.2. Comparison of HSEA Results with Molecular Dynamics Simulation.

Our intention was to perform molecular dynamics of tethered structures and compare their flexibility to natural structures using Insight II[®] from Accelrys[™] and the AMBER_PLUS force field.^[128] This force field includes parameters supporting aspects of oligosaccharide conformation^[129] and steric parameters to account for L-sugars in the ¹C₄ chair.^[134] Prior to these experiments, the HSEA-based GEGOP program was used to perform an incremental grid search to calculate a potential energy surface for the native trisaccharide. This was conducted by examining the ϕ and ψ angles of the BC and CD disaccharides separately. While this calculation was only performed for the two

disaccharides, it gives a good measure of the potential energy surface for the two linkages.

The starting point for molecular dynamics used the bound conformation of the native trisaccharide removed from the crystal structure with SYA/J6. A potential energy minimization was performed on this structure. The dynamics were run at 450 °K with a dielectric constant of 80 to simulate the presence of water. The experiment allowed the trisaccharide to move for one nanosecond, with four thousand conformations being recorded during the trial. The glycosidic torsional angle was plotted *versus* time (Figure 4.2).

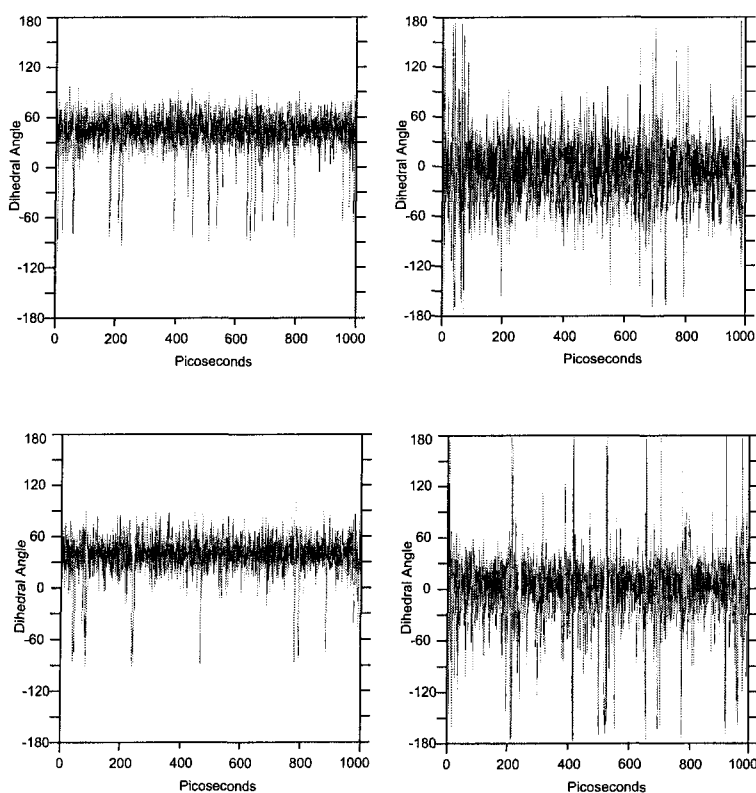


Figure 4.2: The ϕ vs. time (left) and ψ vs. time (right) for the BC (top) and CD (bottom) portions of the native trisaccharide **22**.

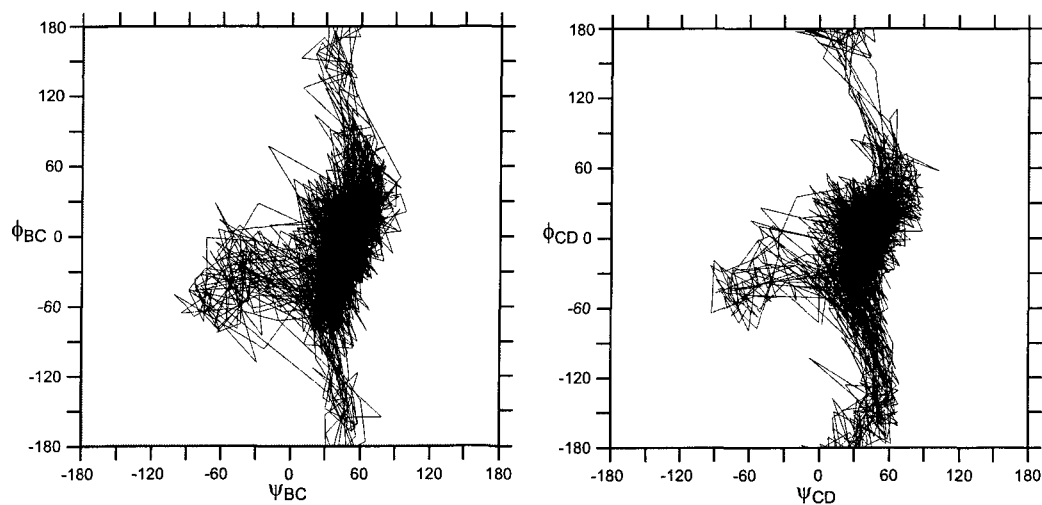
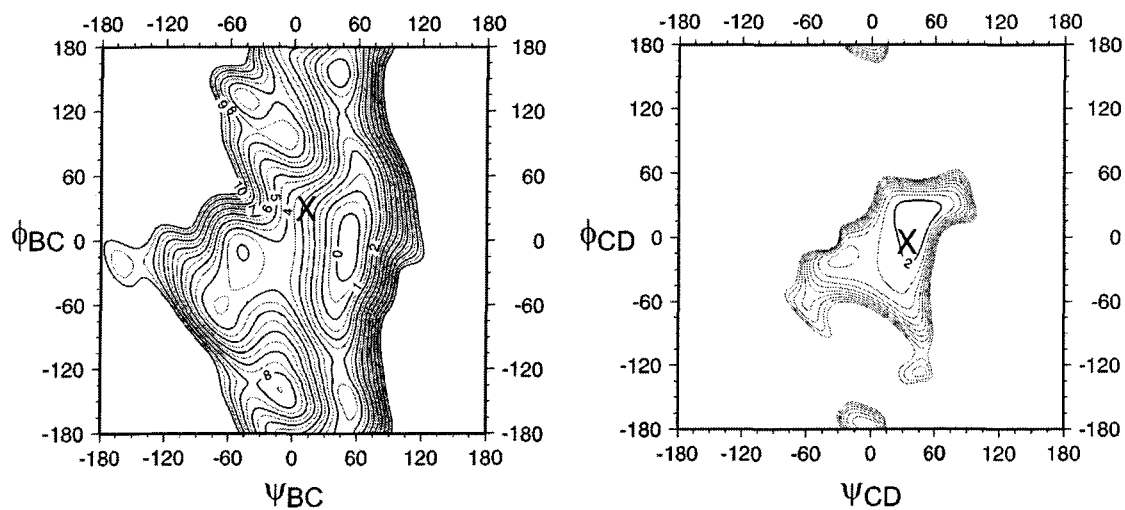
A**B**

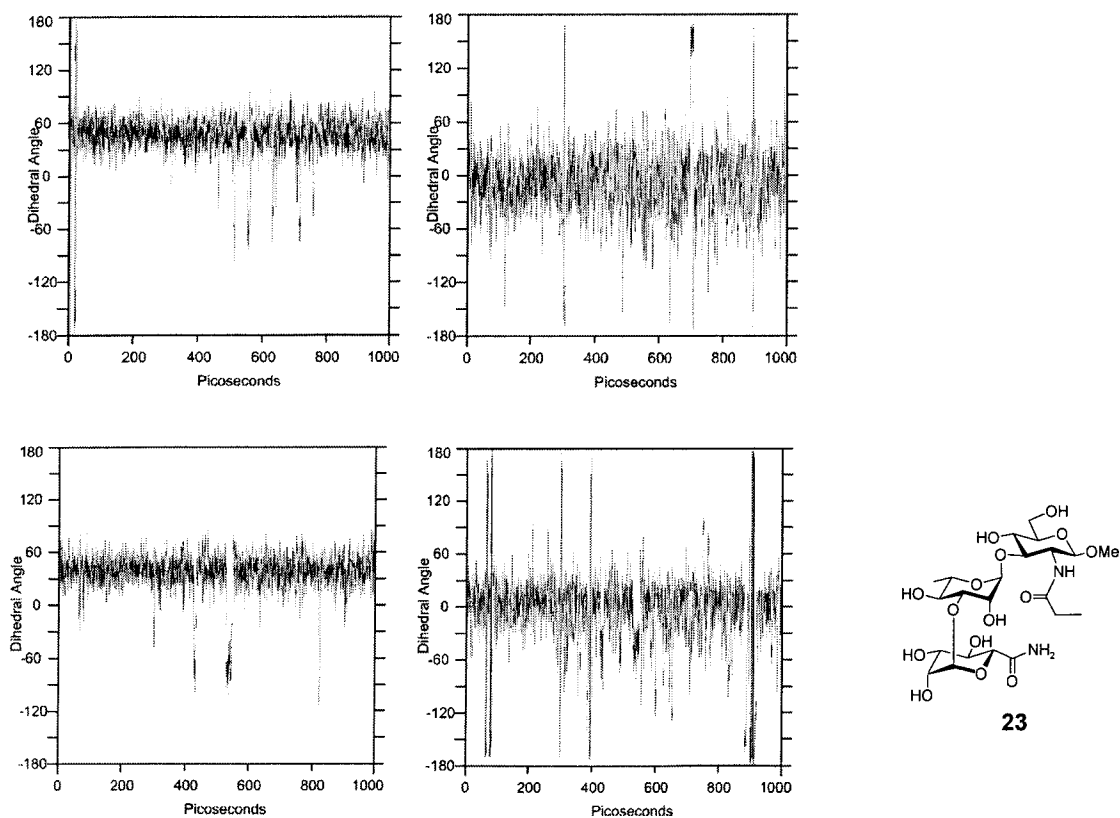
Figure 4.3: Comparisons of the dynamics calculations of native **22** from *Insight II* (A) and potential energy surfaces from GEGOP (B). The GEGOP figures are plotted with 0.5 Kcal increments. The X marks the conformation of bound **22**.

The GEGOP potential energy surfaces match closely to the Insight II derived dynamics plots. Similar results between the two programs encouraged the use of Insight II for the calculation of molecular dynamics for all trisaccharides. Dynamics were not performed with the inclusion of specific water molecules, and thus the ϕ versus ψ plots depicting dynamics may show a broader range of allowable conformation. It has been shown that glycosidic torsion in dynamics simulations were dampened by the presence of explicit water.

4.2.3. Dynamics Calculations of Acyclic Trisaccharides **23** and **24**.

The cyclic derivative of the native structure (**21**) was shown to have a highly constrained geometry, and pre-organized into a conformation very similar to that of the bound BCD trisaccharide (**22**).^[56, 87] The molecular dynamics of non-macrocyclic control trisaccharides **23** (Figure 4.4) and **24** (Figure 4.5) were studied and found to be slightly more flexible about their glycosidic bonds than **22**. This is likely due to the bulk of the synthetically introduced amides at the 6''-position of **23** and **24**. Additionally, the flexibility of the amide at the Man B residue of **23** was explored. The dihedral defined by H5''-C5''-C6''-O6'' was calculated to have no defined conformational preference (Figure 4.5). The B residue amides of **23** and **24** are considerably more bulky than the methyl group native to the 6''-position. The amides are also hydrogen bond donors and acceptors and it is likely that one or both of these factors causes them to bind with a four-fold reduction in binding affinity compared to native **22**. Additionally, the methyl groups of the amides of **23** and **24** may have contributed to hydrophobic interactions with protein.

A



B

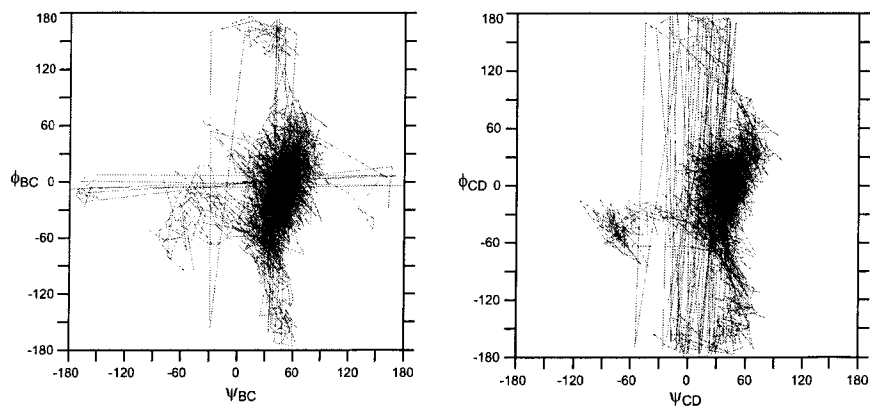
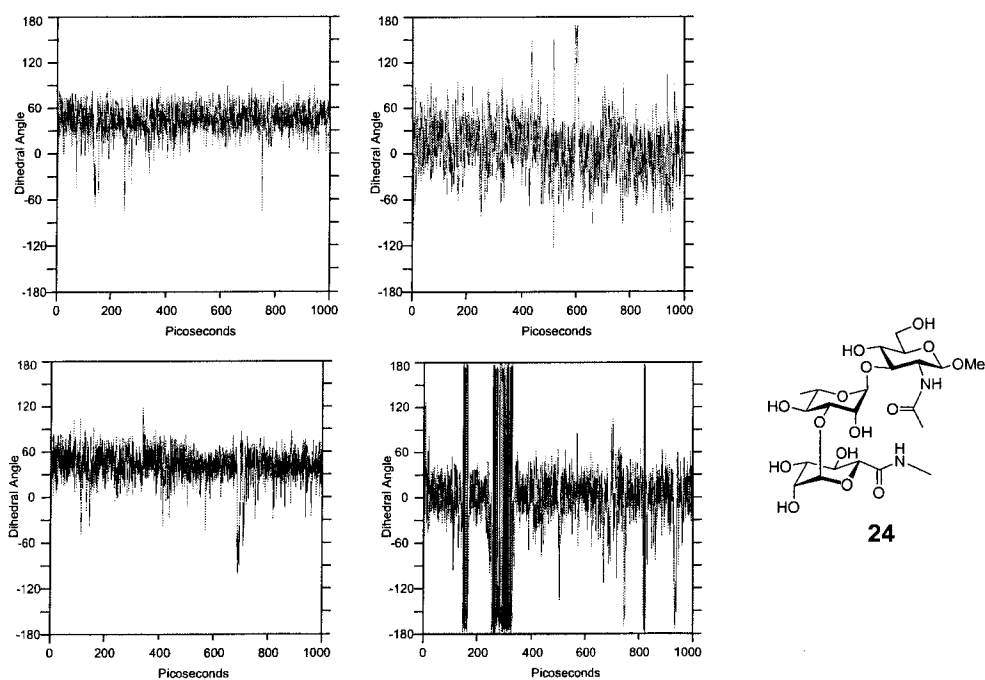


Figure 4.4: Molecular dynamics for **23**. (A) The plots of ϕ and ψ versus time for the BC glycosidic bond (top) and the CD glycosidic bond (bottom). (B) The plot of ϕ versus ψ for each linkage.

A



B

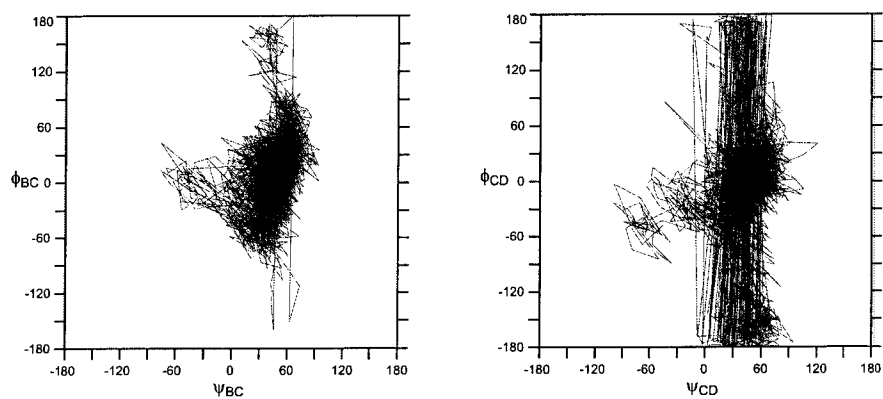


Figure 4.5: Molecular dynamics for 24. (A) The plots of ϕ and ψ versus time for the BC glycosidic bond (top) and the CD glycosidic bond (bottom). (B) The plot of ϕ versus ψ for both linkages.

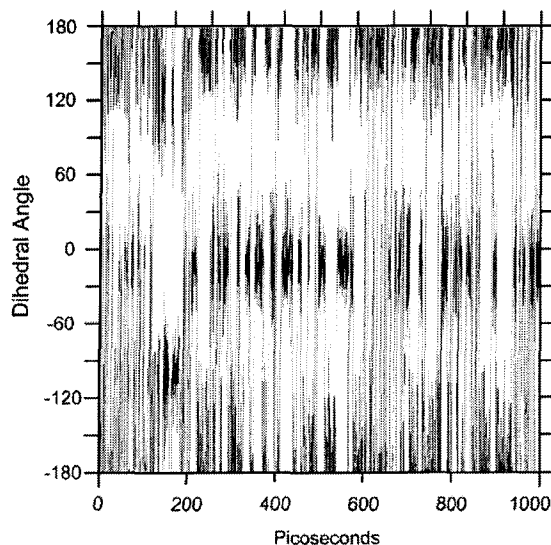


Figure 4.6: *The calculated conformation of the ω angle of 24.*

4.2.4. Conformation of the 2'-Chloro-2'-Deoxy Cyclic Trisaccharide.

The AMBER_PLUS force field does not have support for a covalent carbon chlorine bond, and is only capable of assigning potentials for an ionic chlorine atom. Therefore, the molecular dynamics of cyclic 2'-chloro-2'-deoxy **25** could not be performed. It has been demonstrated that the solution conformation of macrocycle **21** closely resembles that of the bound native trisaccharide and the substitution of a chlorine atom for a hydroxyl would not likely cause a dramatic change in conformation. GEGOP was used to examine the potential energy surfaces for the BC and CD disaccharides corresponding to the 2'-chloro-2'-deoxy derivative **3**.

Because the calculated surfaces are very similar, we can conclude that **3** is in a very similar conformation as native trisaccharide **22**. Additionally, cyclic-chloro

derivative **25** should be pre-organized in a conformation very similar to that of cyclic **21** and the bound native BCD trisaccharide. Figure 4.6 compares the potential energy surfaces of **3** and **22**. The molecular dynamics of macrocyclic **21** were re-calculated to show its highly constrained conformational nature and are shown in Figure 4.7. It is likely **25** has similar conformational properties.

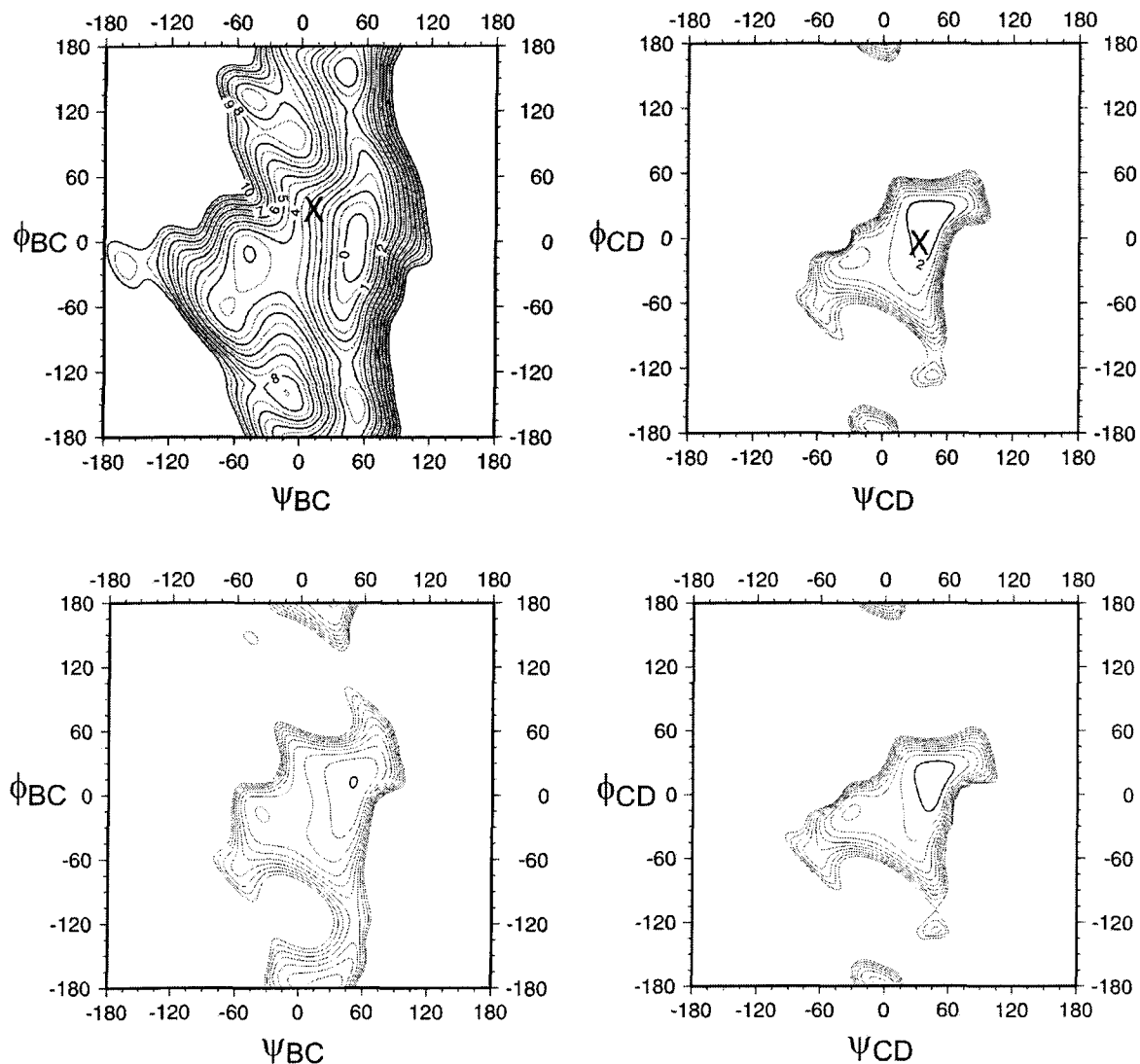


Figure 4.7: The potential energy diagrams for native **22** (top) and the 2'-chloro-2'-deoxy BCD derivative **3** (bottom). The *X* marks the conformation of bound **22** from crystal structure data.

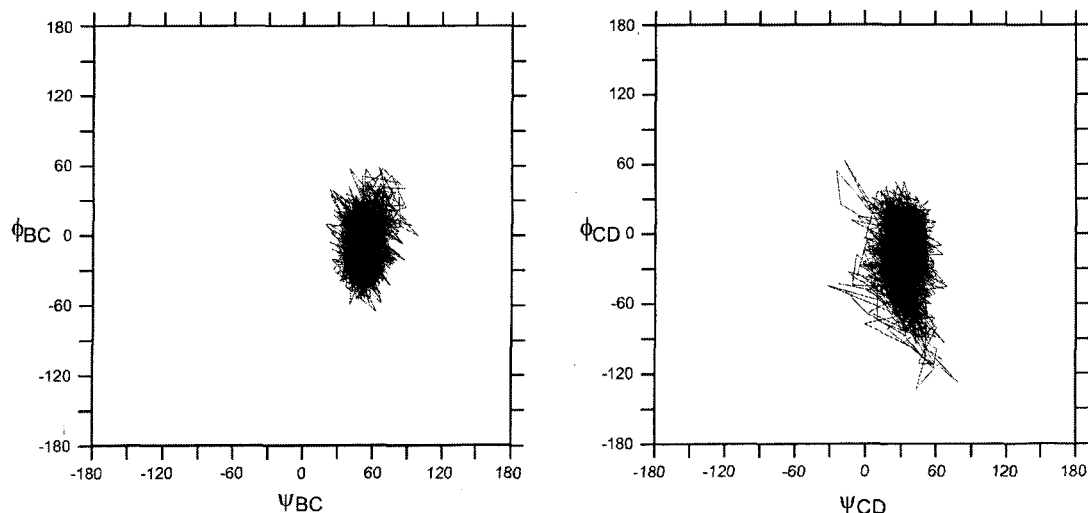


Figure 4.8: *Molecular dynamics calculations for macrocyclic 21.*

4.2.5. Calculated Conformation of Tethered 2'-Deoxy Trisaccharide 26.

The dynamics of 2'-deoxygenated **2** were calculated and the results are displayed in Figure 4.9. It is apparent that the ψ angle of the CD glycosidic bond is considerably more flexible than the native trisaccharide. The dynamics calculations of deoxygenated cyclic **26** were also performed and found to have a restricted conformation compared to its parent structure, 2'-deoxygenated trisaccharide **2** (Figure 4.9). The calculated ϕ and ψ angles of the BC glycosidic bond indicate a reduced degree of torsion compared to compound **2**. Similarly, the tether considerably restricts the CD glycosidic bond although the ψ_{CD} angle is somewhat more mobile than the others. The global energy minimum structure of **26** was superimposed on the extracted structure of **2** from the binding site of SYA/J6. This is illustrated in Figure 4.10 along with the glycosidic torsion angles of the bound trisaccharide and simulated conformation. Both structures are in very close conformation.

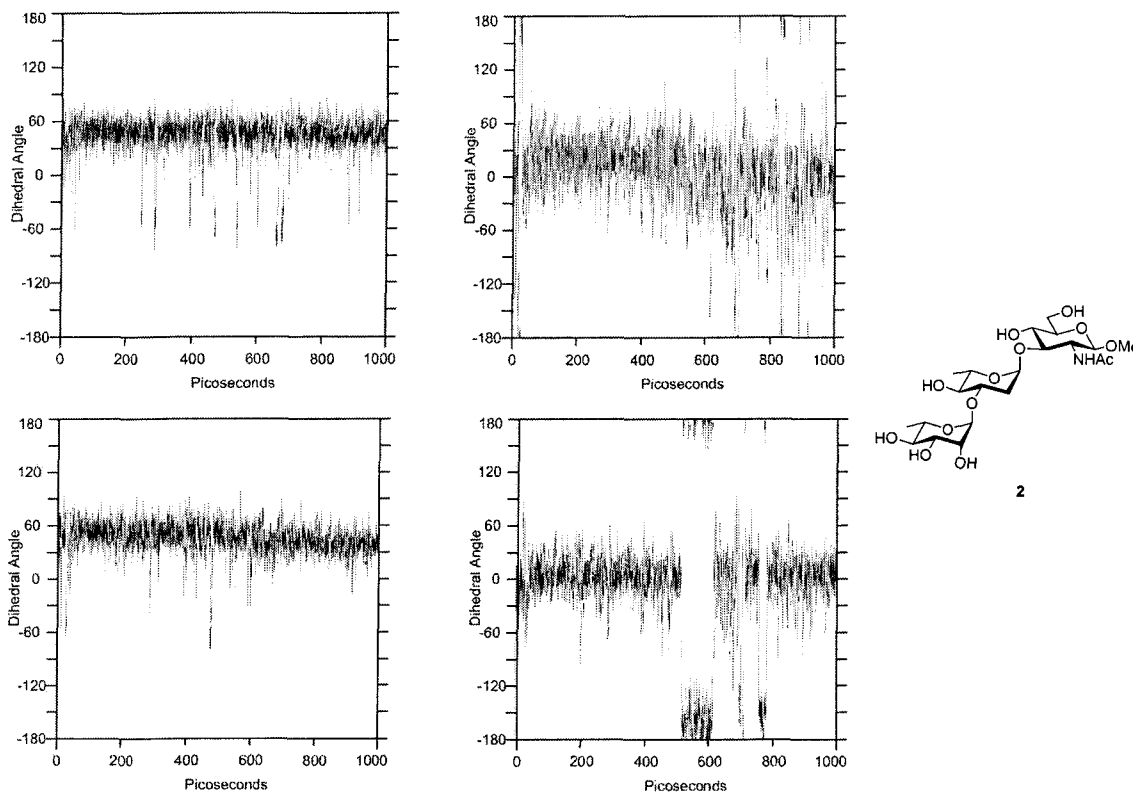
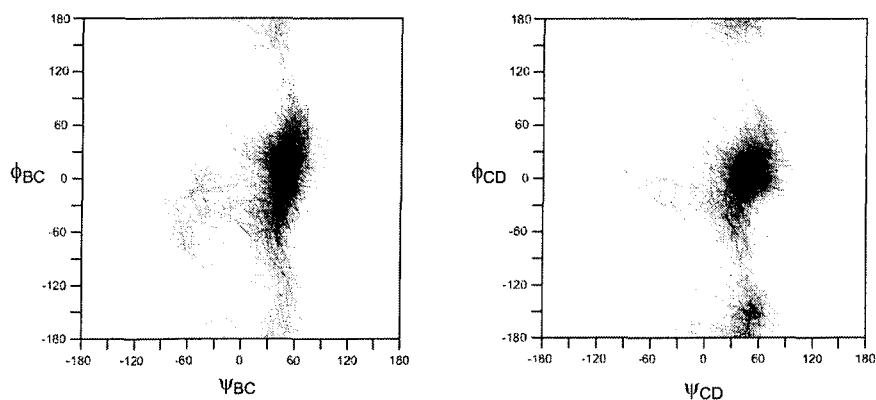
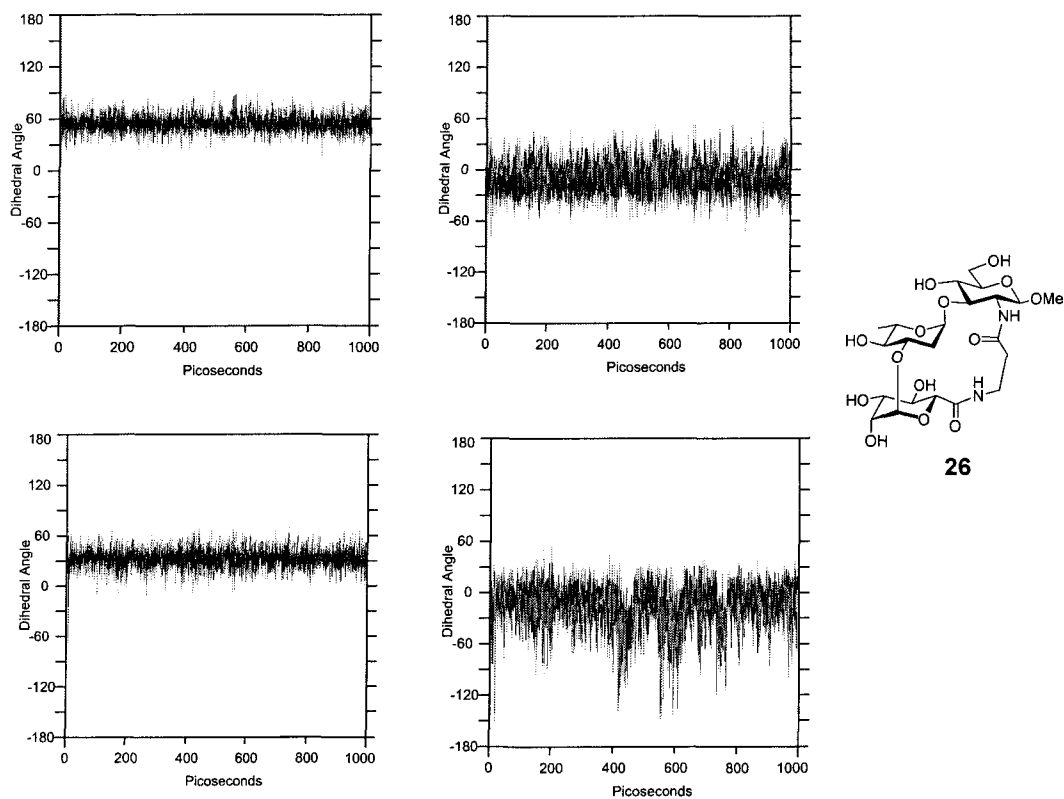
A**B**

Figure 4.9: ϕ and ψ torsional diagrams for compound 2. (A) ϕ versus time (left) and ψ versus time (right) for the BC (top) and CD (bottom) glycosidic bonds. (B) ϕ versus ψ for 2.

A



B

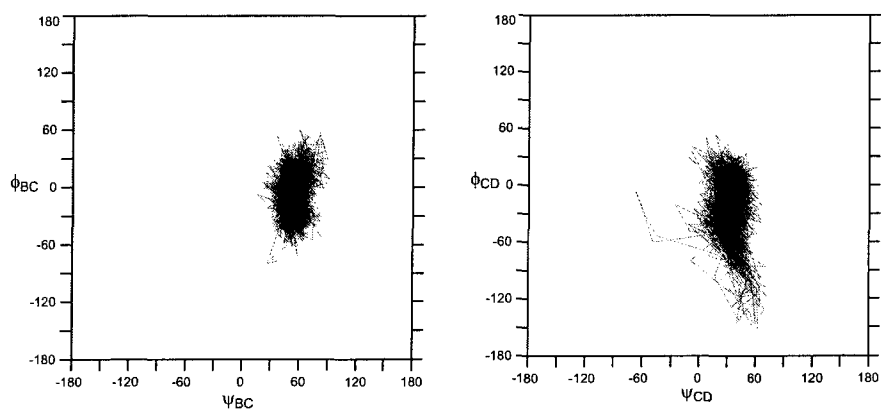
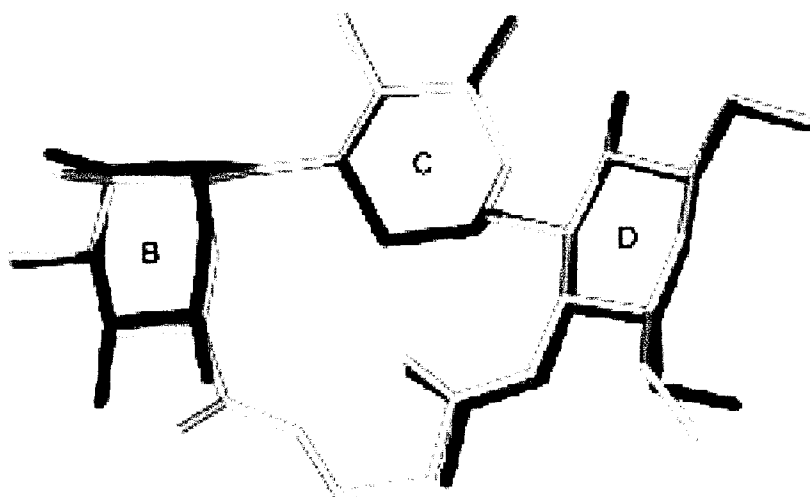


Figure 4.10: ϕ and ψ torsional diagrams for compound 26. (A) ϕ versus time (left) and ψ versus time (right) for the BC (top) and CD (bottom) glycosidic bonds. (B) ϕ versus ψ for 26.



Linkage	Rha- α -(1,3)-Rha		Rha- α -(1,3)-GlcNAc	
	ϕ	ψ	ϕ	ψ
Bound 2 (x-ray data)	56.48°	-8.49°	38.99°	7.26°
Calculated 26	53.59°	-18.24°	41.80°	-2.48°

Figure 4.11: The global energy minimum (1000 ps) of **26** (yellow) superimposed on the bound structure of **2** (magenta).

One measure of the flexibility of cyclic **26** was visualized at the amide of the 6''-position of the Man B residue. The dihedral defined by H5''-C5''-C6''-O6'' was measured from the dynamics simulation (Figure 10). It was found that this angle was more promiscuous than the glycosidic angles of trisaccharide **26** and had maintained an average angle of -160° throughout the dynamics simulation.

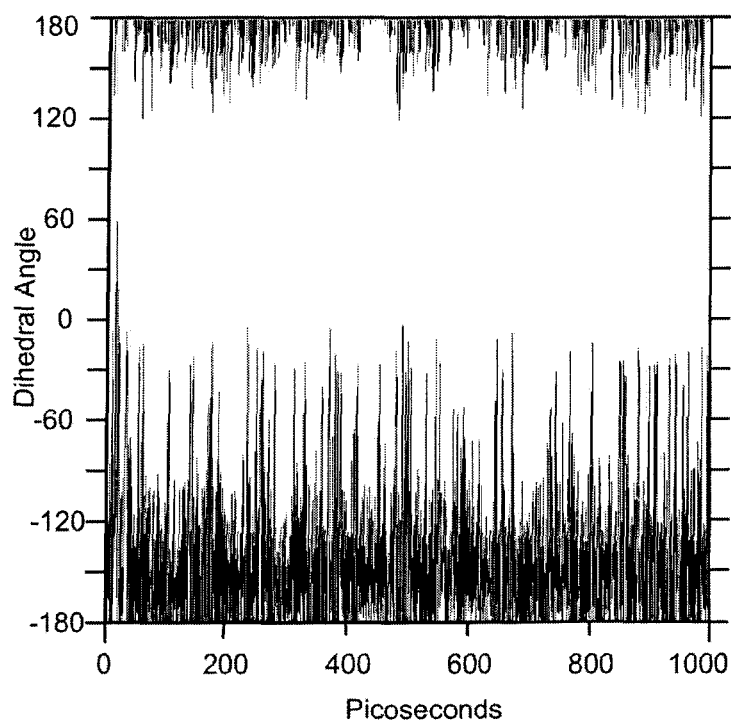


Figure 4.12: Molecular dynamics of rotation around the C5''-C6'' bond, ω .

4.3. Docking of **26** into the SYA/J6 Binding Site.

The molecular dynamics simulations do not appropriately explain the lower than expected binding affinity of **26** despite effective pre-organization in a fashion quite similar to the bound conformation of **2**. To deduce the nature of the incompatibility between the intramolecular tethering and deoxygenation at the 2'-position, the global energy minimum of **26** was docked into the binding site of SYA/J6. The central rhamnose C residues were superimposed, and compound **2** was removed from the binding site for clarity. Inspection of this simple docking is only valid if **2** and **26** bind in

the same mode, and although this is a static image of the complex, a steric clash of the tether with the protein surface would be evident. Figure 4.13 and 4.14 show various views of the docked 26-SYA/J6 complex. The binding site encompasses the ligand, but the tether is close to the protein surface. It is known that the 2'-deoxygenated 2 sinks deeper in the binding site. The preferred orientation of bound 2 could bring the tether into contact with the protein surface. A shift in binding mode would explain the observed ITC measurements and be consistent with disrupted contact with the protein surface.

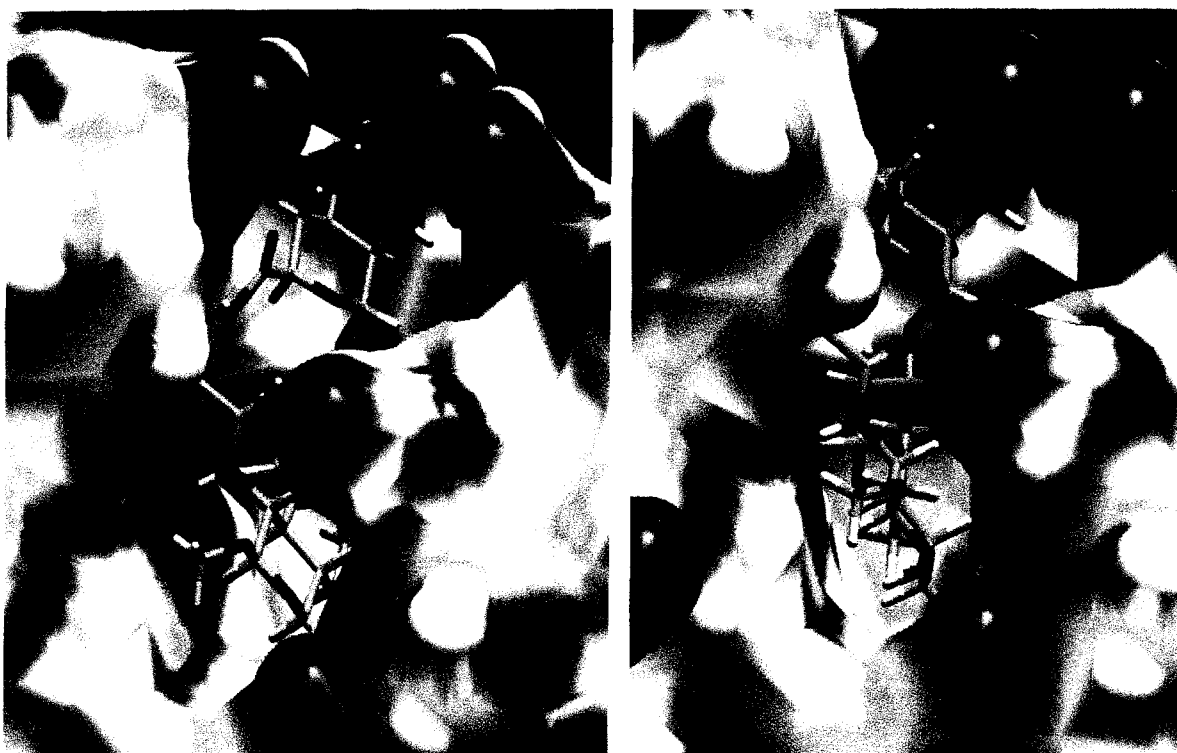


Figure 4.13: *A view of docked 26 in the SYA/J6 binding site with both the protein and 26 are colored by atom. The antibody is rendered as a high-detail Connolly surface.*

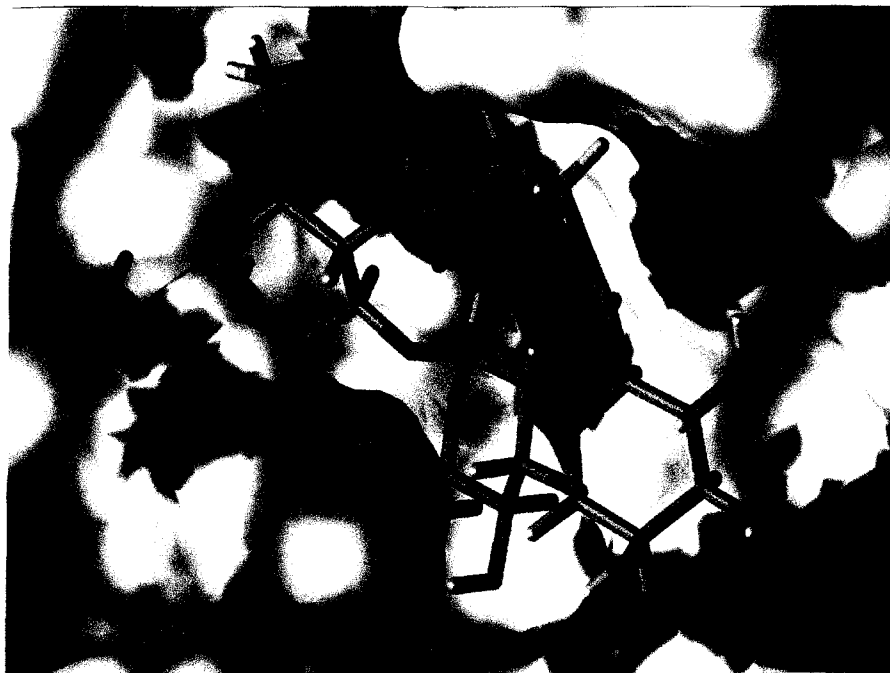


Figure 4.14a: *Additional views of docked 26 with SYA/J6. In the above picture, carbon and hydrogen are both colored white.*

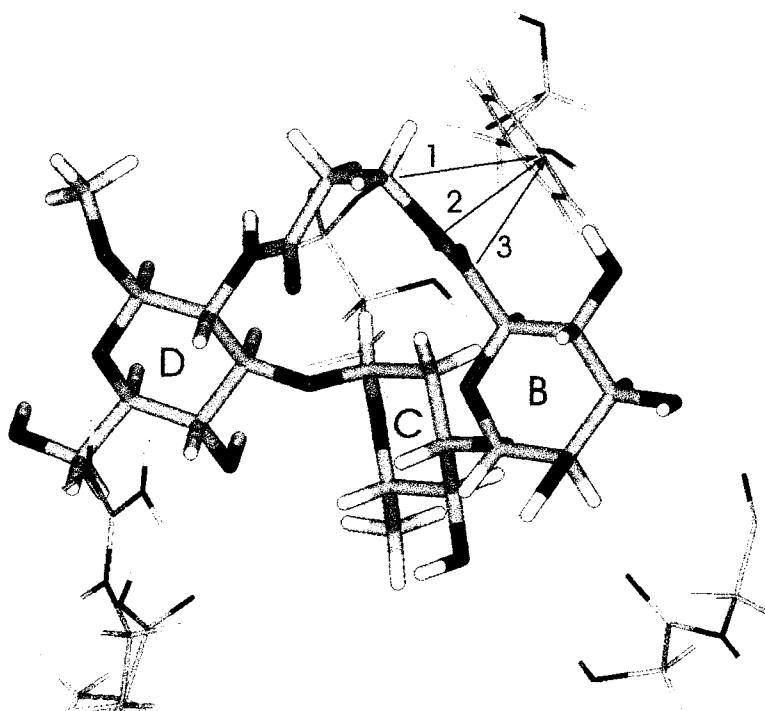


Figure 4.14b: *A stick rendition of macrocyclic 26 docked with SYA/J6 viewed in the same orientation as 4.14a. Selected amino acid residues making polar contacts to the original ligand (2) are included. Selected interatomic distances between the tyrosine oxygen and tether heavy atoms 1, 2 and 3 are respectively 3.3, 2.8 and 3.0 Å.*

Figure 4.14b depicts the stick model of **26** docked with SYA/J6. Arrows 1, 2, and 3 represent the distances between the propionamido carbon of the tether (β to the carbonyl), the nitrogen and carbonyl carbon atoms of the Man B-residue amide. The distances to the phenolic oxygen of the adjacent tyrosine residue (L32) are 3.3, 2.8 and 3.0 Å respectively. This distance is within the limit of a possible van der Waal's contact between the tether and the aromatic ring, and could be a possible cause for altering the binding mode of **26**. Additionally, the polar atoms of the amide could form hydrogen bonds with the phenol of Tyr L32, causing a shift in the side chain thereby disrupting the optimal mode of binding.

Dynamics calculations depict an increased flexibility for acyclic control trisaccharides **23** and **24** that are consistent with a lower binding affinity as measured by ITC. While dynamics calculations of macrocyclic 2'-chloro derivative **25** were not feasible, the HSEA-based GEGOP indicates that the substitution of a hydroxyl for chlorine does not drastically alter the solution conformation of linear trisaccharides, as seen for native **21** and 2'-chloro **3**. The dynamics simulations do not readily explain the lower than expected affinity of cyclic 2'-deoxygenated **26** or the slight degree of additivity seen for the pairing of intramolecular tethering and 2'-chloro-2'-deoxygenation in the case of **25**. The simulations indicate that macrocycle **26** exhibits a calculated solution conformation consistent with the bound conformation of **2** with SYA/J6, but simple docking analysis reveals the possibility of a lipophilic stabilization or polar contact with an adjacent tyrosine residue that could alter the binding mode of **26**.

Chapter 5

Qualitative Comparison of Trisaccharide Binding Modes

Using Saturation Transfer Difference NMR

5.1. Detecting Binding with NMR Techniques.

The molecular events that occur during the binding process of a small molecule ligand and protein receptor are crucial for the design and development of improved drugs and therapeutic agents. NMR studies and x-ray crystallography have been of critical importance to shed light on aspects of protein-carbohydrate interactions. The process of co-crystallization with ligand solutions has provided a number of oligosaccharide-bound crystal structures.^[51-53, 135-138] Co-crystallization can be problematic, as many proteins do not crystallize in ligand soaked solution, as multiple binding modes of ligands disrupt the crystal lattice. NMR methods for determining ligand binding, or the epitope thereof, have been of great interest, especially with respect to the drug industry.

NMR-based methods have been used to detect binding since the early 1970's.^[139-141] Numerous methods have been designed to identify binding and the amino acid residues of the receptor.^[142] Identifying the portion of the ligand in contact with the protein using NMR can be a more difficult task. Methods have focused on chemical shift changes or line broadening upon of the ligand upon binding.^[143] Two methods have emerged to define the epitope map of ligands of smaller size: Water-LOGSY,^[144, 145] and saturation transfer difference (STD)-NMR.^[146, 147] Many ligands bind to protein while still partially exposed to water molecules or *via* water-mediated hydrogen bonds. The

water-LOGSY experiment was designed to use bulk water to detect the binding of ligands to proteins. STD-NMR was used in this study, and relies on selective irradiation of protein that is transferred to a binding ligand that is subsequently detected. Both methods are robust and do not require isotopically enriched protein receptors.

5.1.1. General Features of the Saturation Transfer Difference NMR Technique.

The saturation transfer difference (STD) NMR technique was developed in 1999 by Mayer and Meyer.^[146] The basic STD-NMR spectrum is a one-dimensional (1D) spectrum of ligand resonances and involves saturating the protein resonances with radio frequency energy that is transferred to a binding ligand (Figure 5.1). Difference spectroscopy is used to measure the intermolecular transfer of energy. The intensities of individual ligand peaks arise from the amount of magnetization transferred between the protein surface and ligand contacts, thereby giving a map of the epitope. The exploitation of the fast T_2 relaxation of larger molecules effects this fast saturation of the protein.^{[147,}
^{148]} STD-NMR can be used to screen mixtures of components provided that the numbers of potential binding components in solution do not produce severe spectral overlap.^[149] Binding components are clearly visible as non-binding compounds are effectively subtracted from the spectra.^[142]

The technique can be performed with as little as one nmol of protein with a mass greater than 10 kDa. Typically, a 100-fold excess of ligand is used to maximize signal to noise and the population of the bound state. This allows protein concentrations to be in the low μM range.

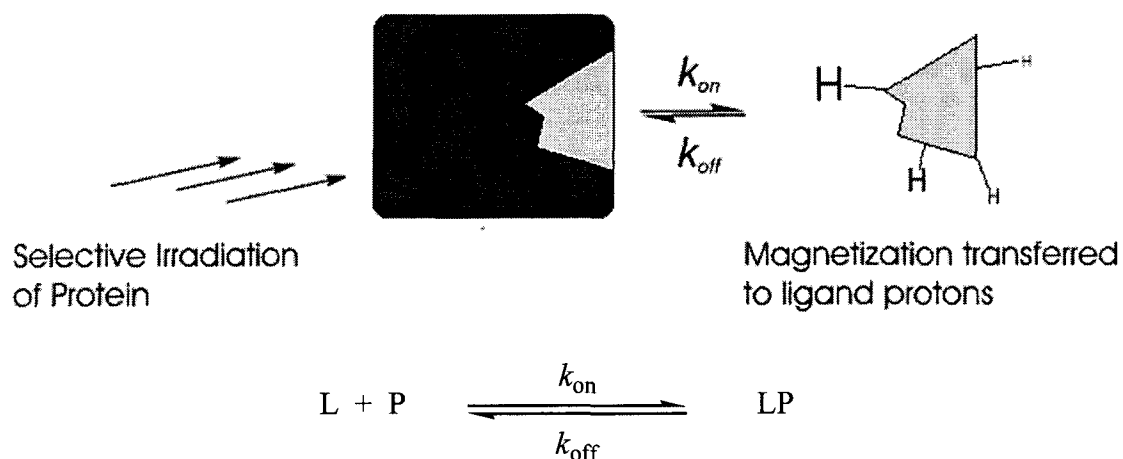


Figure 5.1: A cartoon representation of the STD technique. The protein is selectively saturated with energy that is transferred to the ligand to differing extents based on its proximity to the protein surface when bound.

The intensity of the peaks ultimately depends on the off rates of the ligand where k_{on} and k_{off} represent the rates of association and dissociation of a ligand with its receptor (Figure 5.1). The practical application of this kinetic information is correlated to K_D values. If the association is of lower affinity (10^{-3}), the ligand may not contact the protein for a sufficient period of time for magnetization transfer to occur. Additionally, if the K_D is stronger than 100 nm, the chemical exchange of ligand is slow on the NMR time-scale, and ligand is not released for detection. Competition STD-NMR has been developed for tighter-binding ligands (greater than 10^{-8}) and uses a ligand of known affinity as an internal standard and titrations of the higher-affinity ligand can provide an estimate of K_D and the epitope map. An additional advantage of the STD-NMR method is that the protein and ligand do not require isotopic labeling, thus saving the time and expense, and increasing throughput efficiency. The spectra can be acquired within minutes or hours depending on protein concentration and the affinity the binding partners.

5.1.2. Specific Features of the STD-NMR Experiment.

The essence of the STD-NMR experiment is the successive alternation of gathering saturation transfer data (on-resonance), followed by the acquisition and subtraction of a control spectrum (off-resonance), where the protein is not saturated. The saturation of protein resonances is applied as a cascade of selective gradient pulses at frequencies well removed from those of the ligand. Larger proteins typically have proton resonances ranging from negative parts per million (ppm) region to greater than 10 ppm. Placement of the selective on-resonance cascade is within the region of the protein resonances but sufficiently removed from ligand resonances to eliminate direct irradiation of the ligand. The total duration of selective irradiation can be as little as 250 ms. Signal-to-noise increases with longer magnetization times but doing so for longer than two to three seconds can produce unreliable epitope maps. These inaccuracies are due to the non-uniformity of T_1 proton relaxation of the ligand. The selective pulse requires no ligand resonances be within a minimum of ± 1 ppm. Due to the selectivity of the on-resonance pulse, STD-NMR has been used to study carbohydrates, glycopeptides, peptides and drug-like substances such as heterocycles and aromatic compounds.^[142, 147, 150-157] Initial attempts to utilize STD-NMR were not successful, and it was concluded that the power of the selective pulse was too low.^[158] The selective cascade was arbitrarily set to repeat 30 gradient pulses, each of 50 ms in duration, for a total magnetization time of approximately 1.5 seconds.

Following the on-resonance irradiation of the protein, a full sweep width 90° pulse is applied. This affects all resonances in the spectrum, and is termed a “read pulse”. The effects of saturation transfer on the ligand are small, and this is necessary for

proper subtraction of data. The remainder of the pulse sequence consists of a spin-lock pulse ($T_1\rho$ filter) that is applied to erase signals arising from the broad protein resonances, followed by water suppression and recording of the free induction decay (FID).

The subtraction of on-resonance from off resonance data is performed automatically by the Varian, Inc. spectrometer, generating a single FID for the STD spectrum. A separate reference spectrum is generated to measure the relative intensities of the STD spectrum. The reference is essentially a one-dimensional spectrum of the ligand, recorded using the same sample. This process uses the STD-NMR pulse sequence and therefore, the amount of time taken per scan is the same. Acquiring the reference spectrum in this fashion is the method most consistent with the STD-NMR data, as the T_1 relaxation times of the protons can range from less than a second to several seconds.^[159] To acquire a reference spectrum the difference function is turned off. No data will be subtracted on successive scans. The on-resonance and off-resonance pulses are now set to the same frequency (30 ppm). Because there are no protein resonances in this spectral region, no saturation transfer will occur. The number of scans used for the reference is divided by two, as there is no alternation and subtraction of on-resonance/off resonance. The 90° read pulse generates signal for the ligand in the same fashion as described before, and the $T_1\rho$ and water suppression remain the same.

The Varian VNMR[®] software is used to measure the intensities of both the STD and reference spectra. The absolute intensity is measured *via* a linear vertical scale and only resonances that have no overlapping signal can be measured. The intensity of

individual peaks are converted to the same vertical scale and are then converted to STD amplification factors (η) via the following equation:

$$\eta = I_0 - I_{\text{sat}} / I_0 \times \text{ligand excess}$$

where $I_0 - I_{\text{sat}}$ is the intensity of the saturation transfer effects from the difference spectra and I_0 is the intensity of the same peak in the reference spectra. Amplification factors are then represented as percentages, and the highest value is normalized to 100%. All other amplification factors are scaled by the same normalization parameter, and are then used to describe the epitope map.

This chapter describes the first use of the STD-NMR technique at the Department of Chemistry at the University of Alberta. The programming and compiling of the pulse sequence was performed by Dr. Albin Otter, and a visiting professor, Dr. Thomas Peters, was available for expert technical advice. It was under their guidance that the optimization of this pulse sequence was conducted, and will be described in further detail.

5.2. Optimal STD-NMR Pulse Sequence Parameters.

Considerable time was spent optimizing parameters of the STD-NMR pulse sequence for use with *S. flexneri* trisaccharide congeners. The position and selectivity of the selective protein saturation cascade must be placed far enough from ligand signals so they were not directly irradiated. Also, some resonances for the anomeric proton resonances fall extremely close to the HOD signal (~ 4.8 ppm), and therefore the pulse width of the water suppression sequence was optimized to be as narrow as possible, at the precise resonance of the HOD signal. The water suppression is done using the gradient-

tailored excitation method (WATERGATE W5).^[160] Figure 5.2 shows the STD-NMR pulse sequence.

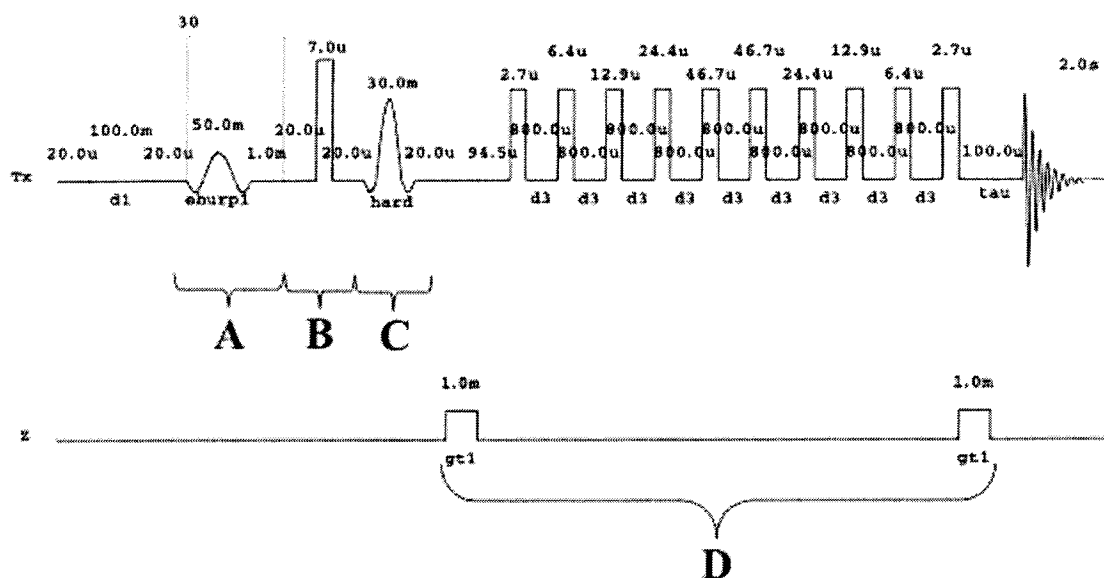


Figure 5.2: The STD-NMR pulse sequence. (A) The selective irradiation cascade. Set to 7.0 ppm for the on-resonance and 30.0 ppm for the off-resonance pulses. (B) The 90° read-pulse. (C) The $T_{1\rho}$ filter. (D) The WATERGATE W5 water suppression sequence. Times are measured in units of s (seconds), m (milliseconds) or u (microseconds).

5.2.1. Placement of the Selective On-Resonance Pulse Cascade.

Solutions of ligand in deuterium oxide were subjected to the STD pulse sequence to determine the position where the selective cascade (A, Figure 5.2) would not irradiate ligand signals. Arrays of spectra were acquired using the gaussian pulse profile at both the aromatic (Figure 5.3) and aliphatic region (Figure 5.4). Any visible ligand peaks are the result of direct irradiation from the selective pulse. While 8.0 ppm was deemed satisfactory for the irradiation of the aromatic SYA/J6 protons, it was preferable to set

this value closer to 7.0 ppm, as the 1D spectrum of the protein showed more aromatic resonances at this chemical shift. Irradiation of the aliphatic region was not feasible due to the direct magnetization of the ligand protons at 1.3 ppm. Even when the selective pulse was placed as far away as -2.0 ppm, direct irradiation of the ligand was detected, and this chemical shift near the upfield boundary for aliphatic protein resonances.

It was envisioned that changing the shape of the gradient pulse could increase the selectivity of the on-resonance pulse. The E-BURP-1 pulse profile is known to be an extremely selective pulse with a narrow width. The arrays portrayed in Figures 6.3 and 6.4 were re-acquired using the E-BURP-1 profile. Repeating the experiments described for the gaussian profile showed ligand resonances are no longer irradiated when the selective pulse was placed at -2.0 ppm, but again, this is an outer limit for protein saturation. Arrays of on-resonance pulses in the aromatic region show the E-BURP-1 is selective enough to allow the on-resonance frequency to be set at 7.0 ppm, the most intense region of aromatic resonances in the 1D ^1H NMR spectrum of SYA/J6 (Figure 5.5 and 6.6).

The y-axes of Figures 5.3 to 5.6 are labeled as absolute spectrometer frequency (in Hz). The arrays of individual spectra have their on-resonance pulses moved by 300 Hz (0.5 ppm) increments. For arrays in the aliphatic region, -3000 Hz corresponds to 0 ppm, and -4200 Hz is -2.0 ppm. The aromatic region shows arrays from 8.5 ppm (2065 Hz) to 6.5 ppm (865 Hz). The arrays were recorded using the full STD pulse sequence with native trisaccharide **22** in deuterium oxide was used as the sample, with no SYA/J6 protein present. When direct irradiation of the ligand has taken place, peaks nearest the selective pulse are seen in varying intensity depending on the distance to the pulse. Other

resonances that are intense and sharp in the 1D spectrum are seen. The appearance of these peaks are artifacts from inefficient subtraction of data acquired from on- and –off resonance pulses.

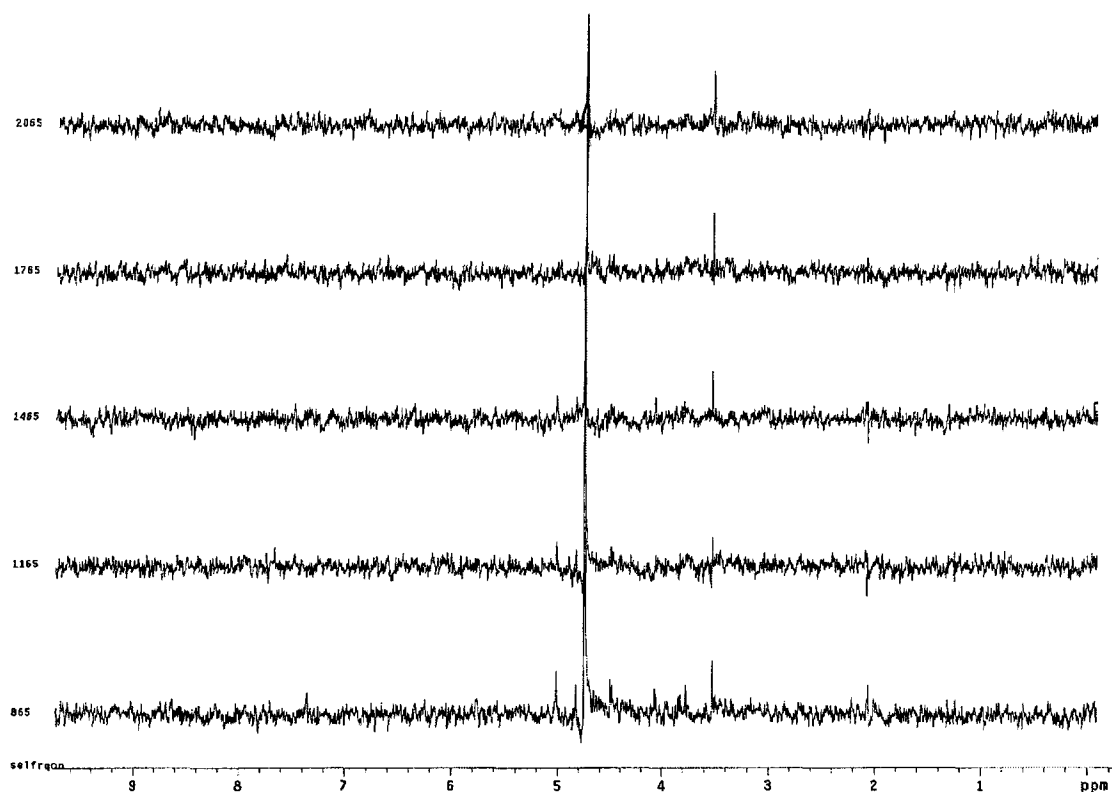


Figure 5.3: *Array of the gaussian on-resonance pulse in the aromatic region. Note the direct irradiation of anomeric proton signals (5.0 ppm) occurring until the placement of the on-resonance pulse was greater than 1765 Hz (8.0 ppm, second spectrum from top)*

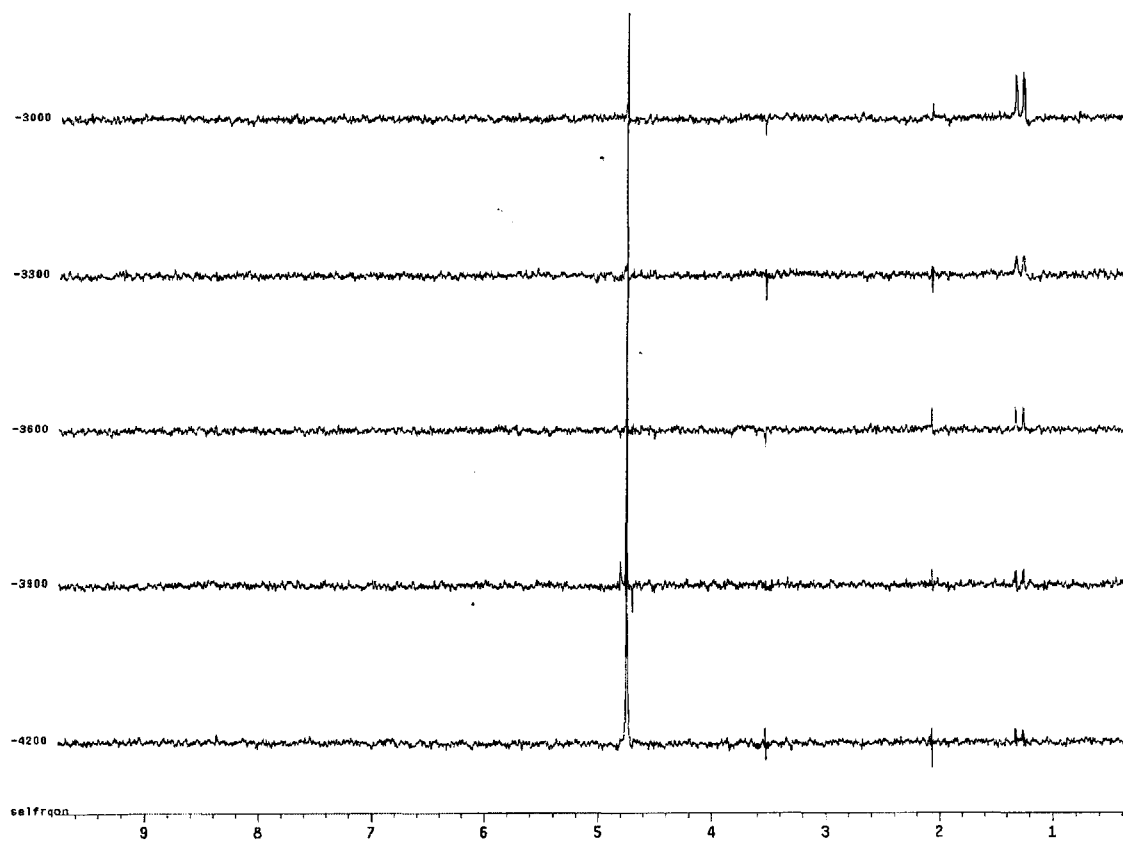


Figure 5.4: Array of the gaussian on-resonance pulse in the aliphatic region. The selective pulse cascade ranged from -3000 Hz (0 ppm, top spectrum) to -4200 Hz (-2 ppm, bottom spectrum). Strong irradiation of ligand methyl groups is seen at 1.25 ppm when the selective pulse was placed as far away as -4200 Hz (-2.0 ppm).

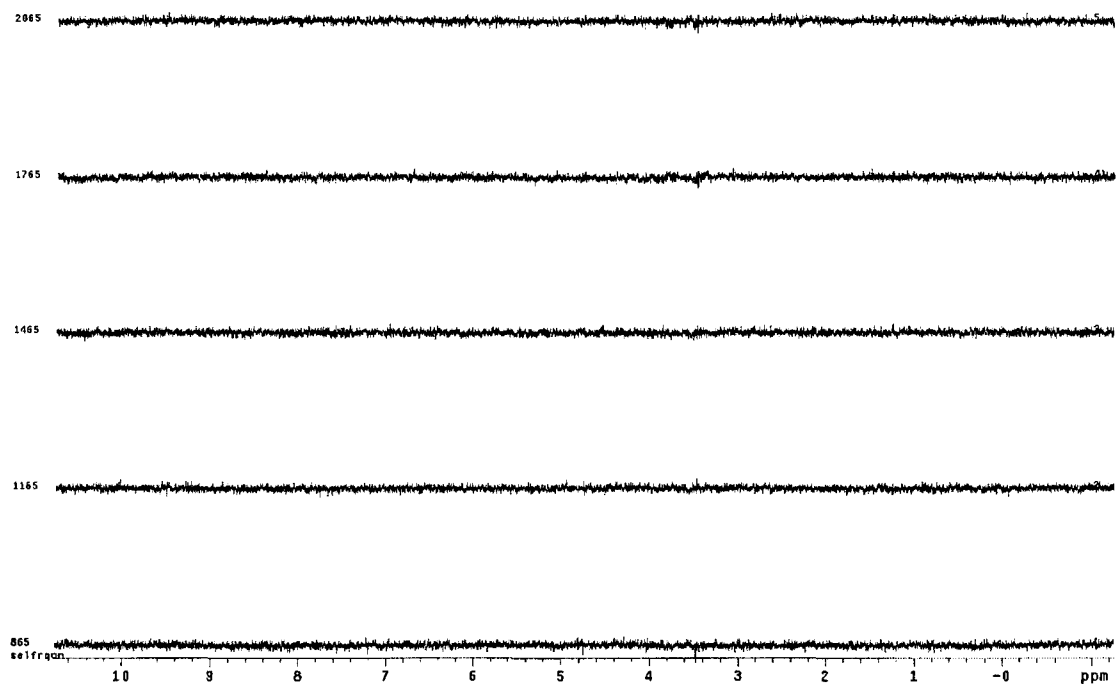


Figure 5.5: Array of the on-resonance pulse using the E-BURP-1 pulse profile in the aromatic region. There is no direct ligand irradiation even when the selective pulse is placed at 6.5 ppm (865 Hz, bottom spectra).

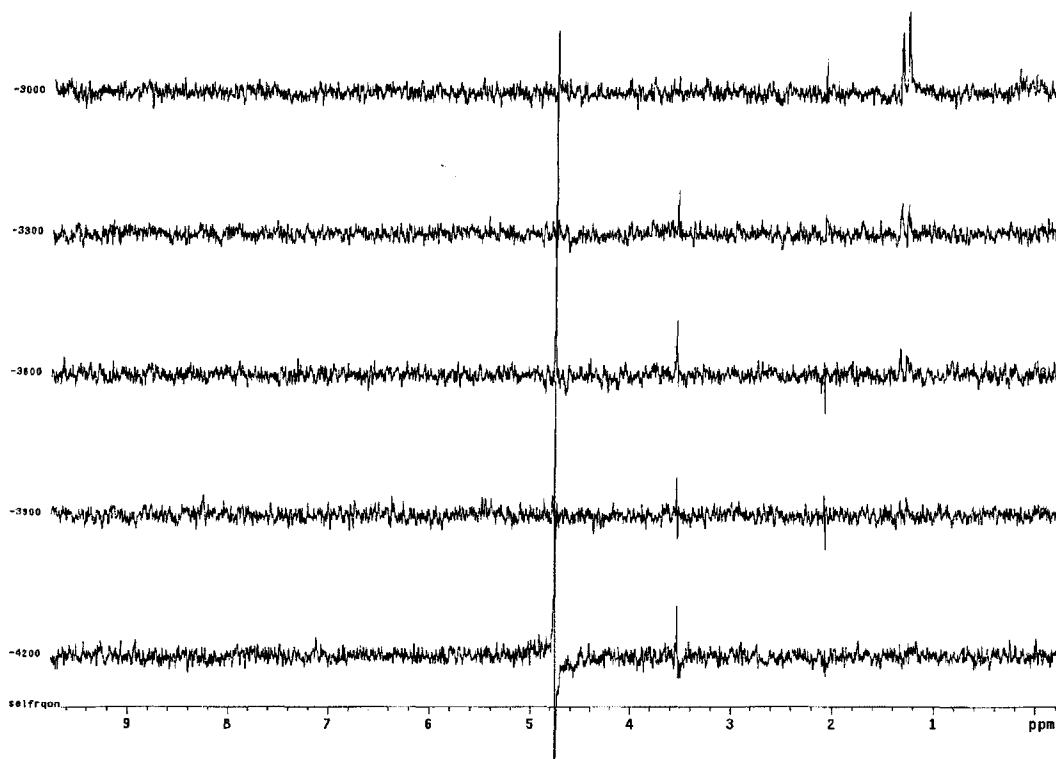


Figure 5.6: Array of the on-resonance pulse using the E-BURP-1 pulse profile in the aliphatic region. Note the unacceptable level of ligand irradiation of methyl group doublets at 1.25 ppm that occurs from -3000 Hz (0 ppm) until -4200 Hz (-2.0 ppm).

The nature of the gaussian wave function prohibits excitation from ever reaching zero in either direction from the pulse frequency, causing a wider pulse width of the on-resonance selective pulse. The E-BURP-1 profile is known to be more selective than the gaussian variant and is visualized in the arrayed experiments of the selective on-resonance frequencies.^[161] The aromatic region was irradiated at 7.0 ppm (1165 Hz) for all STD-NMR spectra recorded.

5.2.2. Optimization of HOD Suppression.

For a standard 1D NMR spectrum in D_2O , a simple pre-saturation sequence is used to eliminate the HOD signal arising from residual water. NMR studies involving protein are often performed at the milli- to micromolar range, especially with the increased sensitivity of modern spectrometers. Consequently, when water (H_2O) is present in the sample, even in small amounts, the HOD signal (~ 4.8 ppm) can become so large that important resonances are obscured or the spectrum can be rendered useless (Figure 5.7). The intensity of an HOD peak can be greatly increased when molecules containing exchangeable protons are involved, or when water is used as a co-solvent with

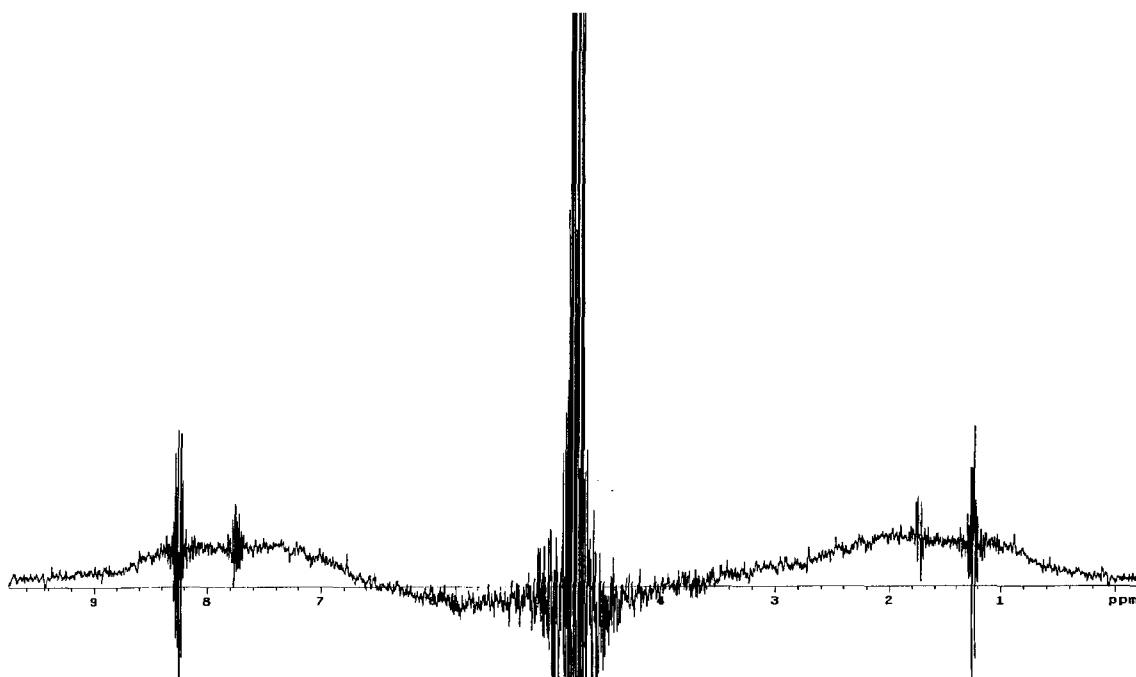


Figure 5.7: The 1D spectrum of a “wet” sample of SYA/J6. It was acquired with the $T_1\rho$ filter to suppress protein signal and no pre-saturation of water.

deuterium oxide. Because of this problem, and an ever growing library of NMR experiments, the suppression of solvent signals in NMR spectroscopy has become a major focus.^[162] Solvent signal suppression is divided into two main categories with regards to its implementation in the pulse sequence, before or after data acquisition. The former is preferable because saturation of the receiver can result and cause spectral artifacts in the latter. As mentioned, the WATERGATE W5 suppression sequence was implemented in our STD-NMR experiment.^[160] It is a more selective variant of a previous program, WATERGATE 3-9-19.^[163]

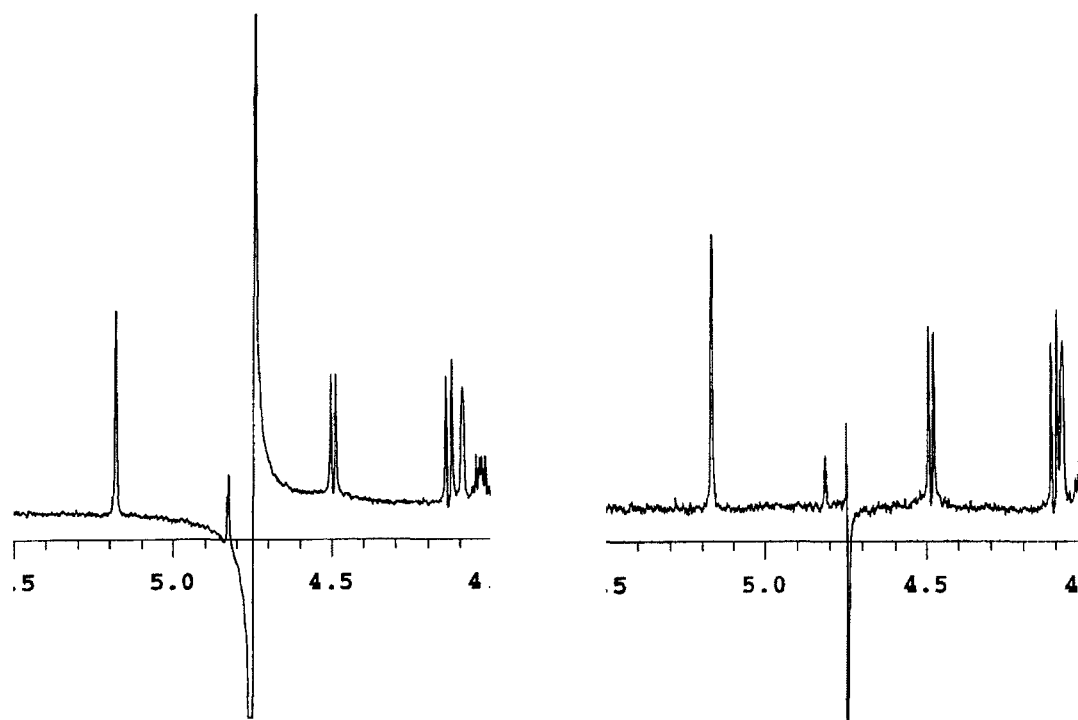


Figure 5.8: *The effect of precise water suppression. The anomeric resonance at 4.83 ppm (left spectrum) is not measurable because the baseline extends below the zero-point of the threshold used to measure peak intensities. This is due to the carrier frequency of the WATERGATE sequence not being directly on the HOD resonance. The spectrum on the right shows precise suppression. These spectra were measured using the same sample depicted in Figure 5.7.*

The key to successful water suppression is two-fold: The precise frequency of the water peak must be located (± 0.1 Hz), and the pulse sequence delay labeled d3 (D, Figure 5.2) must be set as to increase selectivity. The consequences of not applying the WATERGATE sequence directly on the HOD signal causes the baseline to become skewed, where a region of the baseline extends below the zero level of the threshold used to measure the intensity of the peaks. Therefore, some anomeric resonances near the 4.8 ppm cannot be measured for use in epitope mapping. The precise frequency for water suppression is measured using an array of spectra, varied only by the carrier frequency of HOD suppression. Figure 5.8 illustrates this result.

The second variable affecting performance of the water suppression involves lengthening the d3 delay, which is the time between pulses of the suppression sequence. Longer delays increase the selectivity of the irradiation of the water signal, reducing suppression of nearby anomeric proton signals. The W5 suppression sequence produces “null points” in the spectra at regular intervals depending on the d3 setting. These nulls have the same effect as the main suppression at 4.8 ppm on all regions of the spectrum where they are present. For an NMR experiment such as the STD method, where intensities are variable and unintentional suppression gives erroneous data, arrays of spectra are acquired at a range of d3 values to ensure nulls are not suppressing saturation transfer effects (Figure 5.9). The arrays are run on complete STD-NMR samples (SYA/J6, ligand in deuterated phosphate buffer), but the pulse program is set to acquire a reference spectrum, affording a 1D spectrum of the ligand acquired with the STD pulse sequence. A value for d3 is set to 200 μ s and rises in successive 200 μ s increments. The

d_3 of 800 μs was found to be extremely selective, while null points at this setting did not interfere with the ligand resonances of any trisaccharides investigated.

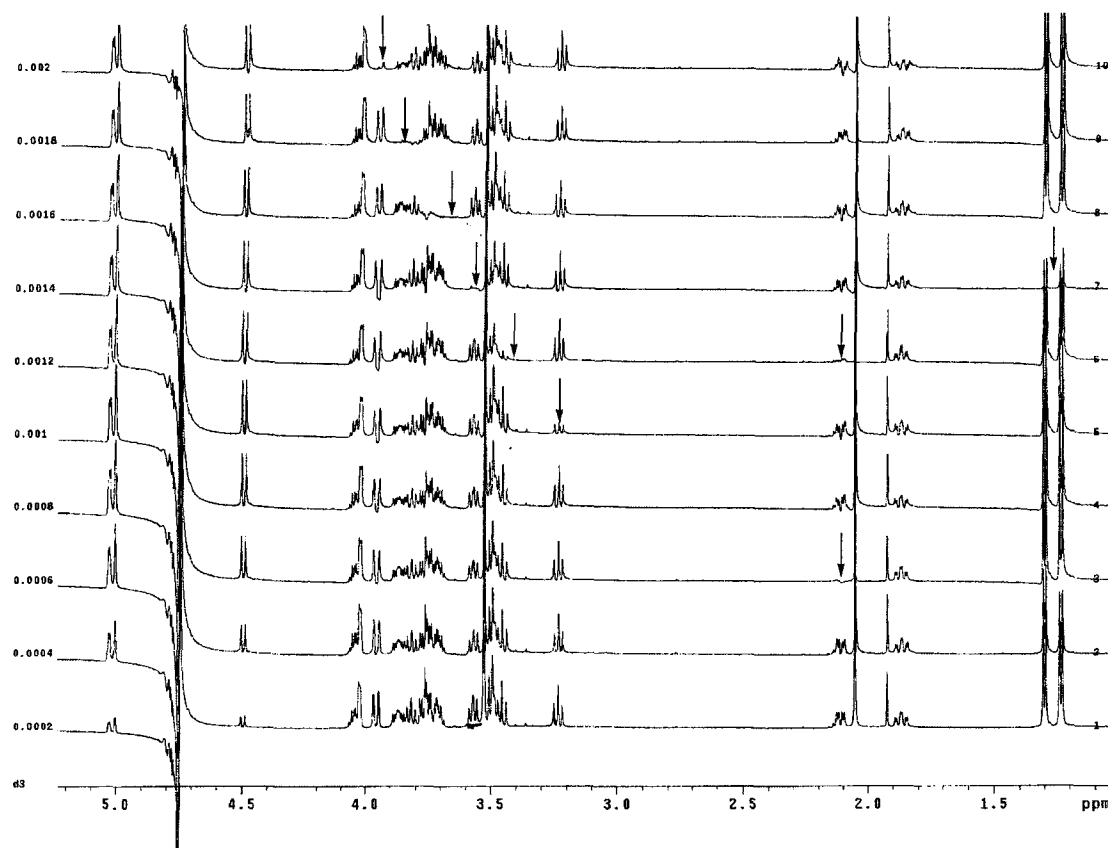


Figure 5.9: Array of reference spectra for determination of an optimal WATERGATE d_3 values (listed in seconds). The null points are easily seen as regions of suppressed signal (noted with arrows). HOD suppression is not optimally set and variation in d_3 interacts with the placement of the WATERGATE pulse itself. The optimal value was selected as 800 μsec (0.0008 sec, fourth trace from bottom) as suppression of the anomeric resonances is minimized and nulls do not appear in the spectrum. The ligand is 2'-deoxygenated BCD derivative 2.

5.3. STD-NMR Analysis of *Shigella flexneri* BCD Trisaccharide Congeners.

5.3.1. Comparison of STD-NMR Derived Epitope Maps: General Considerations.

The comparison of epitope maps between the compounds tested was expected to validate or disprove assumptions of the similarities of binding modes between certain compounds. Conclusions could be made about the origins of the changes in binding affinity if these assumptions proved correct. In fact, it was immediately evident that the compounds did not behave as a homogeneous group with a uniform mode of binding. Figure 5.10 shows ligands grouped having suspected similarities in the modes of binding. We were interested to test whether the acyclic derivatives (**23** and **24**) and macrocycle **21** were binding in the same manner. If **23** and **24** bound in the same mode as cyclic **21** it would reinforce the conclusion that tethering was solely responsible for affinity gains of **21**. Secondly, ITC analysis showed that cyclic 2'-deoxy derivative **26** bound to SYA/J6 with an affinity that was much lower than expected. Therefore, it is assumed that **26** is not binding in the same mode as its parent structure, the un-tethered 2'-deoxy BCD derivative **2**. STD-NMR should provide evidence on this point. Finally, we postulated that 2'-chloro derivative **3** would bind in the same mode as native trisaccharide **22**, as the size and electronegativities of the hydroxyl group and chlorine atom are similar. It was also expected that cyclic **21** would bind in the same mode as the native trisaccharide. If these two assumptions proved correct, 2'-chloro macrocyclic **25** may bind in the same mode as **3**, **21** or **22**. We could then correlate the thermodynamic ramifications of pairing functional group modification with intramolecular tethering (Figure 5.10).

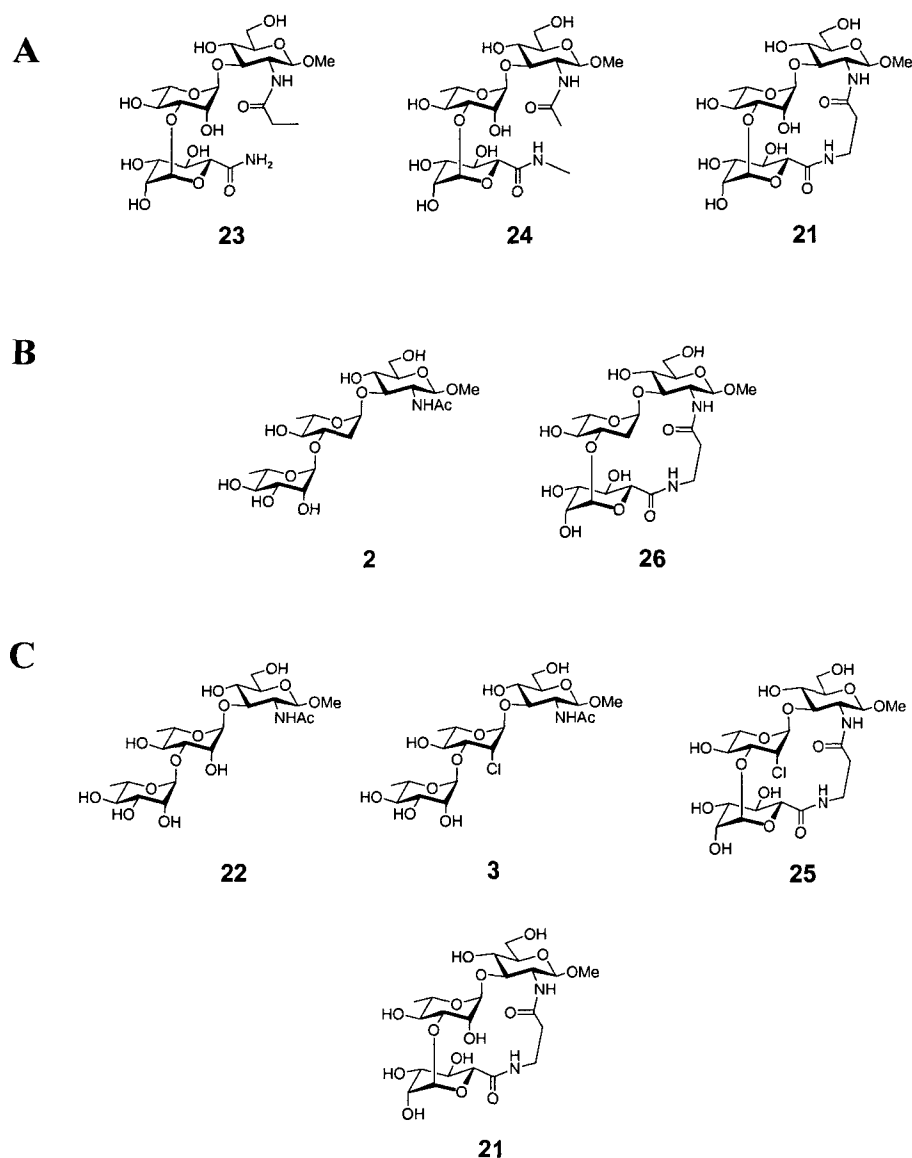


Figure 5.10: *The three groups of ligands compared by epitope mapping derived by STD-NMR. (A) Acyclic ligands vs. cyclic 21. (B) 2'-deoxygenated compounds 2 and cyclic 26. (C) The comparison of 2'-chloro modifications and cyclic derivatives.*

STD-NMR was conducted on trisaccharides **2**, **3** and **21** to **26**. A representative STD-NMR and reference spectrum are shown in Figure 5.11. All spectra were processed in an identical manner. When possible, the comparable protons with the greatest

intensity on different molecules were scaled to 100%. As many as possible comparable resonances are listed for each compound (as epitope map percentages). For reasons discussed below, the error in comparing epitope maps is $\pm 5\%$. The maximum distance of saturation transfer is likely on a par with the maximum distance of observable NOE effects, approximately 5 Å.

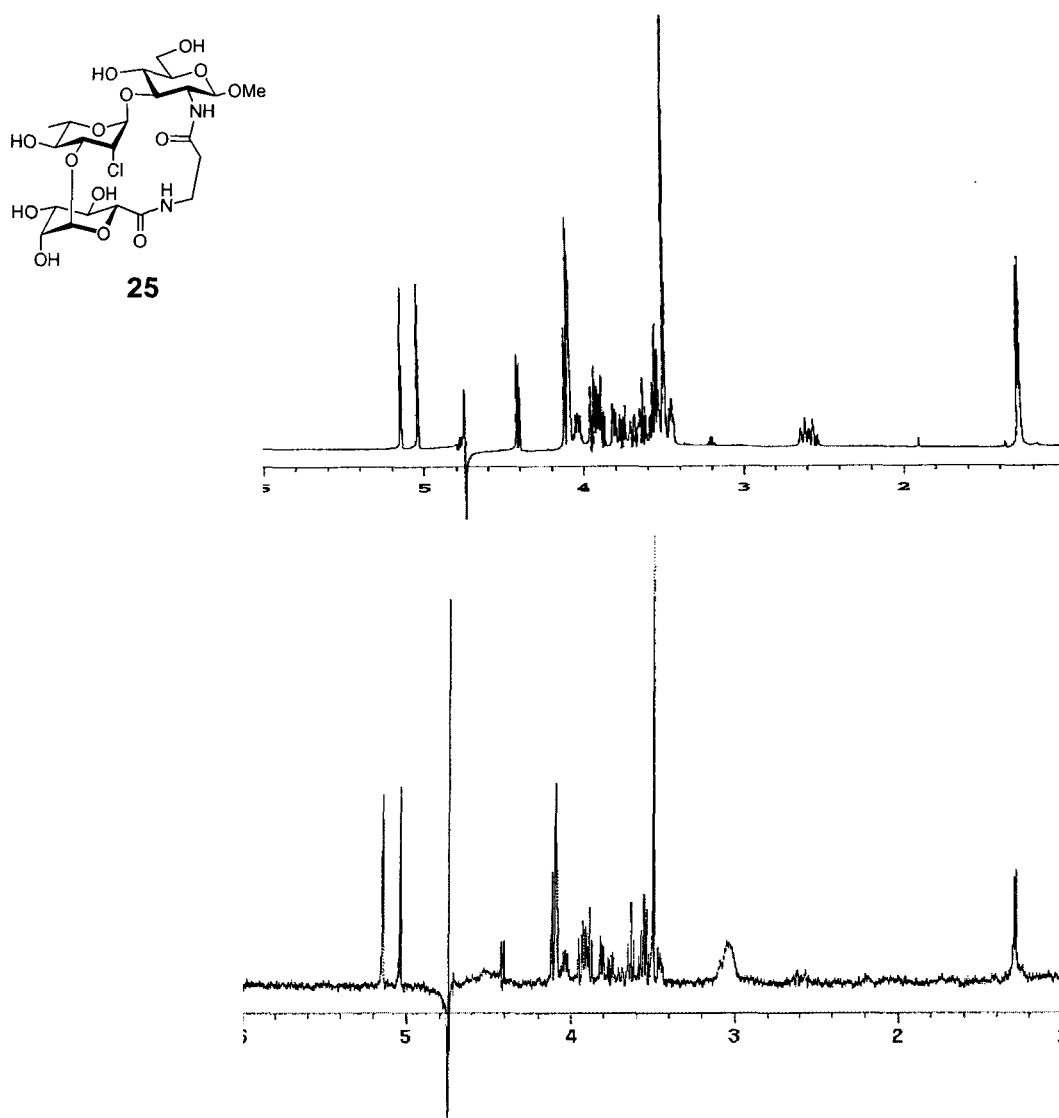


Figure 5.11: *Representative STD-NMR (bottom) and reference spectrum (top) for 25.*

5.3.2. Comparison of STD-NMR Derived Epitope Maps.

The epitope maps of acyclic compounds **23** and **24** are compared to cyclic derivative **21** in Figure 5.12. It is seen that both the acyclic derivatives bind to SYA/J6 in a similar mode. The methyl group of the propionamido in compound **23** is scaled to 110% for further comparison (see below). This group receives the most magnetization from the protein relative to the others, and it is known that increasing the size of the *N*-acyl group is not tolerated. When comparing the acetamido of **24** and the propionamido group of **23**, the latter is treated as an outlier due to close contact with the protein surface. The next most intense resonance of **23** is H-4', and when it is scaled to 100% it is apparent that the two acyclic compounds are in approximate, but not perfect, agreement with respect to their binding mode.

Cyclic derivative **21** shows significant differences in its epitope map compared to acyclic compounds **23** and **24**. The most significant differences in the epitope map of **21** occur at the Man B and Rha C residues. This indicates that the tether of **21** is holding the L-mannosyl ring in a different average bound conformation than this residue in **23** and **24**. It is known from crystallography of the pentasaccharide (1) ABCDA' sequence that the Rha residues A and B are considerably more exposed to bulk solvent than the C and D pyranosyl residues. It is likely that the increased steric bulk at the 6'' position of residue B in **23** and **24** have caused them to bind in different a mode than that of **21**. Additionally, for the un-tethered compounds, the exposure to bulk solvent would allow more movement of the Rha B residue when bound. It was also noted that the methylene groups of the tether receive a considerable degree of saturation transfer from the protein surface. However, the intensities of the two signals are the lowest of the molecule. To

our knowledge, the average distances from the protein surface involved in saturation transfer have not been correlated to peak intensity, but calculations have been developed to predict STD-NMR peak intensities^[164]

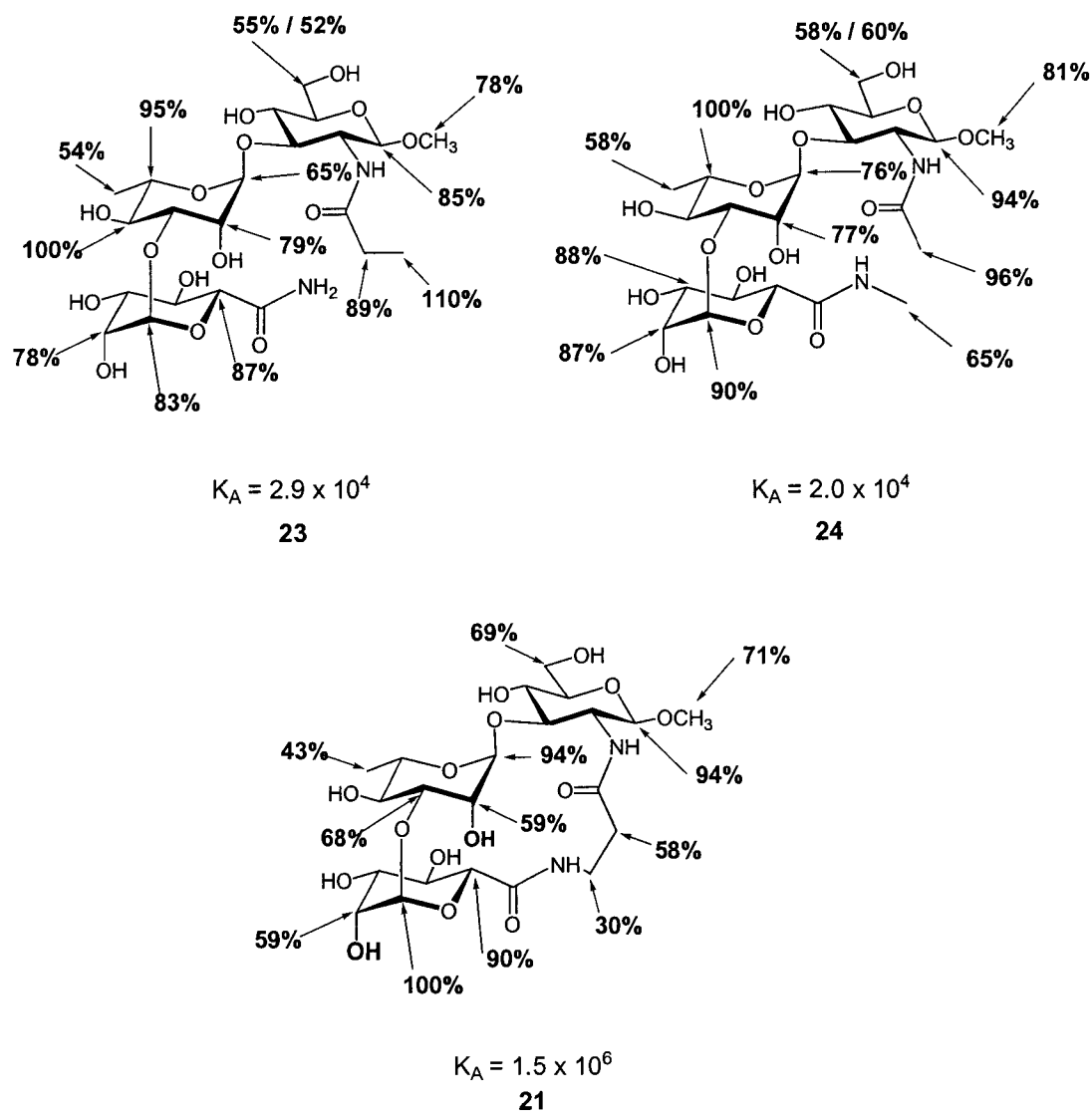


Figure 5.12: The epitope maps of 21, 23 and 24. It is seen that the epitope maps of 23 and 24 are similar; neither of which match that of 21.

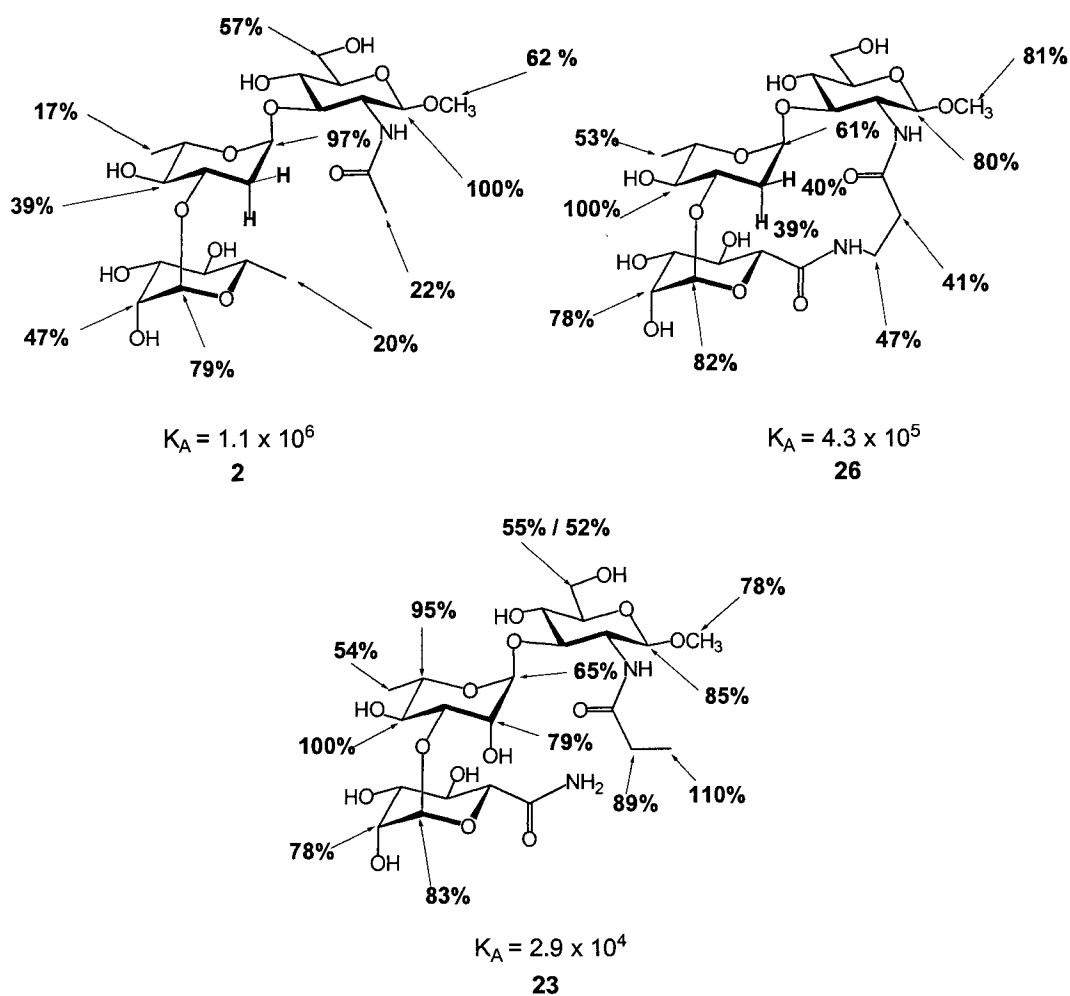


Figure 5.13: The epitope maps for **2**, **26** and **23**. Compounds **2** and **26** do not have comparable epitope maps, but that of **26** matches compound **23**.

Comparing the epitope maps of 2'-deoxygenated **2** and cyclic 2'-deoxygenated **26** show there is little similarity in their binding mode (Figure 5.13). This is not surprising as the affinity and thermodynamic binding parameters of each are quite different. The epitope map of cyclic 2'-deoxygenated **26** did, however, correlate with acyclic derivative **23**. This reinforces the notion that the propionamido methyl group experienced an extensive quantity of saturation transfer from the protein, and when the next most intense

proton of **23** is scaled to 100%, the epitope maps between **23** and **26** match within an error of 5%. The distinct epitope maps indicate that the tether is not allowing **26** to bind in the same manner as **2**, with the result that the beneficial free energy induced by 2'-deoxygenation cannot be realized for the tethered compound. Compound **26** cannot sink into the binding site as deeply as **2**, and binds in the same mode as **23**, which has a hydroxyl at its 2'-position. It is difficult to ascribe forces contributing the slight increase in affinity compared to native BCD trisaccharide **22** to structural features.

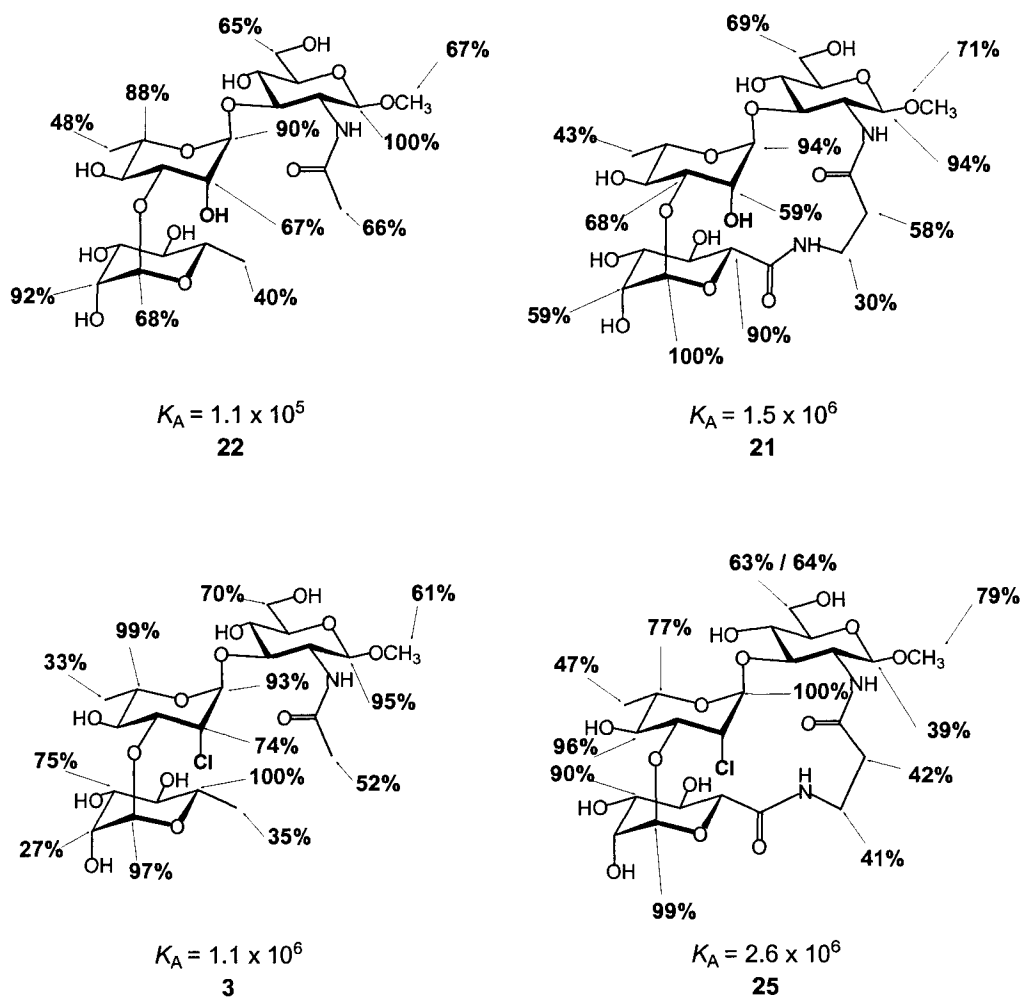


Figure 5.14: Epitope map values for **3**, **21**, **22** and **26**. The C and D residues of these compounds exhibit similar binding environments.

Figure 5.14 illustrates the epitope maps for tethered **21** and **25**, 2'-chloro derivative **3**, and native trisaccharide **22**. Comparison of the epitope map values for **22** and **3** show considerable similarity between the Rha C and GlcNAc D residues. These results correlate well with observations from the X-ray data of SYA/J6 complexed with pentasaccharide **1**. These two residues are located deep in the binding pocket and experience good contacts with the protein surface strongly, making numerous hydrogen bonds and van der Waals contacts.^[46] As seen in Figure 5.13, there is a varying degree of saturation transfer effects about the Rha B residue when the ligands are not tethered.

Both cyclic compounds, **21** and **25**, exhibit very similar epitope maps with each other and their un-tethered counterparts **3** and **22** except for the value for H-1 of **25** is 39% compared to a range of 94% to 100% for **3**, **21**, and **22** (Figure 5.14). It is not known why this proton receives such a small amount of magnetization from the protein, but the relative extent of the magnetization of the tether protons suggests that cyclic **21** and **25** bind in slightly different modes. It has been suggested that the chlorine atom of **3** may make a stabilizing contact with an aromatic residue in the binding pocket.^[46] Possibly, the combination of the tether making a hydrophobic contact with protein and the chlorine atom at the 2'-position has caused an aromatic amino acid side-chain to shift, affecting the transfer of magnetization to H-1. This effect could be more pronounced because it is the aromatic residues that are selectively saturated during the STD-NMR experiment. Epitope maps can vary depending on whether the aromatic or aliphatic residues are saturated and the proportion of each in the binding site.^[165]

In conclusion, STD-NMR has provided insight into the binding modes of the ligands involved in this study. The structural differences in the ligands have, in most

cases, caused subtle changes in the manner in which they bind. The free energy gains associated with having a 2'-chlorine atom paired with intramolecular tethering are not additive, and it is likely that slight shifts in the binding pocket are responsible for this.

This body of work is the first to report a comparison of similar ligands varying by modification. Even though NMR spectrometers cannot detect motions or reaction occurring faster than the millisecond range, the technique is capable of measuring epitope maps with a high degree of precision.

Chapter 6

Summary and Conclusions

Trisaccharide derivatives of *Shigella flexneri* lipopolysaccharide were synthesized to explore two related concepts in the search for univalent ligands with increased affinity. Previous work in the Bundle group has investigated the structural basis for the recognition of the trisaccharide, α -L-Rha-(1 \rightarrow 3)- α -L-Rha-(1 \rightarrow 3)- β -D-GlcNAc-OMe, by an IgG monoclonal antibody, SYA/J6. These studies identified two functional group modifications, namely 2'-deoxygenation and 2'-chloro-2'-deoxygenation that produced trisaccharides with increased affinity. Additionally, a macrocyclic trisaccharide aimed at reducing entropic penalties upon binding was previously developed using X-ray data from co-complexed antibody with oligosaccharide ligands. This work continued the evaluation of the macrocyclic trisaccharide by synthesizing two acyclic derivatives of the parent macrocyclic structure. Two additional trisaccharides were synthesized to investigate the possible affinity increases when functional group modification was paired with intramolecular pre-organization.

All four trisaccharides were synthesized using optimal and convergent routes. During these efforts, an improved synthesis was developed for the introduction of chlorine to an L-rhamnol derivative. Solid-phase binding assays and isothermal titration microcalorimetry were used to evaluate the biological activity of all trisaccharide ligands. The acyclic trisaccharides based on the previously reported macrocyclic derivative

showed substantially reduced binding affinities, thus confirming that intramolecular pre-organization was successful and was the cause of observed binding affinity of the previously described macrocyclic trisaccharide. Oligosaccharides placed in a conformation pre-organized for binding by macrocyclization have typically failed to achieve an order of magnitude increase in affinity displayed by the macrocyclic ligand.

The pairing of functional group modifications and intramolecular tethering illustrated the difficulties in predicting affinity gains based on rational ligand design. In the case of a macrocyclic trisaccharide with a 2'-chloro-2'-deoxy functional group change, its affinity to monoclonal antibody SYA/J6 was the highest of all comparable trisaccharide derivatives. The free energies associated with the individual modifications were not synergistic and complete additivity of free energy was not observed. Conversely, the macrocyclic 2'-deoxygenated trisaccharide had a substantially lowered affinity than was expected. Molecular dynamics calculations showed that the trisaccharide was constrained in a bioactive conformation, but pairing of the two modifications were counter productive.

The use of saturation transfer NMR was employed to obtain a semi-quantitative estimate of the contact areas for the cyclic trisaccharide derivatives. This study marks the first efforts to directly compare ligand binding between multiple compounds with structural changes, and correlate the data to observed thermodynamic parameters of binding. The structural modifications caused small shifts in the binding modes of most trisaccharides but two compounds were found to bind in an identical manner, encouraging conclusions as to the causes for observed changes in binding modes. The

evidence strongly indicates that the tether assembly prevents the pre-organized ligands from achieving their optimal position in the binding site.

The interpretation of the STD-NMR experiment conducted here is clearly inadequate for development of a complete picture of the binding mode for each ligand. For ligands bound in an antibody groove as opposed to a shallow binding site, numerous ligand resonances experience STD effects. Extensive modeling and iterative recalculation of expected versus observed STD effects would provide a more definitive picture. However, it is doubtful whether these calculations are warranted since there is sufficient evidence to suggest that segmental re-positioning of the three carbohydrate residues is the underlying cause of the diverse, affinity enhancements for the tethered ligands.

Modification at the 6-position of the GlcNAc residue is known to produce trisaccharides that exhibit a substantial increase in binding affinity when chlorine is substituted for the hydroxyl group. The combination of a trisaccharide containing 2',6-dichloro-2',6-dideoxy functional group modifications coupled with intramolecular pre-organization has the potential to produce a derivative that could have an association constant that could reach the 10^8 range. The increased rotational freedom of the 6-position could allow an increased measure of additivity of affinities for the individual modifications. The study of this compound would serve to finalize the proof of concept study described in the previous sections. However, when compounds with such high K_A values are studied, comparison to existing data would likely require the use of competitive versions of isothermal titration microcalorimetry and STD-NMR if the affinity gains were too great.

Chapter 7

Experimental Section

General:

Reagents and Chromatography: All reagents were used as supplied from commercial sources. When noted, solvents were distilled and dried according to common literature protocol.^[166] *N,N*-Dimethylformamide was stored over 3Å molecular sieves and placed under vacuum (~1 mm Hg) prior to use. Chlorine gas was purchased (Aldrich) and used without any further purification. **Caution:** Chlorine gas is extremely poisonous, corrosive, and oxidizing. Proper preventive backflow devices were used in apparatus piping. Solvents were removed via rotary evaporator using a maximum bath temperature of 50 °C. Thin layer chromatography used plates coated with silica gel 60-F₂₅₄ (Merck) using ultraviolet light and 5% sulfuric acid in ethanol or acidic cerium ammonium molybdate followed by heating.

Medium pressure column chromatography was conducted with silica gel (230-400 mesh, 60Å, Silicycle, Quebec) using a flow rate of 2-20 mL min⁻¹. High-performance liquid chromatography utilized a Waters Delta 600 system using an absorbance detector. Separations were done using a C₁₈-silica semi-preparative reverse-phase column (Beckman) with an increasing linear gradient of methanol in water as eluent. Flow rates

ranged from 0.5-2.5 mL min⁻¹. Solid-phase extraction cartridges (Sep-Pak, C₁₈,) were purchased from Waters Corp. (Milford, MA, USA).

NMR Spectroscopy: ¹H NMR spectra were recorded on Varian INOVA 500 or 600 MHz spectrometers and ¹³C NMR spectra were recorded at 125 MHz. They were calibrated to residual solvent signals and reported in ppm ($\delta = 7.24$ for CDCl₃, 4.80 for HOD). For samples in D₂O, external acetone was used as a reference ($\delta = 2.225$). Proton resonances corresponding to diastereotopic methylene protons of the tether are labeled as α - or β - with respect to the amide carbonyl of the glucosamine residue. Of the protons in each pair, H_A denotes the more downfield, while H_B is the more upfield resonance.

Purification of monoclonal antibody SYA/J6: Antibody was purified from ascites fluid by centrifugation (30 min, 64 000 g) to pellet cells and fatty tissue. After filtration first through a Millex AP 20 pre-filter (Millipore) and then through a Millex-GV 0.22 μ m low-binding sterilization filter (Millipore), the filtrate was loaded onto a Sepharose Protein-A (Pharmacia Biotech) column equilibrated with running buffer (50 mM Tris, 150 mM NaCl, 0.02% NaN₃, adjusted to pH 8.0). The column was washed with running buffer until serum proteins were eluted (absorbance at 280 nm below 0.1). Antibody was then eluted with citrate buffer (100 mM citric acid, 150 mM NaCl, 0.02% NaN₃, adjusted to pH 4.0). Fractions with an absorbance greater than 0.1 were collected, pooled and dialyzed (24 h) against the initial Tris buffer for calorimetry measurements, or against phosphate buffered saline (PBS) for ELISA measurements.

Enzyme-linked immunosorbent assays: ELISA was carried out with a PBS solution of protein A purified SYA/J6 antibody coated on microtitre plates (1 mg mL⁻¹) and *O*-polysaccharide coupled to biotin. Streptavidin-HRP conjugate (Sigma Chemical

Co., St. Louis, Mo.) served as the disclosing reagent. Inhibition experiments with increasing concentration of synthetic inhibitors were done in triplicate according to a previously reported protocol.^[43, 44]

Isothermal titration microcalorimetry. Dialyzed antibody was concentrated to 30 μM and equilibrated against the above-described TRIS buffer used for calorimetry in CentriPrep units (Amicon). Antibody concentration was determined spectrophotometrically using a calculated extinction coefficient of 1.53 mg mL^{-1} .^[43] Dried saccharide samples were dissolved to 0.060 mM, a 20-fold excess over the protein concentration. In all cases, the value C , defined as the product of the binding constant K_A and the concentration of protein (or binding sites), was in the range of 1–500 and ligand concentrations were such that the final ligand concentration was at least $10K_A$. Isothermal titration measurements were made using the Microcal VP-ITC titration microcalorimeter (MicroCal Inc., Northampton, MA).^[25, 35] Purified antibody (IgG, 30 μM) was placed in the cell (1.41 mL) and 30–35 $8 \mu\text{L}$ injections of ligand were introduced over 16 s, with each injection being 300 s apart. Measurements were evaluated by the ORIGIN software package and data were processed using a single binding site model that assumes no cooperativity between sites.^[35] Non-negligible heats of dilution were subtracted prior to data processing.

Preparation of SYA/J6 for STD NMR: Saturation transfer difference NMR spectroscopy used samples ($650 \mu\text{L}$, 4 mg mL^{-1}) of purified SYA/J6 (145 KDa) monoclonal antibody in deuterated phosphate buffer (PBS-D) that was prepared by lyophilizing PBS (0.10 mM PBS, 0.15 M NaCl, 0.1% NaN_3) from D_2O three times. Antibody in protonated buffer had the volume exchanged five-fold with PBS-D in an

Amicon filter with a 30 KDa membrane cutoff, followed by concentration in the same device. The samples were subsequently filtered (0.22 μ M, Millipore) and portioned into 650 μ L aliquots.

Saturation Transfer Difference NMR: STD-NMR measurements were made on a Varian Inova 600 MHz spectrometer equipped with an inverse triple resonance probe at a temperature of 300 K. The pulse sequence followed that of Mayer and Meyer^[147] and used WATERGATE W5 for HOD suppression. The delay d3 was set to 800 ms for optimal results. One-dimensional STD NMR spectra were generated by subtraction of data acquired from the on-resonance pulse (7 ppm) and the off-resonance (40 ppm). The excitation of the protein consisted of 30 selective EBURP^[161] shaped pulses, each being 50 ms in length. They were spaced 1 ms apart, thereby giving the protein a total of 1.53 s of irradiation. The number of transients ranged from 4 K to 48 K depending on the signal-to-noise.

The peak heights from reference spectra were used to measure the STD amplification factors and epitope map percentages were estimated using the following equation: ^[147]

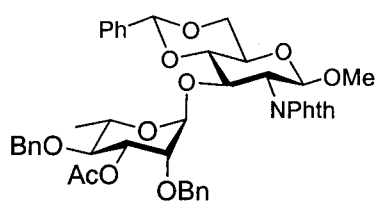
$$\eta = (I_o - I_{sat} / I_o) * \text{ligand excess}$$

where $(I_o - I_{sat})$ is the peak height in the 1D STD NMR spectrum and I_o is the that of the reference spectrum. Ligand excess was 100-fold with respect to concentration of antibody (50-fold excess in terms of binding sites). The reference spectra do not involve excitation of the protein and thus, the selective on-resonance pulse was placed at 30 ppm with transmitter power set to the lowest setting. The subtraction of spectra was turned off

and the experiment was run for 2 K to 24 K scans, corresponding to one half the number of the 1D STD spectra. All spectra were calibrated to the HOD signal at 4.8 ppm.

Analytical Measurements: All mass spectrometry analysis was performed using positive mode electrospray ionization on a ZabSpec Hybrid Sector-TOF instrument. For high resolution measurements, the spectra were obtained using a voltage scan over a narrow mass range at a resolution of 10,000. All spectra were measured by the mass spectrometry service at the University of Alberta. Optical rotation was measured with a Perkin Elmer 241 polarimeter, and values are reported with the units $\text{degr. mL g}^{-1} \text{ dm}^{-1}$. Elemental analysis and optical rotations were measured by the analytical service of this department.

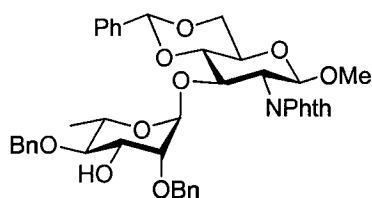
Compounds:



39

Methyl 3-O-(3-O-acetyl-2,4-di-O-benzyl- α -L-rhamnopyranosyl)-4,6-O-benzylidene-2-deoxy-2-phthalimido- β -D-glucopyranoside (39): Anhydrous dichloromethane (30 mL) was added to glycosyl donor **34**^[101] (1.89 g, 4.40 mmol), acceptor **30**^[100] (1.55 g, 3.83 mmol) and 4 Å molecular sieves (1.5 g) and stirred under an argon atmosphere for 1 h at room temperature. Silver trifluoromethanesulfonate (0.40 g, 1.90 mmol) and *N*-iodosuccinimide (1.03 g, 4.6 mmol) were added and the solution was stirred for 1 h. The dark purple solution was then filtered through Celite and the resulting solution was washed with saturated sodium thiosulfate, water, and dried over

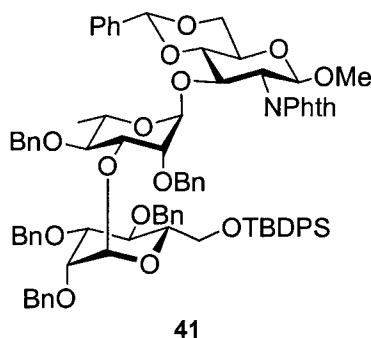
sodium sulfate. The solvent was evaporated and the product was purified using silica gel chromatography (hexanes:ethyl acetate, 2:1). The protected disaccharide **39** was isolated as a colorless solid (3.07 g, 91%): $[\alpha]_D -24.0$ (c 0.9, CH_2Cl_2). ^1H NMR (300 MHz, CDCl_3) δ 7.85-7.68 (m, 4H, Ar-*H*), 7.32-7.14 (m, 13H, Ar-*H*), 6.90-6.95 (m, 2H, Ar-*H*), 5.55 (s, 1H, *CH*-Ph), 5.19 (d, 1H, $J = 8.6$ Hz, H-1), 5.08 (dd, 1H, $J = 3.5, 9.5$ Hz, H-3'), 4.66 (dd, 1H, $J = 9.7, 10.3$ Hz, H-3), 4.59 (d, 1H, $J = 1.8$ Hz, H-1'), 4.46-4.50 (m, 2H, CH_2 -Ph), 4.41 (dd, 1H, $J_{\text{vic}} = 4.0$ Hz, $J_{\text{gem}} = 12.5$ Hz, H-6_a), 4.30 (dd, 1H, $J = 8.5, 10.2$ Hz, H-2), 3.96 (dq, 1H, $J = 6.2, 9.7$ Hz, H-5'), 3.94 (d, 1H, CH_2 -Ph), 3.83-3.86 (m, 1H, H-6_b), 3.76 (d, 1H, CH_2 -Ph), 3.68-3.73 (m, H, H-4, H-5), 3.51 (dd, 1H, $J = 2.0, 3.5$ Hz, H-2'), 3.42 (s, 3H, OMe), 3.35 (dd \approx t, 1H, $J = 9.5$ Hz, H-4'), 1.90 (s, 3H, OAc), 0.79 (d, 3H, $J = 6.2$ Hz, H-6'). ^{13}C NMR (125 MHz, CDCl_3) δ 172.4, 163.5, 138.3, 134.4, 132.1, 132.0, 131.0, 129.3, 129.2, 129.1, 128.7, 128.6, 127.9, 126.8, 127.6, 125.3, 101.9, 99.5 ($J_{\text{C1-H1}} = 164.6$ Hz, C-1), 97.7 ($J_{\text{C1-H1}} = 167.3$ Hz, C-1'), 81.4, 76.3, 74.4, 74.1, 70.9, 69.7, 65.6, 57.3, 57.0, 56.1, 20.8, 17.2. Anal. Calc'd for $\text{C}_{44}\text{H}_{45}\text{NO}_{12}$: C, 67.77; H, 5.82; N, 1.80. Found: C, 67.40; H, 5.83; N, 1.74. ES HRMS calc'd for $\text{C}_{44}\text{H}_{45}\text{NO}_{12}\text{Na}$ (M+Na): 802.2839, Found: 802.2832.



40

Methyl 3-*O*-(2,4-di-*O*-benzyl- α -L-rhamnopyranosyl)-4,6-*O*-benzylidene-2-deoxy-2-phthalimido- β -D-glucopyranoside (40): Distilled methanol (40 mL) was added to the acetate **39** (1.07 g, 1.33 mmol), sodium (50 mg, 2.17 mmol) was added, and the

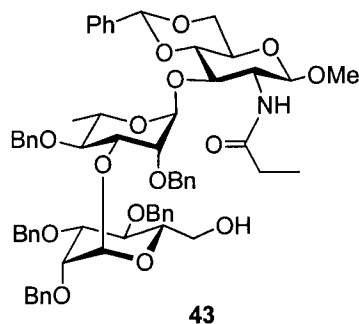
reaction was allowed to stir for 24 h at room temperature. Rexyn 101 (H^+) cationic exchange resin was then added to neutralize the solution that was subsequently filtered through Celite. The solvent was evaporated and the product was purified by silica gel chromatography (toluene:ethyl acetate, 5:1). Alcohol **40** was isolated as a white solid (0.856 g, 85%): $[\alpha]_D -37.2$ (c 1.0, CH_2Cl_2). 1H NMR (600 MHz, $CDCl_3$) δ 7.88-7.68 (m, 4H, Ar-*H*), 7.32-7.14 (m, 13H, Ar-*H*), 6.86-6.91 (m, 2H, Ar-*H*), 5.56 (s, 1H, CH-Ph), 5.19 (d, 1H, $J = 8.5$ Hz, H-1), 4.70 (d, 1H, $PhCH_2O-$), 4.64 (d, 1H, $J = 1.3$ Hz, H-1'), 4.60 (dd, 1H, $J = 9.6, 10.4$ Hz, H-3), 4.46 (d, 1H, $PhCH_2O-$), 4.41 (dd, 1H, $J_{vic} = 4.3$ Hz, $J_{gem} = 10.3$ Hz, H-6_a), 4.26 (dd, 1H, $J = 8.5, 10.2$ Hz, H-2), 3.78-3.82 (m, 4H, H-6_b, H-3', H-5', $PhCH_2O-$), 3.63-3.67 (m, 3H, H-4, H-5, $PhCH_2O-$), 3.42 (s, 3H, OMe), 3.35 (dd, 1H, $J = 1.6, 3.8$ Hz, H-2'), 3.05 (dd \approx t, 1H, $J = 9.5$ Hz, H-4'), 2.01 (d, 1H, OH), 0.72 (d, 3H, $J = 6.2$ Hz, H-6'). ^{13}C NMR (125 MHz, $CDCl_3$) δ 158.8, 138.6, 137.3, 137.0, 134.5, 131.4, 129.1, 128.34, 128.26, 127.8, 127.7, 127.5, 127.3, 126.5, 123.7, 102.1, 99.3, 97.3, 82.0, 80.6, 79.5, 74.5, 74.1, 72.3, 70.9, 69.8, 67.5, 66.5, 57.0, 56.6, 17.2. Anal. Calc'd for $C_{42}H_{43}NO_{11}$: C, 68.37; H, 5.87; N, 1.90. Found: C, 68.14; H, 6.02; N, 1.88. ES HRMS calc'd for $C_{42}H_{43}NO_{11}Na$ ($M+Na$): 760.2734, Found: 760.2748.



Methyl 3-*O*-(2,4-di-*O*-benzyl-3-*O*-[2,3,4-tri-*O*-benzyl-6-*O*-*tert*-butyl-diphenylsilyl- α -L-mannopyranosyl]- α -L-rhamnopyranosyl)-4,6-*O*-benzylidene-2-

deoxy-2-phthalimido- β -D-glucopyranoside (41): Anhydrous dichloromethane (15 mL) was added to mannosyl donor **38**^[87] (0.670 g, 1.01 mmol) and acceptor **40** (0.582 g, 0.788 mmol). The solution was cooled to -78 °C, and *N*-iodosuccinimide (267 mg, 1.19 mmol) and 200 μ L dichloromethane saturated with trifluoromethanesulfonic was added. The solution was allowed to reach room temperature, and the resulting dark purple solution was then filtered through Celite. The organic layer was washed with saturated sodium thiosulfate, water, and dried over sodium sulfate. The solvent was evaporated and the product was purified by silica gel chromatography (hexanes:ethyl acetate, 2:1). Trisaccharide **41** was isolated as a white solid (0.950 g, 85%): $[\alpha]_D -112.3$ (*c* 1.1, CH₂Cl₂). ¹H NMR (600 MHz, CDCl₃) δ : 7.82-6.78 (m, 44H, Ar-H), 5.54 (s, 1H, PhCH₂O-), 5.19 (d, 1H, *J* = 8.5 Hz, H-1), 5.12 (bs, 1H, H-1''), 4.92 (d, 1H, PhCH₂O-), 4.65 (d, 1H, PhCH₂O-), 4.56 (dd, 1H, *J* = 9.6, 10.4 Hz, H-3), 4.53 (d, 1H, *J* = 1.3 Hz, H-1'), 4.51 (dd, 1H, *J*_{vic} = 4.3 Hz, *J*_{gem} = 10.3 Hz, H-6_a), 4.36-4.44 (m, 6H, PhCH₂O-), 4.36 (dd \approx t, 1H, *J* = 9.6 Hz, H-4''), 4.18 (dd, 1H, *J* = 8.5, 10.1 Hz, H-2), 3.97 (dd, 1H, *J*_{vic} = 2.5 Hz, *J*_{gem} = 11.5 Hz, H-6_a''), 3.76-3.86 (m, 7H, H-6_b, H-3', H-5', H-3'', H-5'', H-6_b''), PhCH₂O-, 3.60-3.70 (m, 4H, H-4, H-5, H-2'', PhCH₂O-), 3.42 (s, 3H, OMe), 3.26 (m, 2H, H-2', H-4'), 1.04 (s, 9H, *t*-Bu), 0.74 (d, 3H, *J* = 6.2 Hz, H-6'). ¹³C NMR (125 MHz, CDCl₃) δ 168.9, 139.7, 138.62, 138.61, 138.2, 137.7, 136.6, 135.2, 133.6, 131.1, 129.3, 129.1, 128.94, 128.87, 128.5, 128.47, 128.44, 128.2, 128.11, 128.05, 127.7, 127.6, 127.5, 127.4, 127.2, 127.1, 125.4, 123.9, 102.1, 99.5 (*J*_{C1-H1} = 165.0 Hz, C-1), 99.5 (*J*_{C1-H1} = 171.1 Hz, C-1''), 97.6 (*J*_{C1-H1} = 168.0 Hz, C-1'), 81.5, 79.7, 78.3, 77.6, 76.1, 74.6, 74.5, 74.3, 74.1, 73.4, 73.1, 72.7, 71.3, 68.9, 67.6, 65.3, 61.1, 61.0, 56.0, 55.5, 26.05, 17.4, 14.8,

5.4. Anal. Calc'd for $C_{85}H_{89}NO_{16}$: C, 72.47; H, 6.37; N, 0.99. Found: C, 72.24; H, 6.24; N, 1.01. ES HRMS: (M+Na): 1430.5838, Found: 1430.5848.



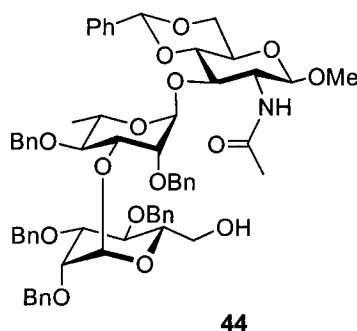
Methyl 4, 6-*O*-benzylidene-2-propionamido-3-*O*-(2,4-di-*O*-benzyl-3-*O*-(2, 3, 4-tri-*O*-benzyl- α -L-mannopyranosyl)- α -L-rhamnopyranosyl)- β -D-glucopyranoside

(43): To a suspension of protected **41** (0.457 g, 0.39 mmol) in ethanol (5 mL) was added hydrazine hydrate (2 mL). The solution was refluxed for 24 h and the volatiles were removed under vacuum and the residue co-evaporated with toluene three times. The resultant solid was suspended in methanol (15 mL) and propionic anhydride was added (56 μ L, 0.44 mmol). The reaction was stirred for 2 h until clear, and potassium carbonate (100 mg) was added. The solvent was removed under a vacuum and the residue was dissolved in CH_2Cl_2 treated with excess TBAF in THF (5 mL). After 6 h the solvent was evaporated and washed with water. The organic layer was dried with sodium sulfate, filtered and evaporated to dryness. The residue was chromatographed (6:4:1 cyclohexane:ethyl acetate:acetone) to afford a white foam (0.383 g, 88%): $[\alpha]_D -38.7$ ($c = 1.0$, $CHCl_3$). 1H NMR (600 MHz, $CDCl_3$) δ 7.49-7.15 (m, 30H, Ar-*H*), 6.14 (bd, 1H, $J = 7.4$ Hz, EtC(O)NH-), 5.49 (s, 1H, PhCHO₂-), 5.21 (s, 1H, H-1''), 4.92 (d, 1H, $J_{gem} = 14.4$ Hz, PhCH₂O-), 4.91 (s, 1H, H-1'), 4.61-4.51 (m, 7H, PhCH₂O-), 4.39 (d, 1H, $J_{gem} =$

12.2 Hz, PhCH₂O-), 4.36-4.27 (m, 3H, PhCH₂O-, H-6_a, H-3), 4.14 (dd, 1H, *J* = 2.8, 9.8 Hz, H-3'), 3.99 (m, 1H, H-3''), 3.88-3.81 (m, 2H, H-5', H-6_a''), 3.78 (dd ≈ t, 1H, *J* = 2.3 Hz, H-2'), 3.77-3.71 (m, 4H, H-6_b, H-2'', H-4'', H-5''), 3.68-3.62 (m, 1H, H-6_b''), 3.53-3.47 (m, 3H, H-4, H-5, H-4'), 3.43 (s, 3H, -OCH₃), 3.16 (ddd ≈ q, *J* = 9.3 Hz, H-2), 2.04-1.91 (m, 2H, -CH₂CH₃), 1.01 (t, 3H, 7.6 Hz, -CH₂CH₃), 0.84 (d, 3H, *J* = 7.62 Hz, H-6').

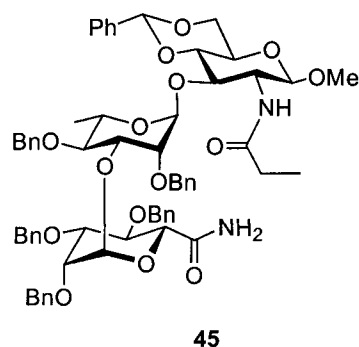
¹³C NMR (125 MHz, CDCl₃) δ 174.2, 138.74, 138.69, 138.53, 138.39, 138.35, 129.2, 128.34, 128.31, 128.28, 128.2, 128.13, 128.1, 127.7, 127.6, 127.55, 127.53, 127.51, 127.4, 127.35, 127.34, 126.9, 126.3, 101.7, 100.5, 99.6, 99.2, 81.1, 80.8, 79.9, 78.0, 76.9, 76.5, 75.6, 74.9, 74.6, 73.1, 72.6, 72.3, 72.2, 68.8, 66.2, 63.2, 58.4, 57.1, 29.6, 18.9, 9.7.

Anal. calc'd for C₆₄H₇₃NO₁₅: C, 68.68; H, 6.57; N, 1.25. Found C, 68.53; H, 6.64; N, 1.30. ES MS calc'd for C₆₄H₇₃NO₁₅Na (M+Na): 1118.5. Found 1118.5.



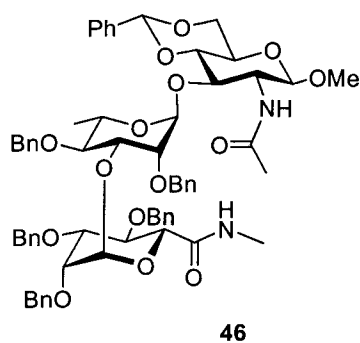
Methyl 4,6-*O*-benzylidene-2-acetamido-3-*O*-(2,4-di-*O*-benzyl-3-*O*-(2,3,4-tri-*O*-benzyl- α -L-mannopyranosyl)- α -L-rhamnopyranosyl)- β -D-glucopyranoside (44): To a suspension of protected **41** (0.496 g, 0.429 mmol) in ethanol (5 mL) was added hydrazine hydrate (2 mL). The solution was refluxed for 24 h and the volatiles were removed under vacuum and the residue co-evaporated with toluene three times. Amine

42 was treated analogously for the production of **43** using acetic anhydride (42 μ L, 0.451 mmol) as the acylation agent. Similar work-up and chromatography gave the target compound (0.413 g, 89%) as colorless foam: $[\alpha]_D = -36.8$ ($c = 1.1$, CHCl_3). ^1H NMR (600 MHz, CDCl_3) δ 7.52-7.14 (m, 30H, Ar-H), 6.39 (bd, 1H, $J = 7.3$ Hz), 5.51 (s, 1H, PhCHO_2 -), 5.22 (d, 1H, $J = 1.0$ Hz, H-1''), 4.94 (d, 1H, $J = 1.7$ Hz, H-1''), 4.92 (d, 1H, $J_{\text{gem}} = 11.2$ Hz, PhCH_2O -), 4.78 (d, 1H, $J = 8.3$ Hz, H-1), 4.66-4.52 (m, 7H, PhCH_2O -), 4.43-4.32 (m, 2H, HO-, H-6_a), 4.21 (dd \approx t, 1H, $J = 9.2$ Hz, H-3), 4.14 (dd, 1H, $J = 2.8$, 9.7 Hz, H-3'), 3.91 (dd, 1H, $J = 3.0$, 8.6 Hz, H-3''), 3.88-3.84 (m, 2H, H-5', H-6_a''), 3.81 (dd \approx t, 1H, $J = 2.5$ Hz, H-2'), 3.78-3.72 (m, 4H, H-6_b, H-2'', H-4'', H-5''), 3.65 (dd, 1H, $J_{\text{gem}} = 11.5$ Hz, $J_{\text{vic}} = 7.3$ Hz, H-6_b''), 3.55-3.47 (m, 3H, H-4, H-5, H-4''), 3.42 (s, 3H, - OCH_3), 3.27 (bddd \approx q, 1H, $J = 9.0$ Hz, H-2), 2.74 (bs, 1H, 6''-OH), 1.76 (s, 3H, NHCOCH_3), 0.86 (d, 3H, $J = 6.2$ Hz, H-6'). ^{13}C NMR (125 MHz, CDCl_3) δ 170.5, 138.4, 138.2, 138.1, 138.0, 137.1, 128.9, 128.4, 128.34, 128.31, 128.2, 128.1, 128.0, 127.8, 127.61, 127.58, 127.57, 127.56, 127.53, 127.43, 127.40, 127.36, 126.9, 126.3, 101.7, 100.9, 99.7, 98.9, 81.1, 81.0, 79.8, 77.8, 77.1, 76.7, 75.6, 74.9, 74.6, 73.1, 72.6, 72.2, 68.9, 68.8, 66.1, 63.2, 58.3, 57.0, 23.3, 17.5. Anal. calc'd for $\text{C}_{63}\text{H}_{71}\text{NO}_{15}$: C, 69.92; H, 6.61; N, 1.29. Found C, 69.80; H, 6.38; N, 1.35. ES HRMS calc'd for $\text{C}_{63}\text{H}_{71}\text{NO}_{15}\text{Na}$ (M+Na): 1104.4721. Found 1104.4719.



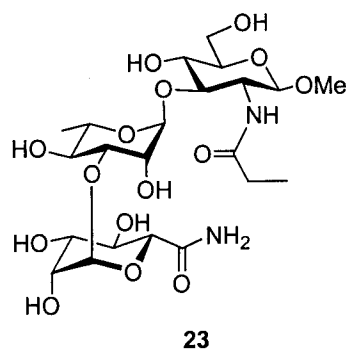
Methyl 4,6-*O*-benzylidene-2-propionamido-3-*O*-(2,4-di-*O*-benzyl-3-*O*-(2,3,4-tri-*O*-benzyl-6-amino- α -L-mannopyranuronoyl)- α -L-rhamnopyranosyl)- β -D-glucopyranoside (45): To a stirred solution of alcohol **43** (0.217 g, 0.198 mmol) in acetonitrile (5 mL) at 0 °C was added 2,2,6,6-tetramethyl-1-piperidiny-*N*-oxide (0.031 g, 0.198 mmol) and an aqueous solution containing potassium bromide (0.198 mmol) and sodium bicarbonate (0.040 mmol) (1.30 mL, pH 10.5 with sodium hydroxide). Sodium hypochlorite (5-6%, 1.50 mL) was added drop-wise and the reaction stirred for 1 h before the addition of hydrochloric acid (1M, 15 mL), and dichloromethane (15 mL). The organic layer was removed, washed with water, dried with sodium sulfate, and evaporated to dryness. The residue was dissolved in dry dichloromethane (5 mL) under argon, carbonyldiimidazole (0.064 g, 0.396 mmol) was added, and the mixture was stirred for 45 minutes before the introduction of ammonia gas (excess). After an additional hour, the ammonia was allowed to evaporate and the solvent was removed under vacuum. Column chromatography (2: 3: 1 cyclohexane: ethyl acetate: acetone) of the residue afforded the target compound as a clear glass (0.149 g, 68%): $[\alpha]_D = -22.7$ ($c = 1.1$, CHCl_3). $^1\text{H NMR}$ (600 MHz, CDCl_3) δ 7.48-7.11 (m, 30H, Ar-*H*), 6.58 (bs, 1H, -CONH_{2a}), 6.26 (bd, 1H, $J = 7.6$ Hz, -NHCOEt), 5.51 (s, 1H, PHCHO₂-), 5.46 (bs, 1H, -CONH_{2b}), 5.39 (d, 1H, $J = 1.8$ Hz, H-1''), 4.97 (d, 1H, $J = 1.7$ Hz, H-1'), 4.82 (d, 1H, J_{gem}

= 10.7 Hz, PhCH₂O-), 4.69 (d, 1H, *J* = 8.3 Hz, H-1), 4.59-4.49 (m, 6H, PhCH₂O-), 4.39-4.32 (m, 3H, PhCH₂O-, H-6_a), 4.18-4.13 (m, 2H, H-3, H-3'), 4.09 (dd ≈ t, 1H, *J* = 9.0 Hz, H-4'), 4.02 (d, 1H, *J* = 9.2 Hz, H-5''), 3.89 (dq, 1H, *J* = 6.1, 9.5 Hz, H-5'), 3.85 (dd, 1H, *J* = 2.9, 8.5 Hz, H-3''), 3.77-3.72 (m, 2H, H-6_b, H-2'), 3.69 (dd ≈ t, 1H, *J* = 2.6 Hz, H-2''), 3.54 (dd ≈ t, 1H, *J* = 9.3 Hz, H-4''), 3.51-3.44 (m, 3H, H-4, H-5, H-4'), 3.42 (s, 3H, OCH₃), 2.10-2.01 (m, 2H, -NHCOCH₂CH₃), 1.01 (t, 3H, -NHCOCH₂CH₃), 0.84 (d, 3H, *J* = 6.1 Hz, H-6). ¹³C NMR (125 MHz, CDCl₃) δ 174.3, 171.5, 138.3, 138.2, 138.1, 138.03, 138.00, 137.1, 128.9, 128.34, 128.29, 128.27, 128.20, 128.14, 128.10, 128.0, 127.58, 127.57, 127.53, 127.51, 127.4, 127.3, 126.9, 126.3, 101.7, 101.4, 99.6, 98.3, 81.1, 80.6, 78.9, 78.1, 76.9, 76.1, 76.51, 76.47, 75.4, 74.7, 74.5, 72.5, 72.4, 68.8, 68.7, 66.2, 57.5, 57.0, 29.6, 17.5, 9.9. Anal. calc'd for C₆₄H₇₂N₂O₁₅: C, 69.30; H, 6.54; N, 2.53. Found: C, 69.15; H, 6.48; N, 2.82. ES MS calc'd for C₆₄H₇₂N₂O₁₅Na (M+Na): 1131.5. Found: 1131.5.

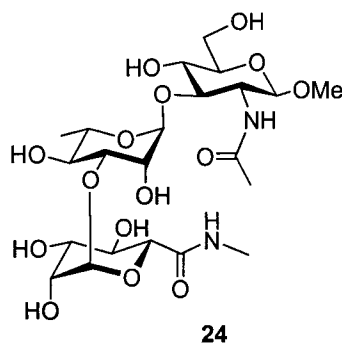


Methyl 4, 6-*O*-benzylidene-2-acetamido-3-*O*-(2,4-di-*O*-benzyl-3-*O*-(2, 3, 4-tri-*O*-benzyl-6-*N*-methylamino- α -L-mannopyranuronyl)- α -L-rhamnopyranosyl)- β -D-glucopyranoside (46): Using the same protocol for the production of **45**, alcohol **44** (0.179 g, 0.182 mmol) was oxidized and converted to its corresponding amide using carbonyldiimidazole (0.061 g, 0.377 mmol) and methylamine (0.10 mL of a 2.0 M

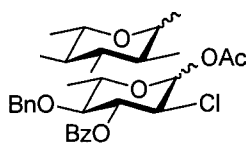
solution in THF, 0.2 mmol) to afford the title compound (0.136 g, 67%) as a white foam. $[\alpha]_D = -33.0$ ($c = 1.0$, CHCl_3). $^1\text{H NMR}$ (600 MHz, CDCl_3) δ 7.48-7.09 (m, 30 H, Ar-H), 6.49 (bd, 1H, $J = 7.1$ Hz, -NHAc), 6.44 (bd, 1H, NHCH₃), 5.52 (s, 1H, PhCHO₂-), 5.24 (d, 1H, $J = 1.4$ Hz, H-1''), 5.04 (d, 1H, $J = 1.50$ Hz, H-1'), 4.81 (d, 1H, $J_{\text{gem}} = 10.9$ Hz, PhCH₂O-), 4.70 (d, 1H, $J = 8.3$ Hz, H-1), 4.64-4.49 (m, 7H, PhCH₂O-), 4.37-4.30 (m, 3H, PhCH₂O-, H-6_a), 4.13 (dd, 1H, $J = 2.7, 9.7$ Hz, H-3'), 4.08 (bdd, 1H, $J_{2,3} \approx J_{3,4} = 9.2$ Hz, H-3), 4.03 (dd \approx t, 1H, $J = 9.0$ Hz, H-4), 3.90-3.85 (m, 2H, H-5', H-5''), 3.83 (dd, 1H, $J = 2.9, 9.7$ Hz, H-3''), 3.76 (dd, 1H, $J_{\text{vic}} \approx J_{\text{gem}} = 10.4$ Hz, H-6_b), 3.72 (dd \approx t, 1H, $J = 2.2$ Hz, H-2'), 3.68 (dd \approx t, 1H, $J = 2.6$ Hz, H-2''), 3.56 (dd, 1H, $J_{3,4} \approx J_{4,5} = 9.2$ Hz, H-4), 3.53-3.41 (m, 6H, -OCH₃, H-2, H-5, H-4'), 2.68 (d, 3H, $J = 4.9$ Hz, -NHCH₃), 1.84 (s, 3H, -NHCOCH₃), 0.91 (d, 3H, $J = 6.2$ Hz, H-6'). $^{13}\text{C NMR}$ (125 MHz CDCl_3) δ 170.7, 169.8, 138.4, 138.2, 138.15, 138.06, 138.05, 137.2, 129.0, 128.43, 128.41, 128.3, 128.2, 128.1, 127.8, 127.64, 127.58, 127.50, 127.4, 126.9, 126.2, 101.59, 101.55, 99.7, 98.3, 81.0, 80.9, 79.1, 77.4, 76.6, 76.5, 76.2, 75.4, 74.8, 74.5, 72.5, 72.3, 72.2, 68.9, 68.7, 66.1, 57.1, 57.0, 26.0, 23.2, 17.5. Anal. calc'd for C₆₄H₇₂N₂O₁₅: C, 69.30; H, 6.54; N, 2.53. Found: C, 69.27; H, 6.63; N, 2.71. ES HRMS calc'd for C₆₄H₇₂N₂O₁₅Na (M+Na): 1131.4830. Found: 1131.4837.



Methyl 2-propionamido-3-O-(3-O-(6-amino- α -L-mannopyranuronyl)- α -L-rhamnopyranosyl)- β -D-glucopyranoside (23): Protected amide **45** (56.1 mg, 50.6 μ mol), was suspended in methanol (10 mL) and water (1 mL). Palladium hydroxide (20% wt., Degussa type, 44 mg) was added and the reaction stirred under a hydrogen atmosphere for 24 h. The reaction mixture was filtered, concentrated, and pre-purified with a Waters C-18 Sep-Pak solid-phase extraction cartridge. Further purification was performed using reverse-phase (C-18) HPLC utilizing a gradient from 0% to 10% methanol in water. The resultant clear glass was lyophilized to a white powder (23.4 mg, 81%): $[\alpha]_D = -63.5$ ($c = 0.6$, H_2O). 1H NMR (600 MHz, D_2O) δ 8.22 (bd, 1H, -NHCOEt), 5.02 (s, 1H, H-1''), 4.81 (s, 1H, H-1'), 4.12 (d, 1H, $J = 8.7$ Hz, H-1), 4.12 (d, 1H, $J = 9.8$ Hz, H-5''), 4.08 (dd \approx t, 1H, $J = 1.7$ Hz, H-2''), 4.03 (dq, 1H, $J = 6.2, 9.8$ Hz, H-5'), 3.93 (d, 1H, $J_{gem} = 12.3$ Hz, H-6_a), 3.91 (d, 1H, $J = 3.3, 9.7$ Hz, H-3''), 3.87 (dd \approx t, 1H, $J = 1.4$ Hz, H-2'), 3.84-3.77 (m, 3H, H-2, H-3', H-4''), 3.74 (dd, 1H, $J_{gem} = 12.3$ Hz, $J_{vic} = 6.0$ Hz, H-6_b), 3.59 (dd \approx t, 1H, $J = 8.5$ Hz, H-3), 3.55-3.43 (m, 6H, -OCH₃, H-4, H-5, H-4'), 2.27 (q, 2H, $J = 7.7$ Hz, COCH₂CH₃), 1.24 (d, 3H, $J = 6.2$ Hz, H-6'), 1.11 (t, 2H, $J = 7.7$ Hz, COCH₂CH₃). ^{13}C NMR (125 MHz, D_2O) δ 177.5, 173.5, 101.9, 100.9, 100.8, 81.3, 78.5, 75.5, 72.1, 70.7, 69.9, 69.4, 69.2, 68.4, 68.1, 68.0, 60.3, 56.6, 54.5, 29.0, 16.0, 9.2. ES HRMS calc'd for C₂₂H₃₈N₂O₁₅Na (M+Na): 593.2164. Found: 593.2159.



Methyl 2-acetamido-3-O-(3-O-(6-N-methylamino- α -L-mannopyranuronyl)- α -L-(rhamnopyranosyl)- β -D-glucopyranoside (24): Protected amide **46** (92.4 mg, 83.3 μ mol) was suspended in methanol (10 mL) and water (1 mL). Palladium hydroxide (10% wt., Degussa type, 67 mg) was added and the reaction stirred under a hydrogen atmosphere (balloon) for 24 h. The reaction mixture was filtered, concentrated, and pre-purified with a Waters C-18 Sep-Pak solid-phase extraction cartridge. Final purification was performed using reverse-phase (C-18) HPLC utilizing a gradient from 0% to 10% methanol in water. The resultant clear glass was lyophilized to a white powder (37.0 mg, 78%): $[\alpha]_D = -50.9$ ($c = 0.6$, H₂O). ¹H NMR (600 MHz, D₂O) δ 5.21 (d, 1H, $J = 1.7$ Hz, H-1"), 4.85 (d, 1H, $J = 1.7$ Hz, H-1'), 4.52 (d, 1H, $J = 8.6$ Hz, H-1), 4.14 (d, 1H, $J = 9.2$ Hz, H-5"), 4.12 (dd, 1H, $J = 1.7, 3.3$ Hz, H-2"), 4.06 (dq, 1H, $J = 6.2, 9.8$ Hz, H-5'), 3.98 (dd, 1H, $J_{gem} = 10.2$ Hz, $J_{vic} = 2.2$ Hz, H-6_a), 3.95 (dd, 1H, $J = 3.3, 9.7$ Hz, H-3"), 3.88 (dd, 1H, $J = 2.0, 2.3$ Hz, H-2'), 3.87-3.77 (m, 4H, H-2, H-6_b, H-3', H-4"), 3.62 (dd, 1H, $J = 8.5, 10.0$ Hz, H-3), 3.59-3.48 (m, 6H, -OCH₃, H-4, H-5, H-4'), 2.86 (s, 3H, -NHCH₃), 1.24 (d, 3H, $J = 6.2$ Hz, H-6'). ¹³C NMR (125 MHz, D₂O) δ 173.4, 171.1, 102.0, 100.8, 100.7, 81.6, 78.1, 75.5, 72.5, 70.7, 69.9, 69.4, 69.3, 68.5, 68.1, 60.2, 56.5, 54.5, 25.3, 21.6, 16.0. ES HRMS calc'd for C₂₂H₃₈N₂O₁₅Na (M+Na): 593.2170. Found 593.2171.

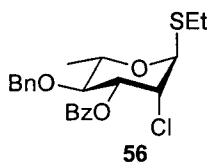


54

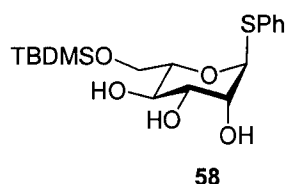
1-*O*-Acetyl-3-*O*-benzoyl-4-*O*-benzyl-2-chloro-2-deoxy- α -L-rhamnopyranose

(54): Chlorine gas was slowly bubbled through a stirring solution of glycal **51** (2.18 g, 6.74 mmol) in carbon tetrachloride (6 mL) in a darkened flask at $-10\text{ }^{\circ}\text{C}$, until a faint yellow color persisted. Excess chlorine gas was removed by bubbling argon through the solution for 1 h, the solvent was removed under reduced pressure and the residue was evacuated under high vacuum for 20 minutes. The light opaque residue was dissolved in glacial acetic acid (5 mL) under an argon atmosphere, silver acetate (0.702 g, 4.20 mmol) was added and the solution was stirred for 12 h at room temperature. The solution was filtered through Celite and concentrated. The light yellow syrup was dissolved in dichloromethane and washed with saturated sodium bicarbonate and water, then dried with sodium sulfate, filtered and evaporated to dryness. The product was purified by column chromatography (6:1 hexanes:ethyl acetate) to afford the target compound as a clear syrup (1.99 g, 88% overall yield; 3.9:1 distribution of α -*rhamno*- and β -*quinovo*-isomers). Data for α -rhamnosyl isomer: $[\alpha]_{\text{D}} +2.00$ (c 2.00, CHCl_3). ^1H NMR (600 MHz, CDCl_3) δ 8.09-7.19 (m, 10H, Ar-*H*), 6.19 (d, 1H, $J = 2.0$ Hz, H-1), 5.61 (dd, 1H, $J = 3.8, 9.1$ Hz, H-3), 4.62 (ABq, 2H, $J = 11.0$ Hz, $\text{PhCH}_2\text{O-}$), 4.52 (dd, 1H, $J = 2.0, 3.8$ Hz, H-2), 3.99 (dq, 1H, $J = 6.2, 9.5$ Hz, H-5), 3.98 (dd \approx t, 1H, $J = 9.3$ Hz, H-4), 2.14 (s, 3H, $-\text{C}(\text{O})\text{CH}_3$), 1.37 (d, 3H, $J = 6.2$ Hz, H-6). ^{13}C NMR (125 MHz, CDCl_3) δ 168.6, 165.6, 137.4, 133.5, 129.8, 129.4, 128.6, 128.0, 93.1 ($^1J_{\text{C1-H1}} = 180.2$ Hz), 77.9, 75.5, 72.3,

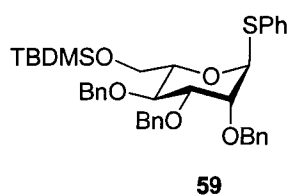
70.5, 57.5, 20.9, 18.0. Anal. calc'd for $C_{22}H_{23}ClO_6$: C, 63.08; H, 5.53. Found C, 63.06; H, 5.57. ES HRMS calc'd for $C_{22}H_{23}ClO_6Na$ (M+Na): 441.1080. Found 441.1072.



Ethyl 3-O-benzoyl-4-O-benzyl-2-chloro-2-deoxy-1-thio- α -L-rhamnopyranoside (56): To a stirring solution of anomeric acetate **54** (3.31g, 7.90 mmol) and 3Å molecular sieves in ethanethiol (0.76 mL, 10.3 mmol) and distilled dichloromethane (50 mL) under argon at 0 °C was added borontrifluoride diethyletherate (1.29 mL, 10.3 mmol). The reaction was allowed to stir for 2 h before the addition of triethylamine (4 mL). The solution was filtered and washed with sodium bicarbonate (sat.) and water. The organic layer was dried with sodium sulfate and concentrated under vacuum. Column chromatography (9:1 hexanes:ethyl acetate) gave a clear syrup (3.04 g, 91%): $[\alpha]_D -62.3$ (*c* 2.6, $CHCl_3$). 1H NMR (600 MHz, $CDCl_3$) δ 8.06-7.20 (m, 10 H, Ar-*H*), 5.53 (dd, 1H, $J = 3.7, 9.2$ Hz, H-3), 5.37 (s, 1H, H-1), 4.71 (dd, 1H, $J = 1.2, 3.6$ Hz, H-2), 4.69 (Abq, 2H, $J = 10.9$ Hz, $PhCH_2O-$), 4.26 (dq, 1H, $J = 6.3, 9.4$ Hz, H-5), 3.80 (dd \approx t, 1H, $J = 9.3$ Hz, H-4), 2.64 (m, 2H, SCH_2CH_3), 1.37 (d, 3H, $J = 6.3$ Hz, H-6), 1.27 (t, 3H, SCH_2CH_3). ^{13}C NMR (125 MHz, $CDCl_3$) δ 165.3, 137.5, 133.3, 129.7, 129.5, 128.5, 128.3, 127.9, 127.8, 84.3 ($J_{C1-H1} = 168.8$ Hz), 78.6, 75.3, 73.2, 68.9, 61.1, 26.0, 18.0, 15.0. Anal. calc'd for $C_{22}H_{25}ClO_4S$: C, 62.77; H, 5.99. Found: C, 62.74; H, 5.89. ES HRMS calc'd for $C_{22}H_{25}ClO_4SNa$ (M+Na): 443.1059. Found 443.1056.

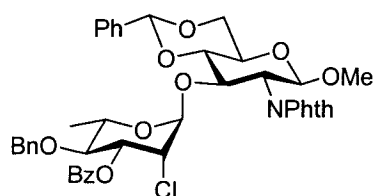


Phenyl 6-*O*-(*tert*-butyldimethylsilyl)-1-thio- α -L-mannopyranoside (58**):** To a stirred solution of triol **57** (1.72 g, 6.34 mmol) in pyridine (15 mL) was added *tert*-butylchlorodimethylsilane (1.43 g, 9.51 mmol). Triethylamine (10 mL) was added in five 1 mL portions over 10 minutes, whereupon the volatiles were evaporated under vacuum. Column chromatography (3:1 ethyl acetate:toluene) gave the title compound as a white foam (2.20 g, 90%): $[\alpha]_D -1.91$ (c 0.76, CHCl_3). ^1H NMR (600 MHz, CD_3OD) δ 7.54-7.23 (m, 5H, Ar-*H*), 5.41 (d, 1H, $J = 1.2$ Hz, H-1), 4.08-4.04 (m, 2H, H-2, H-5), 3.99 (dd, 1H, $J_{\text{gem}} = 11.2$ Hz, $J_{\text{vic}} = 2.0$ Hz, H-6_a), 3.82 (dd, 1H, $J_{\text{gem}} = 11.2$ Hz, $J_{\text{vic}} = 6.7$ Hz, H-6_b), 3.66 (dd, 1H, $J = 2.8, 9.3$ Hz, H-3), 3.63 (dd \approx t, 1H, $J = 9.3$ Hz), 0.89 (s, 9H, $-\text{C}(\text{CH}_3)_3$), 0.07 (s, 3H, $-\text{Si}(\text{CH}_3)_a$), 0.05 (s, 3H, $-\text{Si}(\text{CH}_3)_b$). ^{13}C NMR (125 MHz, CD_3OD) δ 136.2, 132.7, 129.9, 128.3, 90.3 ($^1J_{\text{C1-H1}} = 167.1$ Hz), 76.1, 73.6, 73.2, 69.0, 64.5, 26.4, 19.3, -5.0, -5.1. Anal. calc'd for $\text{C}_{18}\text{H}_{30}\text{O}_5\text{SSi}$: C, 55.92; H, 7.82. Found: C, 55.55; H, 8.00. ES HRMS calc'd for $\text{C}_{18}\text{H}_{30}\text{O}_5\text{SSiNa}$ ($\text{M}+\text{Na}$): 409.1475. Found: 409.1474.



Phenyl 2,3,4-tri-*O*-benzyl-6-*O*-(*tert*-butyldimethylsilyl)-1-thio- α -L-mannopyranoside (59**):** A stirring solution of triol **58** (3.34 g, 8.65 mmol) in dry DMF (70 mL) was cooled to 0 °C under argon and sodium hydride (95% dry, 1.24 g, 51.9 mmol) was

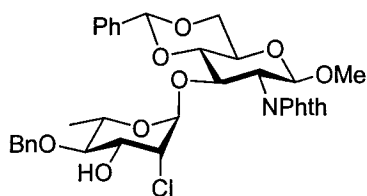
added. The reaction was allowed to stir for 30 minutes before the addition of benzyl bromide (5.15 mL, 43.3 mmol). The mixture was stirred for 16 h before the slow addition of methanol (25 mL). The solvents were removed and the crude mixture was dissolved in dichloromethane and washed with water. The organic layer was dried (sodium sulfate) and evaporated under vacuum. Column chromatography (12:1 hexanes:ethyl acetate) gave a thin clear syrup (5.34 g, 94%): $[\alpha]_D -72.8$ ($c = 0.9$, CHCl_3) ^1H NMR (600 MHz, CDCl_3) δ 7.47-7.23 (m, 20H, Ar-H), 5.57 (dd, 1H, $J = 1.7$ Hz, H-1), 4.96 (d, 1H, $J_{\text{gem}} = 11.0$ Hz, $\text{PhCH}_2\text{O}-$), 4.71-4.62 (m, 5H, $\text{PhCH}_2\text{O}-$), 4.12 (ddd, 1H, $J = 1.7, 4.9, 9.6$ Hz, H-5), 4.03 (dd \approx t, 1H, $J = 9.4$ Hz, H-4), 4.00 (dd, 1H, $J = 1.7, 3.0$ Hz, H-2), 3.93 (dd, 1H, $J_{\text{gem}} = 11.5$ Hz, $J_{\text{vic}} = 5.1$ Hz, H-6_a), 3.89-3.85 (m, 2H, H-3, H-6_b), 0.91 (s, 9H, $-\text{Si}(\text{CH}_3)_3$), 0.08 (s, 3H, $-\text{Si}(\text{CH}_3)_a$), 0.06 (s, 3H, $-\text{Si}(\text{CH}_3)_b$). ^{13}C NMR (125 MHz, CDCl_3) δ 138.7, 138.3, 138.0, 134.8, 131.5, 128.9, 128.4, 138.37, 138.31, 128.0, 127.9, 127.8, 127.7, 127.6, 127.2, 85.6, 80.2, 76.6, 75.2, 74.9, 74.3, 72.2, 71.8, 62.7, 26.0, 18.4, -5.1, -5.3. Anal. calc'd for $\text{C}_{39}\text{H}_{48}\text{O}_5\text{SSi}$: C, 71.30; H, 7.36. Found: C, 71.45; H, 7.33. ES HRMS calc'd for $\text{C}_{39}\text{H}_{48}\text{O}_5\text{SSiNa}$ ($\text{M}+\text{Na}$): 679.2884. Found: 679.2885.



60

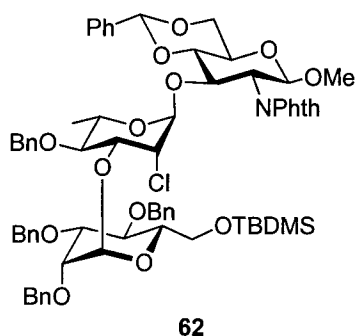
Methyl (3-*O*-benzoyl-4-*O*-benzyl-2-chloro-2-deoxy- α -L-rhamnopyranosyl)-(1 \rightarrow 3)-4,6-*O*-benzylidene-2-phthalimido- β -D-glucopyranoside (60): A solution of

glucosamine acceptor **30**^[100] (2.31 g, 5.62 mmol) and rhamnosyl donor **56** (2.86 g, 6.79 mmol) were dissolved in dry dichloromethane (40 mL) and stirred with 3 Å molecular sieves for 1 h under argon. The flask was darkened and *N*-iodosuccinimide (1.53 g, 6.79 mmol) and silver trifluoromethane sulfonate (1.40 g, 5.43 mmol) were added all at once. The reaction mixture was stirred for 15 min and neutralized with triethylamine (~1 mL) before filtration through Celite. The dichloromethane solution was washed with sodium thiosulfate (10%), sodium bicarbonate (sat.) and water. The organic layer was dried (sodium sulfate) and concentrated under reduced pressure. Gradient column chromatography (5:1-4:1-2:1 hexanes:ethyl acetate) gave a colorless foam (3.98 g, 92%): $[\alpha]_D^{+9.8}$ (*c* 1.1, CHCl₃). ¹H NMR (600 MHz, CDCl₃) δ 7.98-7.06 (m, 19H, Ar-*H*), 5.56 (s, 1H, PhCHO₂-), 5.48 (dd, 1H, *J* = 3.7, 8.7 Hz, H-3'), 5.18 (d, 1H, *J* = 8.5 Hz, H-1), 4.68 (d, 1H, *J* = 1.9 Hz, H-1'), 4.65 (dd, 1H, *J* = 8.9, 10.2 Hz, H-3), 4.58 and 4.46 (d, 1H ea., *J*_{gem} = 11.1 Hz, PhCH₂O-), 4.41 (dd, 1H, *J*_{gem} = 10.5 Hz, *J*_{vic} = 4.8 Hz, H-6_a), 4.30 (dd, 1H, *J* = 8.6, 10.3 Hz, H-2), 4.13 (dd, 1H, *J* = 1.9, 3.7 Hz, H-2'), 4.08 (dq, 1H, *J* = 6.2, 8.9 Hz, H-5'), 3.83 (dd ≈ t, 1H, *J*_{5,6} ≈ *J*_{vic} = 10.1 Hz, H-6_b), 3.72 (dd ≈ t, 1H, *J* = 9.3 Hz, H-4), 3.67 (ddd, 1H, *J*_{5,6} ≈ *J*_{gem} = 9.4 Hz, *J*_{vic} = 4.8 Hz, H-5), 3.49 (dd ≈ t, 1H, *J* = 9.1 Hz, H-4'), 3.41 (s, 3H, -OCH₃), 0.82 (d, 3H, *J* = 6.2 Hz, H-6'). ¹³C NMR (125 MHz, CDCl₃) δ 179.8, 165.5, 137.3, 136.9, 134.3, 133.2, 131.3, 129.7, 129.6, 129.0, 128.4, 128.2, 128.1, 127.7, 127.6, 126.3, 101.9, 100.2 (¹*J*_{C1-H1} = 165.9 Hz), 99.7 (¹*J*_{C1-H1} = 173.2 Hz), 80.6, 78.5, 74.6, 74.3, 71.9, 68.7, 68.4, 58.7, 57.0, 56.3, 17.3. Anal. calc'd for C₄₂ClH₄₀NO₁₁: C, 65.49; H, 5.23; N, 1.82. Found: C, 65.18; H, 5.24; N, 1.69. ES HRMS calc'd for C₄₂ClH₄₀NO₁₁Na (M+Na): 792.2187. Found: 792.2180.



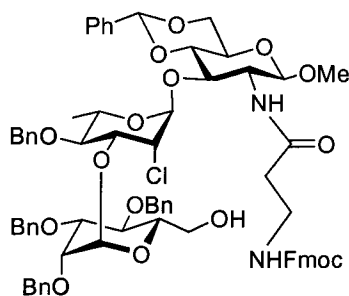
61

Methyl (4-*O*-benzyl-2-chloro-2-deoxy- α -L-rhamnopyranosyl)-(1 \rightarrow 3)-4,6-*O*-benzylidene-2-phthalimido- β -D-glucopyranoside (61): Protected disaccharide **60** (2.13 g, 2.76 mmol) was dissolved in dry dichloromethane (20 mL) under argon at 0 °C. Methanol (40 mL) and sodium metal (88 mg) were added, the reaction warmed to room temperature and stirred for 12 h before neutralization with Rexyn 101 (H⁺) resin. The resin was filtered and the solution was concentrated under vacuum. Column chromatography (2% acetone in chloroform) afforded a white powder (1.49 g, 81%): $[\alpha]_D -55.1$ (*c* 2.1, CHCl₃). ¹H NMR (600 MHz, CD₂Cl₂) δ 7.91-7.23 (m, 14H, Ar-*H*), 5.56 (s, 1H, PhCHO₂-), 5.17 (d, 1H, *J* = 8.6 Hz, H-1), 4.64 (d, 1H, *J* = 11.3 Hz, PhCH₂O-), 4.62 (s, 1H, H-1'), 4.59 (dd, 1H, *J* = 8.9, 9.9 Hz, H-3), 4.52 (d, 1H, *J* = 11.3 Hz, PhCH₂O-), 4.40 (d, 1H, *J* = 4.3, 7.1 Hz, H-6_a), 4.19 (dd, 1H, *J* = 8.6, 10.1 Hz, H-2), 4.00 (ddd, 1H, 3.8, 7.2, 9.0 Hz, H-3'), 3.94-3.87 (m, 2H, H-2', H-5'), 3.85-3.79 (m, 1H, H-6_b), 3.70-3.63 (m, 2H, H-4, H-5), 3.41 (s, 3H, -OCH₃), 3.14 (dd \approx t, 1H, *J* = 9.2 Hz, H-4'), 2.13 (d, 1H, *J* = 7.1 Hz, 3'-OH), 0.79 (d, 3H, *J* = 6.2 Hz, H-6'). ¹³C NMR (125 MHz, CD₂Cl₂) δ 168.3, 138.8, 137.7, 135.0, 131.6, 129.4, 128.7, 128.5, 128.09, 128.07, 126.8, 124.0, 102.3, 100.5, 100.1, 81.6, 81.0, 75.1, 75.0, 70.1, 69.1, 68.8, 66.9, 62.8, 57.5, 57.0, 17.7. Anal. calc'd for C₃₅H₃₆ClNO₁₀: C, 63.11; H, 5.45; N, 2.10. Found: C, 62.75; H, 5.34; N, 2.09. ES HRMS calc'd for C₃₅H₃₆ClNO₁₀Na (M+Na): 688.1925. Found: 688.1924.



Methyl (2,3,4-tri-*O*-benzyl-6-*O*-*tert*-butyldimethylsilyl- α -L-mannopyranosyl)-(1 \rightarrow 3)-(4-*O*-benzyl-2-chloro-2-deoxy- α -L-rhamnopyranosyl)-(1 \rightarrow 3)-4,6-*O*-benzylidene-2-phthalimido- β -D-glucopyranoside (62): Disaccharide acceptor **61** (1.33 g, 2.00 mmol) and thiomannosyl donor **59** (2.37 g, 3.60 mmol) were dissolved in dry dichloromethane (40 mL), protected from light, and cooled to -30 °C under argon. *N*-iodosuccinimide (0.81 g, 3.60 mmol) and a solution of dichloromethane (200 μ L) saturated with trifluoromethanesulfonic acid were added all at once. The reaction mixture was warmed to -20 °C and allowed to stir for 2 h before neutralization with triethylamine (1.5 mL). The reaction mixture was washed with sodium thiosulfate (10%), sodium bicarbonate (sat.) and water. The organic layer was dried with sodium sulfate and concentrated under vacuum. Gradient column chromatography (7:1-6:1-4:1 hexanes:ethyl acetate) afforded a white foam (2.10 g, 86%): $[\alpha]_D -15.7$ (*c* 0.7, CDCl_3). ^1H NMR (600 MHz, CDCl_3) δ 7.83-7.11 (m, 29H, Ar-*H*), 5.56 (s, 1H, PhCHO_2 -), 5.20 (d, 1H, $J = 8.4$ Hz, H-1), 4.97 (d, 1H, $J = 1.8$ Hz, H-1''), 4.88 (d, 1H, $J_{\text{gem}} = 10.8$ Hz, PhCH_2O -), 4.67 (d, 1H, $J_{\text{gem}} = 10.8$ Hz, PhCH_2O -), 4.61 (d, 1H, $J_{\text{gem}} = 11.4$ Hz, PhCH_2O -), 4.58 (d, 1H, $J = 1.8$ Hz, H-1'), 4.56 (dd, 1H, $J = 8.4, 10.2$ Hz, H-3), 4.53-4.46 (m, 3H, PhCH_2O -), 4.43-4.35 (m, 3H, PhCH_2O -, H-6_a), 4.25 (dd, 1H, $J = 8.5, 10.1$ Hz, H-2), 4.08 (dd \approx t, 1H, $J = 9.7$ Hz, H-4''), 4.03 (dd, 1H, $J = 3.7, 9.0$ Hz, H-3'), 3.95-3.91 (m,

2H, H-5', H-6_a''), 3.90 (dd, 1H, $J = 1.6, 3.7$ Hz, H-2'), 3.87-3.81 (m, 3H, H-6_b, H-6_b'', H-3''), 3.69-3.63 (m, 3H, H-4, H-5, H-5''), 3.59 (dd, 1H, $J = 1.9, 2.9$ Hz, H-2''), 3.42 (s, 3H, -OCH₃), 3.19 (dd \approx t, 1H, $J = 9.3$ Hz, H-4'), 0.91, (s, 9H, (CH₃)₃CSi-), 0.77 (d, 3H, $J = 6.1$ Hz, H-6'), 0.12 (s, 6H, (CH₃)₂Si-). ¹³C NMR (125 MHz, CDCl₃) δ 167.9, 138.9, 138.7, 138.5, 138.3, 137.0, 134.4, 131.2, 129.0, 128.3, 128.2, 128.1, 127.8, 127.6, 127.5, 127.4, 127.2, 127.1, 126.3, 123.6, 101.8, 100.2 (¹J_{C1-H1} = 169.8 Hz, C-1''), 99.9 (¹J_{C1-H1} = 172.7 Hz, C-1'), 99.7 (¹J_{C1-H1} = 164.9 Hz, C-1), 80.5, 79.9, 79.3, 77.3, 76.2, 75.1, 74.6, 74.4, 74.0, 73.9, 72.4, 72.3, 68.7, 68.6, 66.4, 61.2, 60.7, 57.1, 56.5, 26.0, 17.2, -5.0, -5.3. Anal. calc'd for C₆₈H₇₈ClNO₁₅Si: C, 67.34; H, 6.48; N, 1.15, found: C, 67.46; H, 6.53; N, 1.13. ESMS calc'd for C₆₈H₇₈ClNO₁₅SiNa (M+Na): 1234.4727. Found: 1234.5.

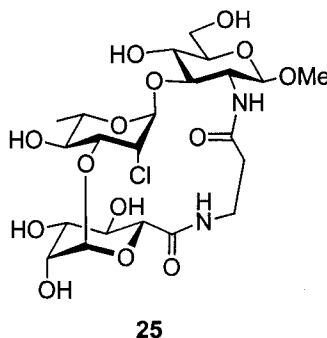


63

Methyl (2,3,4-tri-*O*-benzyl- α -L-mannopyranosyl)-(1 \rightarrow 3)-(4-*O*-benzyl-2-chloro-2-deoxy- α -L-rhamnopyranosyl)-(1 \rightarrow 3)-4,6-*O*-benzylidene-2-deoxy-2-(*N*-fluorenylmethoxycarbonyl- β -alanyl)-amido- β -D-glucopyranoside (63): To a solution of fully protected trisaccharide **62** (0.721 g, 0.595 mmol) in ethanol (15 mL) was added hydrazine hydrate (1.0 mL, 12.9 mmol) and the solution was heated at reflux under argon for 24 h. Upon cooling the reaction was diluted with CHCl₃ and washed with water. The organic layer was evaporated, suspended in boiling ethanol (100%), cooled, filtered, and washed with cold ethanol to afford the free amine which needed no further purification. The

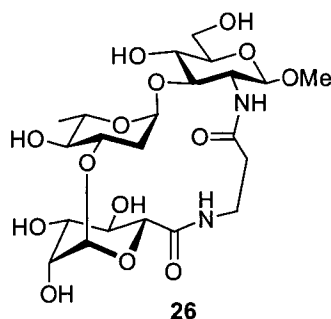
white solid was dissolved in THF and tetrabutylammonium fluoride (1.5 mL, 1.0 M in THF, 1.5 mmol) was added. The solution stirred for 24 h and evaporated to dryness. The brown syrup was filtered through silica using toluene as the eluent, and evaporated to dryness. The resultant white solid (0.467 g, 0.482 mmol) was dissolved in dry DMF (12 mL) and *N*-Fmoc- β -alanine (0.180 g, 0.578 mmol), *O*-(Benzotriazol-1-yl)-*N,N,N',N'*-tetramethyluronium tetrafluoroborate (0.309 g, 0.964 mmol), 1-hydroxybenzotriazole (0.147 g, 0.964 mmol), and *N*-ethylmorpholine (0.24 mL, 1.88 mmol) were added and the reaction was allowed to stir for 2 h. The solvents were removed under vacuum and the residue was dissolved in dichloromethane and washed with water. The organic layer was dried with sodium sulfate, filtered, and evaporated to dryness. Column chromatography (2:3:1 cyclohexane:ethyl acetate:acetone) afforded the target compound as a white powder (0.510 g, 68%): $[\alpha]_D -40.7$ (*c* 1.0, CHCl₃). ¹H NMR (600 MHz, CDCl₃) δ 7.75-7.15 (m, 33H, Ar-*H*), 5.50 (s, 1H, PhCHO₂-), 5.11 (s, 1H, H-1''), 4.88 (s, 1H, H-1'), 4.84 (d, 1H, $J_{gem} = 10.9$ Hz, PhCH₂O-), 4.61 (d, 1H, $J_{gem} = 11.7$ Hz, PhCH₂O-), 4.59-4.40 (m, 8H, H-1, H-2', PhCH₂O-), 4.39-4.32 (m, 3H, H-6_a, -OCH₂CHAr), 4.20-4.16 (m, 2H, H-3', -OCH₂CHAr), 4.01-4.09 (bm, 1H, H-3), 3.97-3.88 (m, 4H, H-5', H-3'', H-5'', H-6_a''), 3.77-3.72 (m, 2H, H-6_b, H-4''), 3.69-3.64 (m, 2H, H-2'', H-6_b''), 3.61-3.53 (m, 1H, H-2), 3.52 (dd \approx t, $J = 9.3$ Hz, H-4), 3.48-3.38 (m, 3H, H-5, tether- $\beta_{a/b}$), 3.38-3.33 (m, 4H, -OCH₃, H-4'), 2.48-2.36 (m, 2H, tether- $\alpha_{a/b}$), 0.81 (d, 3H, $J = 6.0$ Hz, H-6'). ¹³C NMR (125 MHz, CDCl₃) δ 172.1, 157.0, 144.1, 143.8, 138.4, 138.3, 138.2, 138.1, 137.0, 129.0, 128.38, 128.35, 128.31, 128.26, 128.20, 128.1, 127.8, 127.7, 127.6, 127.55, 127.53, 127.51, 127.2, 127.1, 126.3, 125.2, 101.7, 101.4, 100.9, 100.8, 79.94, 79.87, 77.9, 77.7, 75.9, 75.4, 75.1, 75.0, 74.0, 72.7, 72.4, 68.9, 68.7, 66.8, 66.3, 63.0, 61.2, 57.2, 56.8, 37.1,

hexane:ethyl acetate:acetone) to afford an amorphous white solid (0.22 g, 61%): $[\alpha]_D$ -39.6 ($c = 0.9$, CHCl_3). $^1\text{H NMR}$ (600 MHz, $\text{CD}_3\text{C(O)CD}_3$) δ 7.51-7.21 (m, 27 H, Ar-H, 2x N-H), 5.63 (s, 1H, PhCHO₂-), 5.25 (d, 1H, $J = 3.5$ Hz, H-1''), 4.94 (d, 1H $J = 1.3$ Hz, H-1'), 4.78 (d, 1H, $J = 10.3$ Hz, PhCH₂O-), 4.77 (d, 1H, $J = 11.0$ Hz, PhCH₂O-), 4.64-4.58 (m, 5H, PhCH₂O-), 4.52 (d, 1H, $J = 11.3$ Hz, PhCH₂O-), 4.46 (d, 1H, $J = 8.4$ Hz, H-1), 4.34 (dd, 1H, $J = 1.7, 3.7$ Hz, H-2'), 4.29 (d, 1H, $J = 8.8$ Hz, H-5''), 4.27-4.21 (m, 2H, H-6_a, H-2), 4.15 (dd, 1H, $J = 3.7, 9.3$ Hz, H-3'), 3.91-3.75 (m, 10H, OCH₃, tether-βH_a, H-3, H-6_b, H-5', H-2'', H-3'', H-4''), 2.67 (dd \approx t, 1H, $J = 9.5$ Hz, H-4), 3.44 (ddd, 1H, $J = 5.1, 9.7, 9.7$ Hz, H-5), 3.34 (dd \approx t, 1H, $J = 9.4$ Hz, H-4'), 3.24 (m, 1H, tether-βH_b), 2.48 (ddd, 1H, $J_{\text{gem}} = 16.5$ Hz, $J_{\text{vic}} = 3.0$ Hz, tether-αH_a), 2.40 (ddd, 1H, $J_{\text{vic}} = 4.0, 12.0$ Hz, $J_{\text{gem}} = 16.5$ Hz, tether-αH_b), 0.74 (d, 3H, $J = 6.2$ Hz, H-6'). $^{13}\text{C NMR}$ (125 MHz, CDCl_3) δ 171.2, 169.2, 138.3, 138.1, 137.8, 137.1, 129.1, 128.3, 128.28, 128.26, 128.24, 127.9, 127.7, 127.63, 127.58, 127.55, 126.4, 102.6, 102.3, 101.7, 101.6, 82.2, 80.3, 19.1, 78.3, 77.5, 75.1, 73.6, 73.0, 72.8, 72.0, 68.8, 68.6, 66.5, 61.9, 56.7, 54.3, 35.3, 33.5, 17.6. Anal. calc'd for $\text{C}_{57}\text{H}_{63}\text{ClN}_2\text{O}_{14}$: C, 66.11; H, 6.13; N, 2.71. Found: C, 65.86; H, 6.03; N, 2.69. ES MS calc'd for $\text{C}_{57}\text{H}_{63}\text{ClN}_2\text{O}_{14}\text{Na}$ (M+Na): 1057.4. Found: 1057.4.



**Methyl (α-L-mannopyranosyluronyl)-(1→3)-(2-chloro-2-deoxy-α-L-rhamno-
pyranosyl)-(1→3)-2-(3-aminopropionamido)-2-deoxy-β-D-glucopyranoside**

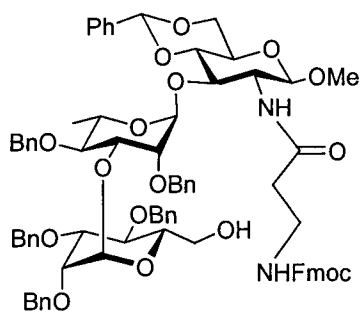
lactam (25): Protected lactam **64** (105 mg, 0.101 mmol), was suspended in methanol (10 mL) and water (1 mL). Palladium hydroxide (10% wt., Degussa type, 85 mg) was added and the solution stirred under a hydrogen atmosphere (balloon) for 24 h. The reaction mixture was filtered, concentrated, and pre-purified with a Waters C-18 Sep-Pak solid-phase extraction cartridge. Further purification was performed using reverse-phase (C-18) HPLC utilizing a gradient from 0% to 15% methanol in water. The resultant clear glass was lyophilized to a fluffy white solid (47.2 mg, 79%). $[\alpha]_D -27.3$ ($c = 0.7$, H₂O). ¹H NMR (600 MHz, D₂O) δ 5.13 (d, 1H, $J = 1.1$ Hz, H-1''), 5.02 (d, 1H, $J = 1.1$ Hz, H-1'), 4.39 (d, 1H, $J = 8.5$ Hz, H-1), 4.12-4.06 (m, 4H, H-2', H-3', H-2'', H-5''), 4.03 (dq, 1H, $J = 6.2, 9.7$ Hz, H-5'), 3.95-3.85 (m, 3H, H-2, H-6_a, H-4''), 3.79 (dd, 1H, $J = 3.4, 9.3$ Hz, H-3''), 3.74 (dd, 1H, $J = 6.1$ Hz, $J_{gem} = 12.4$ Hz, H-6_b), 3.67-3.60 (m, 2H, H-4', tether- β H_a), 3.57-3.51 (m, 3H, H-3, H-4, tether- β H_b), 3.48 (s, 3H, -OCH₃), 3.42 (ddd, 1H, $J = 2.0, 5.9, 8.5$ Hz, H-5), 2.64-2.51 (m, 2H, tether- α H_{a/b}), 1.28 (d, 3H, $J = 6.2$ Hz, H-6'). ¹³C NMR (125 MHz, D₂O) δ 174.5, 170.8, 104.3, 103.1, 102.7, 86.2, 78.7, 76.8, 73.2, 71.9, 71.2, 70.7, 70.4, 69.8, 68.9, 62.0, 61.6, 57.9, 55.1, 35.4, 34.7, 17.5. ES HRMS calc'd for C₂₂H₃₅ClN₂O₁₄Na (M+Na): 609.1674. Found 609.1673.



Methyl 2-(3-aminopropionamido)-3-O-(2-deoxy-3-O-[α-L-manno-

pyranosyluronic acid]-α-L-rhamnopyranosyl)-2-deoxy-β-D-glucopyranoside lactam

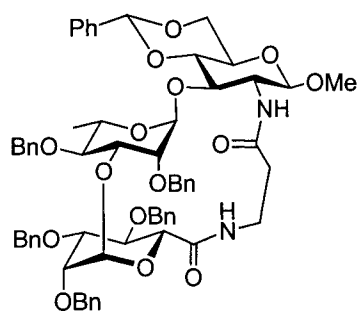
(26): To a solution of **25** (19.4 mg, 33 μ mol) in a 1,4-dioxane: THF mixture (3:1, 2 mL) at reflux was added tri-*n*-butyltin hydride (18 μ L, 66 μ mol) and 2,2-azo-bis-isobutyronitrile (6 mg, 33 μ mol). After stirring for 12 h, the solution was cooled, dichloromethane was added, and allowed to stir for 1 h at 40 °C. The solution was then concentrated under vacuum. The reaction was pre-purified with a Waters C-18 Sep-Pak followed by reverse-phase (C-18) HPLC utilizing a gradient from 0% to 15% methanol in water to give a clear glass that was lyophilized to a white solid (14.1 mg, 77%). $[\alpha]_D = -36.2$ ($c = 0.5$, H₂O). ¹H NMR (600 MHz, D₂O) δ 5.07 (s, 1H, H-1''), 4.94 (d, 1H, $J = 3.5$ Hz, H-1'), 4.40 (d, 1H, $J = 8.7$ Hz, H-1), 4.04 (dd, 1H, $J = 1.6, 3.5$ Hz, H-2''), 3.98-3.86 (m, 6H, H-2, H-6_a, H-3', H-5', H-4'', H-5''), 3.77-3.67 (m, 3 H, H-3'', H-6_b, tether- β H_a), 3.52-3.42 (m, 7H, tether- β H_b, H-3, H-4, H-5, -OCH₃), 3.25 (dd \approx t, 1H, $J = 9.5$ Hz, H-4'), 2.64-2.50 (m, 2H, tether- $\alpha_{a/b}$) 2.05 (dd, 1H, $J_{gem} = 12.5$ Hz, $J_{vic} = 4.9$ Hz, H-2_a'), 1.92 (ddd, 1H, $J_{gem} = 12.5$ Hz, $J_{vic} = 12.5, 4.9$ Hz, H-2_b') 1.24 (d, 3H, $J = 6.2$ Hz, H-6'). ¹³C NMR (125 MHz, D₂O) δ 172.9, 169.6, 102.5, 101.3, 99.9, 84.5, 77.2, 75.4, 74.1, 70.9, 70.5, 69.3, 68.5, 67.5, 60.3, 56.4, 53.7, 37.2, 33.4, 16.4. ES HRMS calc'd for C₂₂H₃₆N₂O₁₄Na (M+Na): 575.2064. Found 575.2065.



66

Methyl 3-O-(2,4-di-O-benzyl-3-O-[2,3,4-tri-O-benzyl- α -L-mannopyranosyl]- α -L-rhamno-pyranosyl)-4,6-O-benzylidene-2-deoxy-2-(*N*-fluorenylmethoxy-carbonyl- β -alanyl)-amido- β -D-glucopyranoside (66): To a solution of fully protected trisaccharide **62** (0.365 g, 0.298 mmol) in ethanol (15 mL) was added hydrazine hydrate (2.0 mL, 25.8 mmol) and the solution was heated to reflux under argon for 24 h. The volatiles were evaporated and the residue concentrated with toluene three times. The resultant white solid was dissolved in THF and tetrabutylammonium fluoride (1.0 mL, 1.0 M in THF, 1.0 mmol) was added. The solution stirred for 24 h. and evaporated to dryness. The brown syrup was filtered through silica using toluene:ethyl acetate (6:1) as eluent, and evaporated to dryness. The resultant white solid was dissolved in dry DMF (12 mL) and *N*-Fmoc- β -alanine (0.90 g, 0.290 mmol), *O*-(benzotriazol-1-yl)-*N,N,N',N'*-tetramethyluronium tetrafluoroborate (0.155 g, 0.470 mmol), 1-hydroxybenzotriazole (0.074 g, 0.470 mmol), and *N*-ethylmorpholine (0.20 mL, 1.70 mmol) were added and the reaction was allowed to stir for 6 h. The solvents were removed under vacuum and the residue was dissolved in dichloromethane and washed with water. The organic layer was dried over sodium sulfate, filtered, and concentrated to dryness. Column chromatography (2:3:1 cyclohexane:ethyl acetate:acetone) afforded the target compound as a white

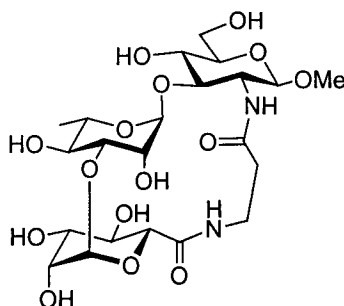
powder (0.245 g, 71%): $[\alpha]_D -21.0$ (c 0.7, CHCl_3). $^1\text{H NMR}$ (300 MHz, CDCl_3) δ : 7.69-7.08 (m, 38H, aromatic), 6.00 (bt, 1H, NH-Fmoc), 5.52 (s, 1H, CH-Ph), 5.11 (d, 1H, $J = 2.2$ Hz, H-1''), 4.86 (bs, 1H, H-1'), 4.80 (d, 1H, $\text{CH}_2\text{-Ph}$), 4.60-4.24 (m, 10H, H-1, $\text{CH}_2\text{-Ph}$), 4.27 (dd, 1H, $J_{\text{vic}} = 5.5$ Hz, $J_{\text{gem}} = 10.5$ Hz, H-6a), 4.08 (bt, $\text{O-CH}_2\text{-CHFmoc}$), 4.01 (dd, 1H, $J = 2.8, 9.7$ Hz, H-3'), 4.01 (dd \approx t, 1H, $J = 9.3$ Hz, H-4''), 3.80-3.90 (m, 6H, H-2', H-5', H-3'', H-6a'', linker), 3.73-3.77 (m, 3H, H-3, H-6b, H-6b''), 3.66-3.69 (m, 2H, H-4, tether αH_a), 3.67 (dd \approx t, 1H, $J = 2.6$ Hz, H-2''), 3.56-3.58 (m, 1H, tether αH_b), 3.52 (t, 1H, $J_{3',4'} = J_{4',5'} = 9.3$ Hz, H-4'), 3.37-3.42 (m, 5H, H-5, $\text{O-CH}_2\text{-CHFmoc}$, H-5'', H-6b''), 3.30 (s, 3H, OMe), 3.24-3.27 (m, 1H, H-2), 2.16-2.19 (m, 2H, tether $\beta\text{H}_{a/b}$), 0.73 (d, 3H, $J = 6.0$ Hz, H-6'). $^{13}\text{C NMR}$ (125 MHz, CDCl_3) δ 144.0, 143.0, 141.3, 138.5, 138.4, 138.3, 138.2, 137.0, 129.0, 128.4, 128.38, 128.35, 128.30, 128.2, 128.1, 127.8, 127.7, 127.65, 127.62, 127.60, 127.5, 127.4, 127.2, 127.1, 127.0, 126.9, 126.3, 101.8, 101.2, 99.8, 98.8, 81, 80.7, 79.8, 75.55, 75.50, 74.9, 74.7, 74.6, 73.2, 72.2, 72.1, 68.8, 68.7, 66.4, 66.48, 66.40, 66.3, 63.2, 63.1, 57.5, 56.8, 47.3, 36.1, 17.2. Anal. Calc'd for $\text{C}_{79}\text{H}_{84}\text{N}_2\text{O}_{17}$: C, 71.15; H, 6.35; N, 2.10. Found: C, 71.27; H, 6.24; N, 2.20. ES HRMS: (M+Na): 1355.3667, found: 1355.3675



67

Methyl 2-(3-aminopropionamido)-3-O-(2,4-di-O-benzyl-3-O-[2,3,4-tri-O-benzylidene-2-deoxy- β -D-glucopyranoside lactam (67)]- α -L-rhamnopyranosyl)-4,6-O-benzylidene-2-deoxy- β -D-glucopyranoside (67): To a solution of primary alcohol **66** (0.21g, 0.18 mmol) in acetonitrile (3 mL) was added 2,2,6,6-tetramethyl-1-piperidinyl-*N*-oxide (0.026 g, 0.18 mmol), 1 M aqueous potassium bromide (0.180 mL), 0.50 M sodium bicarbonate (0.90 mL), and sodium hypochlorite (5-6%, 1.10 mL) at -5°C . The reaction was allowed to stir for 1 h before the addition of methanol (0.5 mL). After 15 min, 1 M hydrochloric acid (15 mL) and dichloromethane (25 mL) were added and the organic layer was removed, washed with water, dried with sodium sulfate, and evaporated. The crude syrup was filtered through a small plug of silica using dichloromethane: methanol (50:1) as eluent. The resultant off-white solid was stirred in 20% piperidine/DMF (5 mL) for 30 min and the solution concentrated under vacuum and co-evaporated with toluene (3 x 10 mL). The resultant syrup was dissolved in DMF (110 mL) and benzotriazol-1-yloxy)tripyrrolidinophosphonium hexafluorophosphate (0.175 g, 0.34 mmol) was added and the reaction stirred for 1 h before evaporation under vacuum. The residue was purified by chromatography (4:2:1 hexane:ethyl acetate:acetone) to afford an amorphous white solid (0.11 g, 64%): $[\alpha]_{\text{D}} +12.1$ (c 0.5, CHCl_3). ^1H NMR (600 MHz, CDCl_3) δ 7.50-7.13 (m, 30H, Ar-*H*), 6.89 (bs, 1H, NH), 5.48 (s, 1H, CH-Ph),

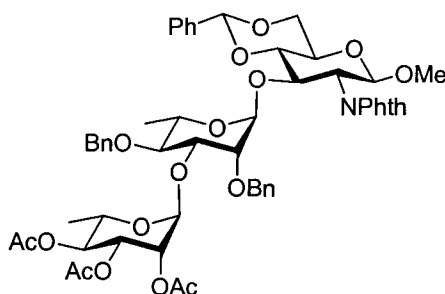
5.42 (d, 1H, *NH*-Glc), 5.14 (d, 1H, $J = 2.3$ Hz, H-1''), 4.91 (d, 1H, $J = 1.3$ Hz, H-1'), 4.71-4.38 (m, 10H, CH_2Ph), 4.30 (dd, 1H, $J = 5.0$ Hz, 10.7 Hz, H-6_a), 4.22 (d, 1H, $J = 8.6$ Hz, H-1), 4.04 (d, 1H, $J = 9.3$ Hz, H-5''), 3.92 (dd \approx t, 1H, $J = 8.6$ Hz, H-2), 3.96 (dd, 1H, $J = 3.0, 9.7$ Hz, H-3'), 3.89 (dd \approx t, 1H, $J = 9.3$ Hz, H-4''), 3.70-3.80 (m, 4H, H-6_b, H-5', H-3'', tether βH_a), 3.59-3.69 (m, 2H, H-3, H-2''), 3.76 (t, 1H, $J_{3,4} \approx J_{4,5} = 9.1$ Hz, H-4), 3.79 (dd \approx t, 1H, $J = 2.3$ Hz, H-2'), 3.52-3.58 (m, 4H, H-4', H-5, tether βH_b), 3.45 (s, 3H, OMe), 2.37-2.39 (m, 2H, tether $\alpha H_{a,b}$), 0.81 (d, 3H, $J = 6.2$ Hz, H-6'). ^{13}C NMR (125 MHz) δ 173.2, 169.8, 138.5, 138.4, 138.2, 137.6, 137.4, 129.8, 128.9, 128.8, 128.5, 128.4, 128.3, 128.3, 127.9, 127.8, 127.74, 127.71, 127.6, 127.5, 126.4, 102.9, 102.1, 101.1, 101.0, 84.2, 82.4, 79.6, 78.1, 77.2, 76.6, 75.0, 74.6, 73.4, 72.4, 72.0, 68.9, 68.6, 66.3, 62.9, 58.5, 54.1, 32.7, 31.2, 17.3. ES HRMS calc'd for $C_{64}H_{70}N_2O_{15}Na$ (M+Na): 1129.4674, found: 1129.4684.



21

Methyl 2-(2-aminopropionamido)-3-O-(3-O-[α -L-mannopyranosyluronic acid]- α -L-rhamnopyranosyl)-2-deoxy- β -D-glucopyranoside lactam (21): The protected cyclic trisaccharide **67** (18 mg, 0.016 mmol) was dissolved in 9 mL water, and 1 mL methanol. Palladium hydroxide (12 mg, 10% wt., Degussa type) was added and the suspension was stirred for 24 h. The reaction was filtered, evaporated and pre-purified

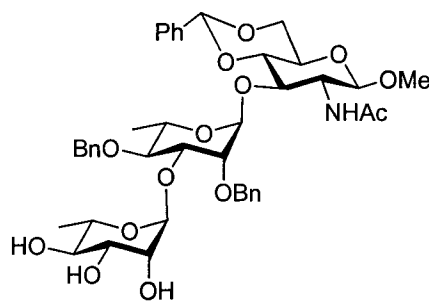
using a Waters solid phase extraction cartridge (C-18). Final purification was done using reverse-phase (C-18) HPLC (0-15% gradient of methanol in water). This gave a clear glass that was lyophilised to a white solid (7.4 mg, 81%): $[\alpha]_D -36.3$ (c 0.5, H_2O). 1H NMR (600 MHz, D_2O) δ 5.11 (d, 1H, $J = 1.5$ Hz, H-1''), 4.77 (d, 1H, $J = 2.2$ Hz, H-1'), 4.41 (d, 1H, $J = 8.6$ Hz, H-1), 4.09 (dd, 1H, $J = 1.5, 3.2$ Hz, H-2''), 4.04 (d, 1H, $J = 9.5$ Hz, H-5''), 3.95-3.99 (m, 2H, H-5', H-6_a), 3.92 (dd, 1H, $J = 8.5, 10.3$ Hz, H-2), 3.89 (dd \approx t, 1H, $J = 9.5$ Hz, H-4''), 3.85 (dd, 1H, $J = 9.3, 3.3$ Hz, H-3''), 3.83 (dd, 1H, $J = 3.3, 9.9$ Hz, H-3'), 3.79 (dd, 1H, $J = 2.2, 3.2$ Hz, H-2'), 3.76 (dd, 1H, $J_{vic} = 5.8$ Hz, $J_{gem} = 12.2$ Hz, H-6_b), 3.65-3.70 (m, 1H, tether αH_a), 3.52-3.57 (m, 4H, H-4', H-3, H-4, tether αH_b), 3.50 (s, 3H, OCH₃), 3.46 (ddd, 1H, $J = 2.2, 6.1, 8.1$ Hz, H-5), 2.58-2.61 (m, 2H, tether $\beta H_{a/b}$), 1.27 (d, 3H, $J = 6.4$ Hz, H-6'). ^{13}C NMR (125 MHz) δ 174.6, 171.2, 104.3, 103.7, 102.8, 86.1, 79.9, 76.7, 72.4, 71.8, 71.55, 71.51, 70.6, 70.3, 70.0, 69.0, 61.6, 57.9, 54.9, 35.3, 34.8, 17.6. ES HRMS calc'd for $C_{22}H_{36}N_2O_{15}Na$ (M+Na): 591.2013, found: 591.2006.



69

Methyl (2,3,4-tri-*O*-acetyl- α -L-rhamnopyranosyl)-(1 \rightarrow 3)-(2,4-di-*O*-benzyl- α -L-rhamnopyranosyl)-(1 \rightarrow 3)-4,6-*O*-benzylidene-2-phthalimido- β -D-glucopyranoside (69): To a stirred solution of alcohol **40**^[56] (0.58 g, 0.79 mmol) and rhamnosyl

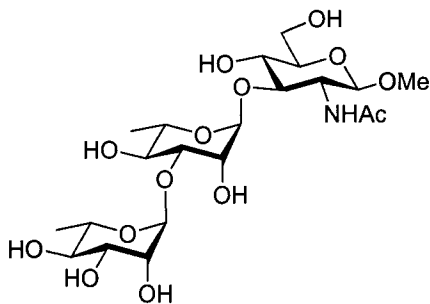
thioglycoside donor **68**^[102] (0.46 g, 1.38 mmol) in dichloromethane (15 mL) was added *N*-iodosuccinimide (0.34 g, 1.38 mmol) and 75 μ L of dichloromethane saturated with trifluoromethanesulfonic acid at -45 °C. The reaction was stirred for 45 min before the addition of triethylamine (3 mL). The reaction was poured into 10% sodium thiosulfate. The organic layer was washed with water, dried over sodium sulfate, filtered and concentrated to dryness. The residue was purified by chromatography (7:1 \rightarrow 4:1 toluene:ethyl acetate) to give a white foam (0.70 g, 88%): $[\alpha]_D -18.3$ (*c* 0.7, H₂O). ¹H NMR (600 MHz, D₂O) δ 7.88-6.92 (m, 19H, Ar-*H*), 5.53 (s, 1H, PhCHO₂-), 5.27 (dd, 1H, *J* = 1.6, 3.4 Hz, H-2'), 5.23 (dd, 1H, *J* = 3.4, 9.2 Hz), 5.20 (d, 1H, *J* = 8.8 Hz), 4.96 (m, 2H, PhCH₂O-), 4.66 (d, 1H, *J* = 11.6 Hz, PhCH₂O-), 4.64 (d, 1H, *J* = 1.2 Hz, H-1''), 4.58 (dd, 1H, *J* = 8.7, 9.2 Hz, H-3), 4.46 (d, 1H, PhCH₂O-, *J* = 11.6 Hz), 4.40 (dd, 1H, *J*_{vic} = 4.5 Hz, *J*_{gem} = 10.2 Hz, H-6_a), 4.24 (dd, 1H, *J* = 8.6, 9.1 Hz, H-2), 3.91 (dd, 1H, *J* = 3.3, 9.6 Hz, H-3''), 3.87-3.80 (m, 2H, H-5, H-5''), 3.70-3.62 (m, 3H, H-5', H-6_b, H-4), 3.42 (s, 3H, OCH₃), 3.39-3.32 (m, 2H, H-4', H-2''), 2.13, 1.92, 1.84 (3 x s, 3H ea, -OCOCH₃), 1.06 (d, 3H, *J* = 6.3 Hz, H-6''), 0.73 (d, 3H, *J* = 6.3 Hz, H-6'). ¹³C NMR (125 MHz) δ 169.9, 169.8, 169.7, 138.2, 137.5, 136.9, 134.5, 128.2, 128.1, 127.7, 127.5, 127.4, 126.8, 126.4, 123.7, 102.1, 99.6, 99.3, 97.3, 80.5, 79.1, 78.2, 75.0, 74.2, 71.9, 71.0, 69.8, 69.1, 68.8, 68.4, 66.7, 66.5, 57.1, 56.7, 20.8, 20.76, 20.70, 17.2, 12.1. ES HRMS calc'd for C₅₄H₅₉NO₁₈Na (M+Na): 1032.3630, found: 1032.3638.



70

Methyl **(α -L-rhamnopyranosyl)-(1 \rightarrow 3)-(2,4-di-O-benzyl- α -L-rhamnopyranosyl)-(1 \rightarrow 3)-2-acetamido- β -D-glucopyranoside (70):** To a solution of **69** (0.44 g, 0.436 mmol) in ethanol (20 mL) at reflux was added hydrazine hydrate (3 mL), and the solution was heated for 24 h. The solution was poured into water and extracted with chloroform (3x). The organic layer was washed again with water, dried over sodium sulfate, filtered and concentrated to dryness. The crude material was dissolved in methanol (3 mL) and acetic anhydride (42 μ L, 0.44 mmol) was added. The mixture was stirred for 2 h and evaporated to dryness. The reaction was purified by chromatography (2:1 acetone:ethyl acetate, 1% acetic acid) to give the target compound as a white powder (0.28 g, 0.36 mmol): $[\alpha]_D -43.6$ (c 1.0, H₂O). ¹H NMR (600 MHz, D₂O) δ 7.46 – 7.12 (m, 15H, Ar-*H*), 5.59 (d, 1H, $J = 7.7$ Hz, N-*H*), 5.49 (s, 1H, PhCHO₂-), 5.01 (s, 1H, H-1''), 4.96 (d, 1H, $J = 1.4$ Hz, H-1'), 4.67 (d, 1H, $J = 7.2$ Hz, H-1), 4.64-4.54 (m, 2H, PhCH₂O-), 4.33 (dd, 1H, $J_{vic} = 6.3$, $J_{gem} = 10.5$ Hz, H-6_a), 4.24 (dd \approx t, 1H, $J = 9.2$ Hz, H-3), 3.94 (dd, 1H, $J = 3.4$, 9.3 Hz, H-3'), 3.92 (dq, 1H, $J = 6.7$, 9.3 Hz, H-5'), 3.79 (bd, 1H, $J = 2$ Hz, H-2''), 3.74 (dd, 1H, $J_{vic} = 4.5$ Hz, $J_{gem} = 10.5$ Hz, H-6_b), 3.69 (dd, 1H, $J = 1.8$, 3.4 Hz, H-2') 3.63 (dd, 1H, $J = 4.5$, 10.0 Hz, H-3''), 3.56-3.42 (m, 9H, H-2, H-4, H-5, H-4', H-3'', H-5'', OCH₃), 1.88 (s, 3H, NHAc), 1.24 (s, 3H, $J = 6.6$ Hz, H-6'), 0.86 (s, 3H,

$J = 6.6$ Hz, H-6''). ^{13}C NMR (125 MHz, CDCl_3) δ 170.4, 138.4, 138.2, 137.1, 128.9, 128.5, 128.4, 128.1, 127.7, 127.6, 127.54, 127.50, 126.3, 101.8, 101.4, 97.9, 81.2, 80.1, 78.3, 75.3, 72.6, 71.6, 71.0, 68.7, 68.4, 68.3, 66.2, 57.7, 56.9, 23.6, 17.6. ES HRMS calc'd for $\text{C}_{42}\text{H}_{53}\text{NO}_{14}\text{Na}$ ($\text{M}+\text{Na}$): 818.3364, found: 818.3359.



22

Methyl (α-L-rhamnopyranosyl)-(1→3)-(α-L-rhamnopyranosyl)-(1→3)-2-acetamido-β-D-glucopyranoside (22): A solution of **70** (102 mg, 0.1281 mmol) was dissolved in 80% aqueous acetic acid and heated to 80 °C for 24 h. The solvents were evaporated, and the residue co-evaporated from toluene (3x). The residue was dissolved in 10:1 methanol:water and palladium hydroxide (40 mg, 10% wt., Degussa type) was added. The suspension was stirred under a hydrogen atmosphere for 24 h and filtered. The crude product was pre-purified using a Waters solid-phase extraction cartridge using water as the eluent. Final purification was done using reverse-phase (C-18) HPLC to give the target compound as a clear glass that was lyophilized to a white solid (79%, 53 mg): $[\alpha]_{\text{D}} -21.1$ (c 0.5, H_2O). ^1H NMR (600 MHz, D_2O) δ 5.05 (d, 1H, $J = 1.6$ Hz, H-1''), 4.82 (d, 1H, $J = 1.7$ Hz, H-1'), 4.48 (d, 1H, $J = 8.7$ Hz, H-1), 4.06 (dd, 1H, $J = 1.6$, 3.3 Hz, H-2''), 4.04 (dq, 1H, $J = 3.5$, 6.3 Hz, H-5''), 3.95 (dd, 1H, $J_{\text{vic}} = 2.2$ Hz, $J_{\text{gem}} = 10.2$ Hz), 3.86 (dd, 1H, $J = 1.9$, 3.3 Hz, H-2'), 3.85 (m, 5H, H-2, H-3', H-4', H-3'', H-5''),

3.59 (dd, 1H, $J_{2,3} \approx J_{3,4} = 9.4$ Hz, H-3), 3.54 (m, 7H, H-4, H-5, H-6_b, H-4'', OCH₃). 1.91 (s, 3H, NHAc), 1.32 (d, 3H, $J = 6.3$ Hz, H-6''), 0.84 (d, 3H, $J = 6.2$ Hz, H-6). ¹³C NMR (125 MHz, CDCl₃) δ 178.5, 101.2, 101.4, 99.8, 80.3, 79.3, 74.3, 72.7, 71.8, 69.2, 69.1, 68.8, 68.6, 68.1, 68.0, 60.6, 55.6, 27.0, 16.0. ES HRMS calc'd for C₂₁H₃₇NO₁₄Na (M+Na): 550.2112, found: 550.2119.

Chapter 8

Bibliography

- [1] A. Varki, *Glycobiology* **1993**, *3*, 97-130.
- [2] Y. C. Lee, *FASEB J.* **1992**, *6*, 3193-3200.
- [3] B. Imperiali, S. E. O'Connor, *Curr. Opin. Chem. Biol.* **1999**, *3*, 643-649.
- [4] F. I. Comer, G. W. Hart, *J. Biol. Chem.* **2000**, *275*, 29179-29182.
- [5] S. Hakomori, *Cancer Res.* **1996**, *56*, 5309-5318.
- [6] R. A. Dwek, *Chem. Rev.* **1996**, *96*, 683-720.
- [7] R. U. Lemieux, *Chem. Soc. Rev.* **1989**, *18*, 347-374.
- [8] P. I. Kitov, J. M. Sadowska, G. Mulvey, G. D. Armstrong, H. Ling, N. S. Pannu, R. J. Read, D. R. Bundle, *Nature* **2000**, *403*, 669-672.
- [9] J. J. Lundquist, E. J. Toone, *Chem. Rev.* **2002**, *102*, 555-578.
- [10] F. Fortune, J. Walker, M. Lefrancois, T. Lehner, *Scand. J. Immunol.* **1994**, *40*, 636-642.
- [11] N. F. Burkhalter, S. M. Dimick, E. J. Toone, in *Carbohydrates in Chemistry and Biology, Vol. 2* (Ed.: B. Ernst), Wiley-VCH, Toronto, **2000**, pp. 863-914.
- [12] H. J. Gabius, *Pharm. Res.* **1998**, *15*, 23-30.
- [13] T. Christensen, E. J. Toone, in *Recognition of Carbohydrates in Biological Systems Pt A: General Procedures, Vol. 362*, **2003**, pp. 486-504.
- [14] K. A. Kronis, J. P. Carver, *Biochemistry* **1985**, *24*, 834-840.
- [15] K. A. Kronis, J. P. Carver, *Biochemistry* **1985**, *24*, 826-833.

- [16] D. H. Williams, J. P. L. Cox, A. J. Doig, M. Gardner, U. Gerhard, P. T. Kaye, A. R. Lal, I. A. Nicholls, C. J. Salter, R. C. Mitchell, *J. Am. Chem. Soc.* **1991**, *113*, 7020-7030.
- [17] I. K. McDonald, J. M. Thornton, *J. Mol. Biol.* **1994**, *238*, 777-793.
- [18] H. J. Bohm, G. Klebe, *Angew. Chem. Int. Ed. Engl.* **1996**, *35*, 2589-2614.
- [19] M. D. Fernandez, F. J. Canada, J. Jimenez-Barbero, G. Cuevas, *J. Am. Chem. Soc.* **2005**, *127*, 7379-7386.
- [20] F. A. Quijcho, *Annu. Rev. Biochem.* **1986**, *55*, 287-315.
- [21] W. Blokzijl, J. Engberts, *Angew. Chem. Int. Ed. Engl.* **1993**, *32*, 1545-1579.
- [22] M. C. Chervenak, E. J. Toone, *Biophys. J.* **1994**, *66*, A359-A359.
- [23] M. S. Searle, D. H. Williams, *J. Am. Chem. Soc.* **1992**, *114*, 10690-10697.
- [24] S. N. Timasheff, *Biochemistry* **2002**, *41*, 13473-13482.
- [25] M. C. Chervenak, E. J. Toone, *J. Am. Chem. Soc.* **1994**, *116*, 10533-10539.
- [26] H. Beierbeck, L. T. J. Delbaere, M. Vandonselaar, R. U. Lemieux, *Can. J. Chem.-Rev. Can. Chim.* **1994**, *72*, 463-470.
- [27] R. U. Lemieux, *Accounts Chem. Res.* **1996**, *29*, 373-380.
- [28] D. Voet, J. G. Voet, *Biochemistry*, 2nd. Ed., John Wiley and Sons, Toronto, **1995**.
- [29] R. A. Goldsby, T. J. Kindt, B. A. Osborne, J. Kuby, *Immunology*, 5th Ed., W.H. Freeman and Company, New York, **2003**.
- [30] A. J. McMichael, J. R. Pilch, G. Galfre, D. Y. Mason, J. W. Fabre, C. Milstein, *Eur. J. Immunol.* **1979**, *9*, 205-210.
- [31] R. Hahn, R. Schlegel, A. Jungbauer, *J. Chromatogr. B* **2003**, *790*, 35-51.

- [32] N. I. A. Carlin, M. A. J. Gidney, A. A. Lindberg, D. R. Bundle, *J. Immunol.* **1986**, *137*, 2361-2366.
- [33] M. Heinrich, *Am. Lab.* **2000**, *32*, 22-+.
- [34] P. Schuck, *Annu. Rev. Biophys. Biomolec. Struct.* **1997**, *26*, 541-566.
- [35] D. R. Bundle, B. W. Sigurskjold, in *Neoglycoconjugates, Pt B, Vol. 247*, **1994**, pp. 288-305.
- [36] V. Pozsgay, C. Y. Chu, L. Pannell, J. Wolfe, J. B. Robbins, R. Schneerson, *Proc. Natl. Acad. Sci. U. S. A.* **1999**, *96*, 5194-5197.
- [37] M. Inouye, in *Bacterial Outer Membrane* (Ed.: M. Inouye), Wiley, New York, **1979**, pp. 1-12.
- [38] D. R. Bundle, E. Altman, F. I. Auzanneau, H. Baumann, E. Eichler, B. Sigurskjold, in *The Alfred Benzon Symposium No. 36, Complex Carbohydrates in Drug Research* (Eds.: K. Bock, H. Clausen), Copenhagen, **1994**, pp. 168-181.
- [39] B. M. Pinto, D. G. Morissette, D. R. Bundle, *J. Chem. Soc.-Perkin Trans. 1* **1987**, 9-14.
- [40] F. I. Auzanneau, D. R. Bundle, *Can. J. Chem.-Rev. Can. Chim.* **1993**, *71*, 534-548.
- [41] F. I. Auzanneau, H. R. Hanna, D. R. Bundle, *Carbohydr. Res.* **1993**, *240*, 161-181.
- [42] F. I. Auzanneau, D. R. Bundle, *Carbohydr. Res.* **1993**, *247*, 195-209.
- [43] P. J. Meikle, N. M. Young, D. R. Bundle, *J. Immunol. Methods* **1990**, *132*, 255-261.
- [44] E. Vorberg, D. R. Bundle, *J. Immunol. Methods* **1990**, *132*, 81-89.

- [45] D. R. Bundle, *Pure Appl. Chem.* **1989**, *61*, 1171-1180.
- [46] N. K. Vyas, M. N. Vyas, M. C. Chervenak, M. A. Johnson, B. M. Pinto, D. R. Bundle, F. A. Quiocho, *Biochemistry* **2002**, *41*, 13575-13586.
- [47] D. R. Bundle, in *Carbohydrates* (Ed.: S. Hecht), Oxford University Press Inc., Oxford, **1998**, pp. 370-440.
- [48] A. M. M. van Roon, N. S. Pannu, J. P. M. de Vrind, G. A. van der Marel, J. H. van Boom, C. H. Hokke, A. M. Deelder, J. P. Abrahams, *Structure* **2004**, *12*, 1227-1236.
- [49] S. Sheriff, C. Y. Y. Chang, P. D. Jeffrey, J. Bajorath, *J. Mol. Biol.* **1996**, *259*, 938-946.
- [50] D. A. Calarese, C. N. Scanlan, M. B. Zwick, S. Deechongkit, Y. Mimura, R. Kunert, P. Zhu, M. R. Wormald, R. L. Stanfield, K. H. Roux, *Science* **2003**, *300*, 2065-2071.
- [51] S. Villeneuve, H. Souchon, M. M. Riottot, J. C. Mazie, P. Lei, C. P. J. Glaudemans, P. Kovac, J. M. Fournier, P. M. Alzari, *Proc. Natl. Acad. Sci. U. S. A.* **2000**, *97*, 8433-8438.
- [52] H. P. Nguyen, N. O. L. Seto, L. Brade, P. Kosma, H. Brade, S. V. Evans, *Acta Crystallogr. Sect. D-Biol. Crystallogr.* **2001**, *57*, 1872-1876.
- [53] M. Cygler, D. R. Rose, D. R. Bundle, *Science* **1991**, *253*, 442-445.
- [54] H. R. Hanna, D. R. Bundle, *Can. J. Chem.-Rev. Can. Chim.* **1993**, *71*, 125-134.
- [55] M. N. Vyas, N. K. Vyas, P. J. Meikle, B. Sinnott, B. M. Pinto, D. R. Bundle, F. A. Quiocho, *J. Mol. Biol.* **1993**, *231*, 133-136.
- [56] R. A. Gagne, Ph.D. Thesis, University of Alberta (Edmonton), **2000**.

- [57] A. Maradufu, A. S. Perlin, *Carbohydr. Res.* **1974**, *32*, 93-99.
- [58] R. Bishop, M. L. Scudder, D. C. Craig, A. Rahman, S. F. Alshahateet, *Mol. Cryst. Liquid Cryst.* **2005**, *440*, 173-186.
- [59] P. Metrangolo, H. Neukirch, T. Pilati, G. Resnati, *Accounts Chem. Res.* **2005**, *38*, 386-395.
- [60] P. Auffinger, F. A. Hays, E. Westhof, P. S. Ho, *Proc. Natl. Acad. Sci. U. S. A.* **2004**, *101*, 16789-16794.
- [61] J. P. Carver, *Pure Appl. Chem.* **1993**, *65*, 763-770.
- [62] M. Mammen, E. I. Shakhnovich, G. M. Whitesides, *J. Org. Chem.* **1998**, *63*, 3168-3175.
- [63] R. U. Lemieux, L. T. J. Delbaere, H. Beierbeck, U. Spohr, *Host-Guest Molecular Interactions: From Chemistry to Biology*, Wiley, London, **1991**, pp. 231-248.
- [64] H. C. Kolb, B. Ernst, *Chem.-Eur. J.* **1997**, *3*, 1571-1578.
- [65] H. C. Kolb, *Bioorg. Med. Chem. Lett.* **1997**, *7*, 2629-2634.
- [66] K. E. Norman, G. P. Anderson, H. C. Kolb, K. Ley, B. Ernst, *Blood* **1998**, *91*, 475-483.
- [67] H. C. Kolb, B. Ernst, *Pure Appl. Chem.* **1997**, *69*, 1879-1884.
- [68] S. Haataja, K. Tikkanen, J. Liukkonen, C. Francoisgerard, J. Finne, *J. Biol. Chem.* **1993**, *268*, 4311-4317.
- [69] M. Wilstermann, J. Balogh, G. Magnusson, *J. Org. Chem.* **1997**, *62*, 3659-3665.
- [70] K. Blount, F. Zhao, T. Hermann, Y. Tor, *J. Am. Chem. Soc.* **2005**, *127*, 9818-9829.

- [71] N. Navarre, N. Amiot, A. van Oijen, A. Imberty, A. Poveda, J. Jimenez-Barbero, A. Cooper, M. A. Nutley, G. J. Boons, *Chem.-Eur. J.* **1999**, *5*, 2281-2294.
- [72] M. C. Galan, A. P. Venot, J. Glushka, A. Imberty, G. J. Boons, *J. Am. Chem. Soc.* **2002**, *124*, 5964-5973.
- [73] M. C. Galan, A. P. Venot, J. Glushka, A. Imberty, G. J. Boons, *Org. Biomol. Chem.* **2003**, *1*, 3891-3899.
- [74] K. B. Wlasichuk, M. A. Kashem, P. V. Nikrad, P. Bird, C. Jiang, A. P. Venot, *J. Biol. Chem.* **1993**, *268*, 13971-13977.
- [75] R. G. Frost, R. W. Reitherman, A. L. Miller, J. S. Obrien, *Anal. Biochem.* **1975**, *69*, 170-179.
- [76] M. I. Khan, M. V. K. Sastry, A. Surolia, *J. Biol. Chem.* **1986**, *261*, 3013-3019.
- [77] U. Spohr, E. Paszkiewicz, N. Morishima, R. U. Lemieux, *Can. J. Chem.-Rev. Can. Chim.* **1992**, *70*, 254-271.
- [78] R. Cromer, U. Spohr, D. P. Khare, J. Lependu, R. U. Lemieux, *Can. J. Chem.-Rev. Can. Chim.* **1992**, *70*, 1511-1530.
- [79] R. U. Lemieux, M. H. Du, U. Spohr, S. Acharya, A. Surolia, *Can. J. Chem.-Rev. Can. Chim.* **1994**, *72*, 158-163.
- [80] O. Hindsgaul, D. P. Khare, M. Bach, R. U. Lemieux, *Can. J. Chem.-Rev. Can. Chim.* **1985**, *63*, 2653-2658.
- [81] S. A. Wacowich-Sgarbi, D. R. Bundle, *J. Org. Chem.* **1999**, *64*, 9080-9089.
- [82] D. R. Bundle, H. Baumann, J. R. Brisson, S. M. Gagne, A. Zdanov, M. Cygler, *Biochemistry* **1994**, *33*, 5183-5192.
- [83] P. Zhang, D. R. Bundle, *Isr. J. Chem.* **2000**, *40*, 189-208.

- [84] R. Alibes, D. R. Bundle, *J. Org. Chem.* **1998**, *63*, 6288-6301.
- [85] R. S. McGavin, R. A. Gagne, M. C. Chervenak, D. R. Bundle, *Org. Biomol. Chem.* **2005**, *3*, 2723-2732.
- [86] J. P. Praly, R. U. Lemieux, *Can. J. Chem.-Rev. Can. Chim.* **1987**, *65*, 213-223.
- [87] R. U. Lemieux, D. R. Bundle, D. A. Baker, *J. Am. Chem. Soc.* **1975**, *97*, 4076-4083.
- [88] R. U. Lemieux, K. B. Hendriks, R. V. Stick, K. James, *J. Am. Chem. Soc.* **1975**, *97*, 4056-4062.
- [89] R. U. Lemieux, S. Koto, D. Voisin, *ACS Symp. Ser.* **1979**, *87*, 17.
- [90] R. U. Lemieux, D. R. Bundle, D. A. Baker, *J. Am. Chem. Soc.* **1975**, *97*, 4076-4083.
- [91] R. U. Lemieux, K. B. Hendriks, R. V. Stick, K. James, *J. Am. Chem. Soc.* **1975**, *97*, 4056-4062.
- [92] R. U. Lemieux, H. Driguez, *J. Am. Chem. Soc.* **1975**, *97*, 4063-4069.
- [93] R. U. Lemieux, H. Driguez, *J. Am. Chem. Soc.* **1975**, *97*, 4069-4075.
- [94] W. Koenigs, E. Knorr, **1901**, *34*, 957-981.
- [95] H. Paulsen, *Angew. Chem.-Int. Edit. Engl.* **1982**, *21*, 155-173.
- [96] J. H. Kim, H. Yang, G. J. Boons, *Angew. Chem.-Int. Edit.* **2005**, *44*, 947-949.
- [97] D. Crich, S. X. Sun, *Tetrahedron* **1998**, *54*, 8321-8348.
- [98] B. Helferich, K. Weis, *Chem. Ber.-Recl.* **1956**, *89*, 314-321.
- [99] B. Helferich, K. F. Wedemeyer, *Liebigs Ann. Chem.* **1949**, *563*, 139-145.
- [100] N. K. Kochetkov, N. E. Byramova, Y. E. Tsvetkov, L. V. Backinowsky, *Tetrahedron* **1985**, *41*, 3363-3375.

- [101] G. H. Veeneman, S. H. van Leuwen, H. Zuurmand, J. H. van Boom, *J. Carb. Chem.* **1998**, *9*, 783-796.
- [102] F. I. Auzanneau, D. R. Bundle, *Carbohydr. Res.* **1991**, *212*, 13-24.
- [103] V. Pozsgay, *Carbohydr. Res.* **1979**, *69*, 284-286.
- [104] T. Ziegler, G. Lemanski, *Eur. J. Org. Chem.* **1998**, 163-170.
- [105] P. L. Durette, D. Horton, **1971**, *3*, 417-&.
- [106] L. T. Delbaere, M. N. G. James, R. U. Lemieux, *J. Am. Chem. Soc.* **1973**, *95*, 7866-7868.
- [107] K. Bock, I. Lundt, C. Pedersen, *Tetrahedron Lett.* **1973**, 1037-1040.
- [108] E. J. Corey, Venkates.A, *J. Am. Chem. Soc.* **1972**, *94*, 6190-&.
- [109] N. J. Davis, S. L. Flitsch, *Tetrahedron Lett.* **1993**, *34*, 1181-1184.
- [110] K. Igarashi, T. Honma, T. Imagawa, *J. Org. Chem.* **1970**, *35*, 610-&.
- [111] P. Fugedi, P. J. Garegg, H. Lonn, T. Norberg, *Glycoconjugate J.* **1987**, *4*, 97-108.
- [112] R. R. Schmidt, W. Kinzy, in *Advances in Carbohydrate Chemistry and Biochemistry, Vol 50, Vol. 50*, **1994**, pp. 21-123.
- [113] D. Kahne, S. Walker, Y. Cheng, D. Vanengen, *J. Am. Chem. Soc.* **1989**, *111*, 6881-6882.
- [114] R. Knorr, A. Trzeciak, W. Bannwarth, D. Gillessen, *Tetrahedron Lett.* **1989**, *30*, 1927-1930.
- [115] J. Coste, D. Lenguyen, B. Castro, *Tetrahedron Lett.* **1990**, *31*, 205-208.
- [116] A. Otter, D. R. Bundle, *J. Magn. Reson. Ser. B* **1995**, *109*, 194-201.
- [117] W. P. Neumann, *Synthesis* **1987**, 665-683.

- [118] V. Stgeorgiev, R. G. Vaninwegen, P. Carlson, *Eur. J. Med. Chem.* **1990**, *25*, 375-378.
- [119] N. Hossain, A. Zapata, M. Wilstermann, U. J. Nilsson, G. Magnusson, *Carbohydr. Res.* **2002**, *337*, 569-580.
- [120] B. Alberts, D. Bray, J. Lewis, M. Raff, K. Roberts, J. D. Watson, *The Molecular Biology of the Cell*, Garland Publishing, New York, **1994**.
- [121] J. F. Brandts, L. N. Lin, T. Wiseman, S. Williston, C. P. Yang, *Am. Lab.* **1990**, *22*, 30-39.
- [122] T. Wiseman, S. Williston, J. F. Brandts, L. N. Lin, *Anal. Biochem.* **1989**, *179*, 131-137.
- [123] R. U. Lemieux, M. H. Du, U. Spohr, *J. Am. Chem. Soc.* **1994**, *116*, 9803-9804.
- [124] T. Peters, B. M. Pinto, *Curr. Opin. Struct. Biol.* **1996**, *6*, 710-720.
- [125] F. Ni, *Prog. Nucl. Magn. Reson. Spectrosc.* **1994**, *26*, 517-606.
- [126] V. V. Krishnamurthy, *J. Magn. Reson. Ser. A* **1996**, *121*, 33-41.
- [127] T. Rundlof, A. Kjellberg, C. Damberg, T. Nishida, G. Widmalm, *Magn. Reson. Chem.* **1998**, *36*, 839-847.
- [128] S. J. Weiner, P. A. Kollman, D. A. Case, U. C. Singh, C. Ghio, G. Alagonia, S. Profeta, P. Weiner, *J. Am. Chem. Soc.* **1984**, *106*, 765-784.
- [129] S. W. Homans, *Biochemistry* **1990**, *29*, 9110-9118.
- [130] B. R. Brooks, R. E. Bruccoleri, B. D. Olafson, D. J. States, S. Swaminathan, M. Karplus, *J. Comput. Chem.* **1983**, *4*, 187-217.
- [131] R. J. Woods, **1998**, *Glycoconj. J.* *15*, 209-216.
- [132] N. L. Allinger, M. Rahman, J. H. Lii, *J. Am. Chem. Soc.* **1990**, *112*, 8293-8307.

- [133] R. Stuikeprill, B. Meyer, *Eur. J. Biochem.* **1990**, *194*, 903-919.
- [134] D. Cameron, D. R. Bundle, *Unpublished Results*.
- [135] D. R. Bundle, E. Eichler, M. A. J. Gidney, M. Meldal, A. Ragauskas, B. W. Sigurskjold, B. Sinnott, D. C. Watson, M. Yaguchi, N. M. Young, *Biochemistry* **1994**, *33*, 5172-5182.
- [136] A. M. M. van Roon, N. S. Pannu, C. H. Hokke, A. M. Deelder, J. P. Abrahams, *Acta Crystallogr. Sect. D-Biol. Crystallogr.* **2003**, *59*, 1306-1309.
- [137] P. D. Jeffrey, J. Bajorath, C. Y. Chang, D. Yelton, I. Hellstrom, K. E. Hellstrom, S. Sheriff, *Nat. Struct. Biol.* **1995**, *2*, 466-471.
- [138] D. A. Calarese, C. N. Scanlan, M. B. Zwick, S. Deechongkit, Y. Mimura, R. Kunert, P. Zhu, M. R. Wormald, R. L. Stanfield, K. H. Roux, J. W. Kelly, P. M. Rudd, R. A. Dwek, H. Katinger, D. R. Burton, I. A. Wilson, *Science* **2003**, *300*, 2065-2071.
- [139] P. Balaram, A. A. Bothnerb-by, J. Dadok, *J. Am. Chem. Soc.* **1972**, *94*, 4015-4017.
- [140] P. Balaram, A. A. Bothnerb-by, E. Breslow, *J. Am. Chem. Soc.* **1972**, *94*, 4017-4018.
- [141] A. Lanir, G. Navon, *Biochemistry* **1971**, *10*, 1024-&.
- [142] B. Meyer, T. Peters, *Angew. Chem.-Int. Edit.* **2003**, *42*, 864-890.
- [143] J. M. Moore, *Curr. Opin. Biotechnol.* **1999**, *10*, 54-58.
- [144] C. Dalvit, P. Pevarello, M. Tato, M. Veronesi, A. Vulpetti, M. Sundstrom, *J. Biomol. NMR* **2000**, *18*, 65-68.

- [145] C. Dalvit, G. Fogliatto, A. Stewart, M. Veronesi, B. Stockman, *J. Biomol. NMR* **2001**, *21*, 349-359.
- [146] M. Mayer, B. Meyer, *Angew. Chem.-Int. Edit.* **1999**, *38*, 1784-1788.
- [147] M. Mayer, B. Meyer, *J. Am. Chem. Soc.* **2001**, *123*, 6108-6117.
- [148] A. Kalk, H. J. C. Berendsen, *J. Magn. Reson.* **1976**, *24*, 343-366.
- [149] M. Vogtherr, T. Peters, *J. Am. Chem. Soc.* **2000**, *122*, 6093-6099.
- [150] M. A. Johnson, B. M. Pinto, *Bioorg. Med. Chem.* **2004**, *12*, 295-300.
- [151] A. Blume, A. J. Benie, F. Stolz, R. R. Schmidt, W. Reutter, S. Hinderlich, T. Peters, *J. Biol. Chem.* **2004**, *279*, 55715-55721.
- [152] A. Bhunia, V. Jayalakshmi, A. J. Benie, O. Schuster, S. Kelm, N. R. Krishna, T. Peters, *Carbohydr. Res.* **2004**, *339*, 259-267.
- [153] M. Rinnbauer, B. Ernst, B. Wagner, J. Magnani, A. J. Benie, T. Peters, *Glycobiology* **2003**, *13*, 435-443.
- [154] O. Kooistra, L. Herfurth, E. Luneberg, M. Frosch, T. Peters, U. Zahring, *Eur. J. Biochem.* **2002**, *269*, 573-582.
- [155] R. Meinecke, B. Meyer, *J. Med. Chem.* **2001**, *44*, 3059-3065.
- [156] T. Haselhorst, T. Weimar, T. Peters, *J. Am. Chem. Soc.* **2001**, *123*, 10705-10714.
- [157] H. Moller, N. Serttas, H. Paulsen, J. M. Burchell, J. Taylor-Papadimitriou, B. Meyer, *Eur. J. Biochem.*, **2002**, *269*, 1444-1455.
- [158] A. Otter, *Personal communication* **2004**.
- [159] D. L. Pavia, G. M. Lampman, G. S. Kriz, *Introduction to Spectroscopy*, Saunders College Publishing, Toronto, **1996**.

- [160] L. Maili, M. Xi-an, Y. Chaohui, H. Huang, J. K. Nicholson, J. C. Lindon, *J. Magn. Reson.* **1998**, *132*, 125-129.
- [161] H. Geen, R. Freeman, *J. Magn. Reson.* **1991**, *93*, 93-141.
- [162] M. Gueron, P. Plateau, M. Decorps, *Prog. Nucl. Magn. Reson. Spectrosc.* **1991**, *23*, 135-209.
- [163] M. Piotto, V. Saudek, V. Sklenar, *J. Biomol. NMR* **1992**, *2*, 661-665.
- [164] V. Jayalakshmi, N. R. Krishna, *J. Magn. Reson.* **2002**, *155*, 106-118.
- [165] T. Peters, *Personal communication.*
- [166] D. D. Perrin, W. L. F. Armarego, *Purification of Laboratory Chemicals, 3rd. Ed.*, Permagon Press, Oxford,